May 2022

Spline Modeling and Localized Mutual Information Monitoring of Pairwise Associations in Animal Movement

Andrew Benjamin Whetten
University of Wisconsin-Milwaukee

SPLINE MODELING AND LOCALIZED MUTUAL INFORMATION MONITORING OF PAIRWISE ASSOCIATIONS IN ANIMAL MOVEMENT

by

Andrew Benjamin Whetten

A Dissertation Submitted in

Partial Fulfillment of the

Requirements for the Degree of

Doctor of Philosophy

in Mathematics

at

The University of Wisconsin-Milwaukee

May 2022

ABSTRACT

SPLINE MODELING AND LOCALIZED MUTUAL INFORMATION MONITORING OF PAIRWISE ASSOCIATIONS IN ANIMAL MOVEMENT

by

Andrew Whetten

The University of Wisconsin-Milwaukee, 2022
Under the Supervision of Professor Vince Larson and Professor David Spade

Advances in Satellite Imaging and GPS tracking devices have given rise to a new era of remote sensing and geospatial analysis. In environmental science and conservation ecology, biotelemetric data recorded is often high-dimensional, spatially and/or temporally, and functional in nature, meaning that there is an underlying continuity to the biological process of interest. GPS-tracking of animal movement is commonly characterized by irregular time-recording of animal position, and the movement relationships between animals are prone to sudden change. In this dissertation, I propose a spline modeling approach for exploring interactions and time-dependent correlation between the movement of apex predators exhibiting territorial and territory-sharing behavior. A measure of localized mutual information (LMI) is proposed to derive a correlation function for monitoring changes in the pairwise association between animal movement trajectories. The properties of the LMI measure are assessed analytically and by simulation under a variety of circumstances. Advantages and disadvantages of the LMI measure are assessed and alternate measures of LMI are proposed to handle potential disadvantages. The proposed measure of LMI is shown to be an effective tool for detecting shifts in the correlation of animal movements, and seasonal/phasal correlatory structure.

TABLE OF CONTENTS

LIST OF FIGURES

LIST OF TABLES

1 ACKNOWLEDGMENTS

The work of this project, although largely completed in solitude during the COVID19 pandemic accompanied by the competing sounds of relaxing instrumental Celtic music and an passionate toddler, was aided by several individuals: Ronaldo Gonclaves Morato for his admirable support of a "random" graduate student from the other hemisphere, and Daniel Gervini for his valuable suggestions and feedback in the early drafting of this work. I also wish to thank the reviewers and editors at Ecology and Evolution, the International Journal of Geographic and Environmental Research, and Remote Sensing for their continued evaluation and support of my work.

There are a few others that I must acknowledge as well: Vince Larson for his extensive support and mentoring in the final stages of these projects, David Spade for his supportive consultation, and most importantly my wife, Hailey Whetten, for her tireless support of my graduate education, and many of my extended family members, who flooded me with positive encouragement.

2 Introduction

In the past two decades, the rapid increase in the quality of GPS-tracking technology has revolutionized the field of movement ecology [1, 2]. The advancements in animal-tracking systems have yielded high-precision and densely recorded datasets of wildlife behavior [3]. The current challenge in the field of movement ecology is the appropriate processing and integration of large volumes of tracked animals and local environmental data into a unified modeling process to improve the quality of population level inferences [4, 5, 6].

Many models have been proposed in recent years to improve animal trajectory estimation, relationships of animal movements, and home-range and land use estimates for individual animals [4, 5, 7, 8, 9, 10, 11, 12, 13, 14, 15]. However, in spite of the exceptional characteristics of these models, there is minimal development of descriptive statistical tools [16, 17, 18, 19]. Descriptive/summary statistics include the widely familiar and elementary topics in statistics and probability such as mean, median, variance, covariance, quantiles, and many others. Additionally, there is rich literature on dissimilarity measures and distance metrics that have paralleled the rise of machine learning modeling [20, 21, 22, 23]. Although a seemingly trivial topic in modern animal movement modeling, these descriptive measures are the foundation of any sound modeling process, and the appropriate construction and selection of a measure inevitably provides increased insight into the process of interest [24, 25].

The correlation coefficient is a descriptive measure used widely across all branches of statistics. A few household measures of correlation are listed here: Pearson, Spearman, Kendall [26, 27]. In information theory, a common measure of association is referred to as mutual information, which is a quantification of the amount of information obtained from the distribution of a random variable by observing another random variable [28]. Although correlation measures are often abused or "over-interpreted," they can be thought of as a measure of similarity/dissimilarity between observations or variables in a dataset [24, 29].

The use of information theoretic measures in movement ecology has modestly increased

in recent years [30, 31, 32, 33, 34, 35, 36], and it is instructive to press forward in evaluating the merits of information theory and its role in animal movement modeling. Single, global estimations of correlation between animals are insufficient for modeling the complex relationships of animals over an extended time-period. Animals of the same or different species can have changes in the relationships of their movement as a result of mating behavior and critical resource allocation as well as seasonal and environmental changes in an ecosystem such as urbanization, deforestation, or climate change [37].

In this work, we propose a bandwidth-derived correlation function that accomplishes the following: (1) locally measures the correlation/association of the movement of two animals, (2) changes in correlation are successfully detected, (3) the measure can successfully detect complex relationships in a local domain, and (4) information about correlation in movement over a larger time-domain can be successfully inferred. The proposed correlation function is a measure of localized mutual information (LMI) using bivariate (longitudinal and latitudinal) animal position data. There is modest work in recent years in defining localized mutual information over a continuum, and the objective of this work is to construct a temporal measure of localized mutual information, thoroughly assess its qualities, and discuss the advantages and disadvantages of its implementation in movement ecology [38, 39].

We investigate the properties of the proposed LMI measure by proof and by simulation where, for a simple example, we confirm the results of an analytical (i.e. by-hand) and the implemented software solution. Several simulations are also shown afterwards to explore more complicated movement relationships. The measure has been previously implemented in a full statistical analysis of a collection of jaguars (Panthera onca) in the Pantanal Ecological Station in Brazil [40]. The measure is shown to be an effective tool for detecting shifts and spikes in animal association, and further, in the investigation of jaguar movement, the measure provides evidence of detecting animals in the same behavioral state, such as two male jaguars exhibiting similar movements in a mating season.

The simulation studies reveal several characteristics of the proposed measure of LMI

which are of important consideration for researchers who intend to study associations in animal movement and behavior or use the measure for other telemetric, GPS tracking applications, such as military or citizen transportation movements, or relationships between animals and human transportation [41]. In the Discussion Section, following the simulations, we propose one alternative measure of LMI that addresses some of the disadvantages of the currently implemented measure, and we mention other information theoretic measures that have the potential to accomplish the same task as mutual information.

3 Background

In this section, we provide brief introductions to key concepts and techniques from information theory, spline smoothing, and density estimation. The topics introduced from information theory pertain to the main focus of this dissertation, and the latter methods pertain to the application of the measure in application section of the paper.

3.1 Information Theoretic Measures

In the field of Information Theory, there are many measures that have been derived to characterize properties of one or more random variables [28]. In this section, we list only the most basic measures required to understand this work. Later in this work, we mention the ideas of *Relative Entropy* and *Total Correlation* or *Multiinformation*. They are not described in any mathematical detail, but they are relevant to future work with localized information theoretic measures.

3.1.1 Entropy

The entropy of a random variable X is the average level of information or uncertainty inherent to the potential outcomes of X. Widely referred to as Shannon's entropy, the concept is, in principle, analogous to the definition of entropy in thermodynamics [28].

Shannon's entropy of X, denoted by $H(X)$, is the expected value of the information content $I(X)$ of a variable expressed by

$$H(X) = E[I(X)] = E[-log(P(X)]. \tag{3.1}$$

The information content $I(X) = -logP(X)$ is an operator that assign a level of surprise where high probability events that can be realized from X are assigned "low surprise" values and low probability (rare) events are assigned "high surprise" values. If there are many low probability events that are possible, we expect the average level of surprise in X to be higher. Entropy can be written explicitly as

$$H(X) = -\sum_{i=1}^{n} P(x_i) log_b P(x_i) \tag{3.2}$$

where x_i correspond to the possible values of a discrete random variable. It is common practice for $b = 2, e$, or 10, and the choice of b only affects the units by which entropy is measured. For a continuous random variable, Shannon's entropy is expressed by

$$H(X) = E[-log(f(x))] = -\int_{\mathcal{X}} f(x) log(f(x)) dx \tag{3.3}$$

where $f(x)$ is the probability density function of the random variable X. Although some variables are defined with underlying continuity, the computation of entropy is achieved using unsupervised discretization strategies in order to efficiently compute $H(X)$ using Equation 3.2. This is discussed further when relevant in this work.

3.1.2 Conditional and Joint Entropy

Conditional entropy is a quantification of the amount of information needed to explain the outcome of a random variable Y given that another random variable X is known [28]. The conditional entropy of Y given X is expressed by

$$H(Y|X) = -\sum_{x\in\mathcal{X},y\in\mathcal{Y}} p(x,y)log\left(\frac{p(x,y)}{p(x)}\right). \tag{3.4}$$

If X and Y are independent, then $H(Y|X) = H(Y)$. Conversely, conditional entropy equals zero only when the value of Y is perfectly explained/determined by the value of X.

Joint entropy is the measure of uncertainty associated with two or more variables. Also referred to as the joint Shannon entropy, it can be expressed for two random variables X and Y by

$$H(X,Y) = -\sum_{x\in\mathcal{X}}\sum_{y\in\mathcal{Y}} p(x,y)log(p(x,y)). \tag{3.5}$$

There are many important properties of all measures of entropy that tie back to the properties of *information*, $I(p)$. For an event with probability p, $I(p)$ has a domain of $p \in (0,1]$. The following properties hold:

1. $I(p)$ monotonically decreases as the probability, p, occurring increases.
2. $I(p)$ is non-negative.
3. If $p = 1$, then $I(p) = 0$. Certain events do not contain information.
4. Independent events, with p_1 and p_2 provide summative information. $(I(p_1 \cdot p_2) = I(p_1) + I(p_2))$.

3.1.3 Mutual Information

Mutual information is a measure of mutual dependence or association between two random variables X and Y, and it is a measure of the amount of information, measured in the same units as entropy, obtained about one variable by observing another. Up until this point, we have used I to denote the *information content*. However, in standard Information Theory notation, mutual information is also defined with the symbol I; the only difference that distinguishes the two is that mutual information is an operator that accepts two random variable inputs as opposed to one. The mutual information, I, of two jointly discrete random variables X and Y is expressed by

$$I(X,Y) = \sum_{y\in\mathcal{Y}}\sum_{x\in\mathcal{X}} p_{(X,Y)}(x,y) log\left(\frac{p_{(X,Y)}(x,y)}{p_{(X)}(x)p_{(Y)}(y)}\right), \tag{3.6}$$

where $p_{(X,Y)}$ is the joint probability mass function (pmf) of X and Y and p_X and p_Y are their respective marginal distributions. Subscripts have been introduced on the all pmfs starting in this section to ensure that the formula consisting of variables for differing pmf and the joint pmf are clearly labeled. The intuition behind the construction of this measure rests in the concept of the magnitude of independence/dependence between two random variables. If X and Y are perfectly independent, then observing either X or Y does not provide any information about the other variable. In Equation 3.6, if X and Y are independent, then equation becomes

$$I(X,Y) = \sum_{y\in\mathcal{Y}}\sum_{x\in\mathcal{X}} p_{(X,Y)}(x,y) log\left(\frac{p_{(X)}(x)p_{(Y)}(y)}{p_{(X)}(x)p_{(Y)}(y)}\right) = \sum_{y\in\mathcal{Y}}\sum_{x\in\mathcal{X}} p_{(X,Y)}(x,y) log(1) = 0. \tag{3.7}$$

Mutual information can be shown to be nonnegative and symmetric measure ($I(X,Y) \geq 0$, and $I(X,Y) = I(Y,X)$) [28]. Mutual information is directly related to joint and conditional entropy, and it is practical to use this relationship to study properties of mutual information. Mutual information is the amount of entropy remaining in a variable, X, after

subtraction that amount of entropy from the same variable given that another variable, Y, was known. By symmetry of the measure and the properties of entropy, mutual information can be expressed in a number of useful forms given in the next steps of work:

$$I(X,Y) = H(X) - H(X|Y) \tag{3.8}$$

$$I(X,Y) = H(Y) - H(Y|X) \tag{3.9}$$

$$I(X,Y) = H(X) + H(Y) - H(Y,X) \tag{3.10}$$

3.2 Smoothing Splines

In the environmental sciences, among many other applications, many processes are observed which are continuous spatially or evolve/change over time in a continous manner. Many of these processes may also have an underlying smoothness which is theorhetically understood, but when empirically measured, the smoothness is lost to (white) noise, random variation, instrumentation error/insensitivity, and gaps in spatial or temporal domain measurements. All of these natural outcomes from empirical data collection can potentially obscure the underlying process which is of interest to study.

Smoothing splines are estimated functions, denoted generally by $\hat{f}(t)$, are obtained from empirical (discretely and often non-uniformly measured) observations y_i where t the spatial or temporal grid on which observations are measured/recorded. They are used to estimate a target $f(t_i)$. Cubic (polynomial) splines are a common choice for many smoothing problems. We briefly outline the general smoothing problem objective function here. More details of the implemented smoothing spline procedure can be found in the *Smoothing Splines of Apex Predator Movement* chapter of this dissertation.

Let (t_i, y_i) with $i = 1, \ldots, n$ be a set of observations which are realization from a random variable Y on a temporal or spatial grid T. These observations are assumed to be modeled by $y_i = f(t_i) + \epsilon_i$ where f is the continuous, differentiable function we are trying to estimate

and ϵ_i are an unknown, independent error term that is "concealing" the process that we are observing only by the raw data, y_i. Generally, it is assumed that ϵ_i has an expected value of zero and has constant variance. This could be violated in cases where some instrumentation is known to have error which has substantial bias or is know to have larger error under some regularly or irregularly occurring conditions while the process is observed.

The cubic smoothing spline estimate $\hat{f}$ of the function f is defined to be the minimizer of

$$\sum_{i=1}^{n}\{y_i - \hat{f}(t_i)\}^2 + \lambda \int \hat{f}''(t_i)^2 dx, \tag{3.11}$$

where $\hat{f}$ is assumed to be twice differentiable, $\lambda \geq 0$ is a smoothing parameter that penalizes the roughness of the estimated function [42, 43]. As $\lambda \to \infty$, all roughness is eliminated from $\hat{f}$ and the estimate converges to a linear least squares estimate through the data y_i. As $\lambda \to 0$, $\hat{f}$ converges to an exact spline interpolation of the raw data. Clearly, in a smoothing application, neither of these are ideal scenarios since a strict interpolation will yield extremely noisy functions with poor differential properties, and linear functions "wash out" all functional features such as local maximia, minima, periodicity, non-monotonicity etc. There are multiple strategies for defining and optimizing a smoothing spline, and we largely follow Ramsay and Silverman's outline of roughness-penalty smoothing spline optimization [42, 43, 45, 44, 46].

3.3 Kernel Density Estimation

Kernel density estimation (KDE) is a nonparametric method used to acquire an estimate of a probability density function of a random variable. The fundamental objective of KDE is interrelated/inseparable from those found in smoothing splines problems since the estimation of a probability density function required the estimation of a smoothed pdf from finitely (and possibly noisy) sampled data.

Let $\{t_i | i = 1, \ldots, n\}$ be independent and identically distributed samples, given by points t_i, drawn from a univariate distribution with an unknown density, f. The shape of the distribution, denoted by f, has a KDE expressed by

$$\hat{f}(t) = \frac{1}{n} \sum_{i=1}^{n} K_h(t - t_i) = \frac{1}{nh} \sum_{i=1}^{n} K\left(\frac{t - t_i}{h}\right), \tag{3.12}$$

where K is the kernel which is a non-negative function, K_h is referred to as the scaled kernel defined $K_h = 1/hK(x/h)$ [62]. Similar to smoothing splines, $h > 0$ is a smoothing parameter called the bandwidth. Many kernel functions can provide appropriate estimates of f but the Gaussian/normal kernel $K(t) = \Phi(t)$ is most often used. Ultimately, KDE is the sum of several (generally identical) functions (kernels) that are each localized around a respective t_i, and the "width of influence" of each function is restricted by h.

4 Author's Note

Prior to the drafting of this dissertation, the application section of this paper entitled *Smoothing Splines of Apex Predator Movement: Functional Modeling Strategies for Exploring Animal Behavior and Social Interactions* has been published [40]. Although improvements to the measure implemented in this paper are proposed later in this work, it is instructive to verify properties of the original measure.

In this work, we add some additional details to the application section, specifically a sensitivity assessment justifying the automatic density-based knot placement technique used to smooth jaguar trajectories.

5 Localized Mutual Information

Consider bivariate vectors $X = (X_1, X_2)$ and $Y = (Y_1, Y_2)$ which define the movement paths, X and Y, of two animals. The pair of variables (X, Y) have values over the space $\mathcal{X} \times \mathcal{Y}$ where X_1 and Y_1 are vectors corresponding to the longitudinal position of the animals on

a unified time grid, and X_2 and Y_2 correspond similarly for the latitudinal position. In this section, we construct the definition of LMI from the respective latitude and longitude components.

The components of LMI, $I_{\mathcal{L}_i}(X_j, Y_j|\lambda)$ with $j = 1,\ 2$, are a measure of localized mutual information for the j^{th} directional component defined by

$$I_{\mathcal{L}_i}(X_j, Y_j|\lambda) = \sum_{x \in \mathcal{X}_{j\mathcal{L}_i}} \sum_{y \in \mathcal{Y}_{j\mathcal{L}_i}} p_{(X_j,Y_j)}(x,y)\ log \frac{p_{(X_j,Y_j)}(x,y)}{p_{X_j}(x) p_{Y_j}(y)} dxdy \ \text{ for } \ j = 1, 2.$$

The restriction of the mutual information to the localized neighborhood is given by the space $\mathcal{X}_{j\mathcal{L}_i} \times \mathcal{Y}_{j\mathcal{L}_i}$. This is a restriction of the domain of X, Y to their respective probability density functions on the time domain defined by $\mathcal{L}_i$. In our work, we define $\mathcal{L}_i = \{t|t \in [t_{i-\lambda}, t_{i+\lambda}]$, where $\mathcal{L}_i$ is a collection of time points, $\{t\}$, that mark the timing of observations of X and Y. The value λ, also referred to as the bandwidth (bw), is an integer value that defines the local collection time points $\{t\}$ that surround the i^{th} time point, t_i.

A joint measure of mutual information, $\mathbb{I}_{\mathcal{L}_i}$, can be constructed from the directional components as follows:

$$\mathbb{I}_{\mathcal{L}_i}(X, Y|\lambda) = \sqrt{I_{\mathcal{L}_i}(X_1, Y_1|\lambda)^2 + I_{\mathcal{L}_i}(X_2, Y_2|\lambda)^2}$$

.

To construct the final LMI measure, we compute the mutual information, $\mathbb{I}_{\mathcal{L}_i}$, at every available time point t_i for the local neighborhood defined by $t \in [t_{i-\lambda}, t_{i+\lambda}]$. The bandwidth, chosen by the user, must be considered with knowledge of the application of interest. The proposed measure of LMI is then defined by

$$\mathcal{I}(t; \lambda) = \mathbb{I}_{\mathcal{L}_i}(X, Y|\lambda) \ \text{ with } \ \mathcal{L}_i = \{t|t \in [t_{i-\lambda}, t_{i+\lambda}]\}.$$

5.1 General Properties

The LMI measure $\mathcal{I}(t;\lambda)$ is expected to carry many of the properties of a global measure of mutual information. Namely, in this section, we verify the non-negativity of the measure and the monotonicity of the relationship between LMI and a correlation coefficient ρ. Ultimately, it is of interest to ensure that any derived measure of association is on a scale that is comparable to a standard correlation coefficient, and further that the measure behaves similarly on such as scale.

Property 1: $\mathcal{I}(t;\lambda)$ is nonnegative (i.e. $\mathcal{I}(t;\lambda) \geq 0$).

Since the mutual information of any collection of realizations is positive, it follows that $I_{\mathcal{L}_i}(X,Y) \geq 0$. More importantly, for any $a, b \in \mathbb{R}$, it follows that $\sqrt{a^2+b^2} \geq 0$. Therefore, it is clear that $\mathcal{I}(t;\lambda) = \mathbb{I}_{\mathcal{L}_i}(X,Y|\lambda) \geq 0$.

Proposition 1: $\mathcal{I}(t;\lambda)$ is symmetric.

It is sufficient to show that $\mathbb{I}_{\mathcal{L}_i}(X,Y|\lambda) = \mathbb{I}_{\mathcal{L}_i}(Y,X|\lambda)$. Since $I_{\mathcal{L}_i}(X_1,Y_1|\lambda) = I_{\mathcal{L}_i}(Y_1,X_1|\lambda)$ and $I_{\mathcal{L}_i}(X_2,Y_2|\lambda) = I_{\mathcal{L}_i}(Y_2,X_2|\lambda)$ for any $\mathcal{L}_i$, it is clear that $\sqrt{I_{\mathcal{L}_i}(X_1,Y_1|\lambda)^2 + I_{\mathcal{L}_i}(X_2,Y_2|\lambda)^2} = \sqrt{I_{\mathcal{L}_i}(Y_1,X_1|\lambda)^2 + I_{\mathcal{L}_i}(Y_2,X_2|\lambda)^2}$. Therefore, $\mathbb{I}_{\mathcal{L}_i}(X,Y|\lambda) = \mathbb{I}_{\mathcal{L}_i}(Y,X|\lambda)$, and $\mathcal{I}(t;\lambda)$ is symmetric $\forall \mathcal{L}_i$. $\square$

Proposition 2: As the linear correlation coefficient of normally distributed X and Y increases, then $\mathcal{I}(t;\lambda)$ increases ($\uparrow$).

Proof: It is sufficient to show that the proposition holds for any $\mathcal{L}_i$ in the time domain $\mathbb{T}$. In other words, for any $\mathcal{L}_i$, it must be shown that as the correlation coefficients for either directional component increase then $\mathbb{I}_{\mathcal{L}_i}(X,Y) \uparrow$.

It is known that the mutual information between two vectors X and Y on an interval $\mathcal{L}_i$ can be expressed by $I_{\mathcal{L}_i}(X,Y) = H_{\mathcal{L}_i}(X) + H_{\mathcal{L}_i}(Y) - H_{\mathcal{L}_i}(X,Y)$. For a continuous random variable, X, subsetted to the realizations on the domain $\mathcal{L}_i = \{t|t \in [t_{i-\lambda}, t_{i+\lambda}]\}$, Shannon's entropy is defined by $H_{\mathcal{L}_i}(X) = -\int_{\mathcal{X}_{\mathcal{L}_i}} f(x)\ln f(x)dx$ [28]. Assume that $X \sim N(0,1)$ and $Y \sim N(0,1)$. We define association here as an increase in the linear correlation coefficient ρ

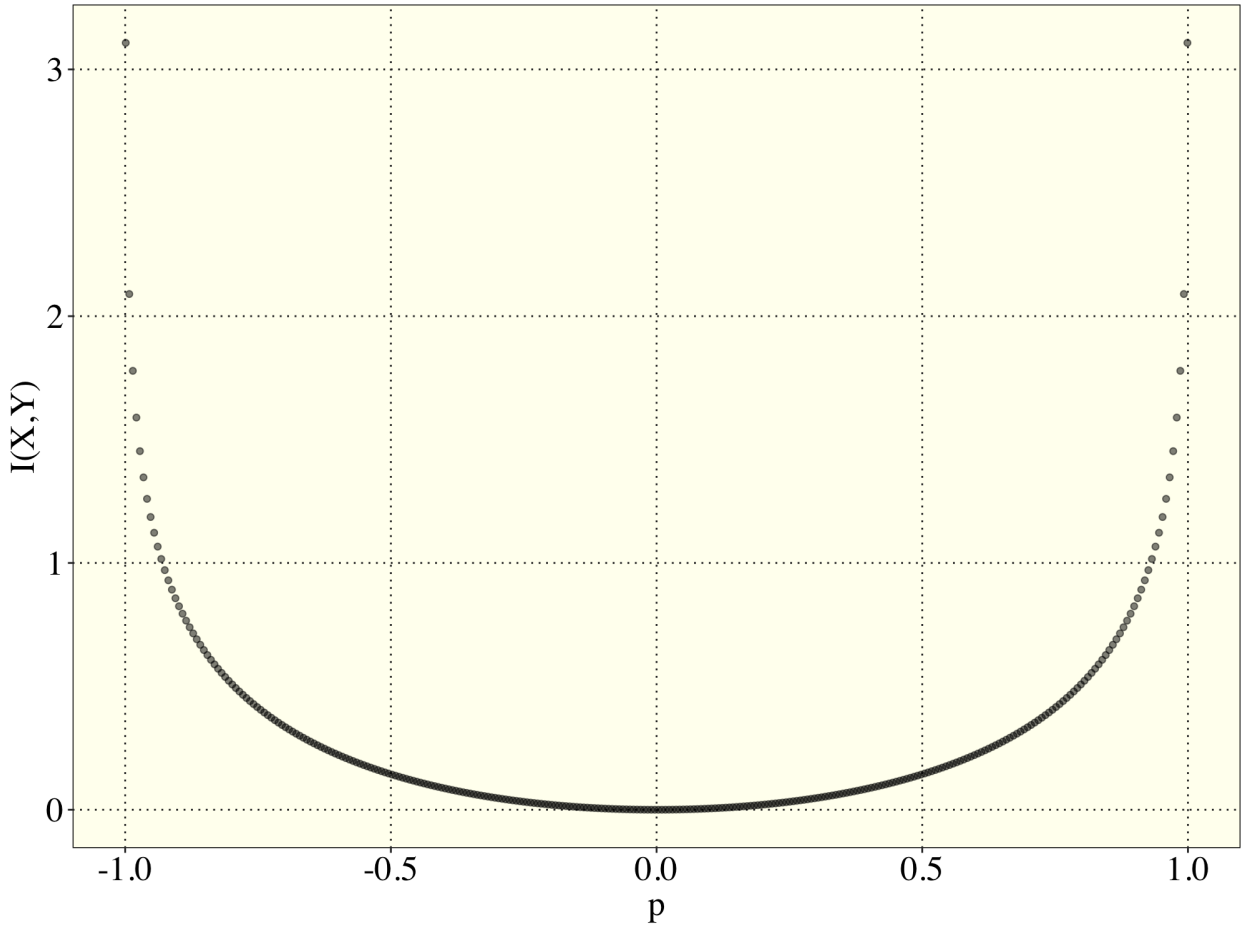

Figure 5.1: The relationship between mutual information and the correlation coefficient, ρ, for normally distributed X, Y using a 300 equally spaced values of $\rho \in (-1, 1)$

between two random variables. Then it follows that

$$\begin{cases} H_{\mathcal{L}_i}(X) = \frac{1}{2} log 2\pi e \\ H_{\mathcal{L}_i}(Y) = \frac{1}{2} log 2\pi e \\ H_{\mathcal{L}_i}(X,Y) = \frac{1}{2} log((2\pi e)^2(1-\rho^2) \end{cases},$$

where ρ is the correlation coefficient between X and Y [28, 47]. It follows that

$I_{\mathcal{L}_i}(X,Y) = \frac{1}{2} log 2\pi e + \frac{1}{2} log 2\pi e - \frac{1}{2} log((2\pi e)^2(1-\rho^2))$

$I_{\mathcal{L}_i}(X,Y) = -\frac{1}{2} log(1-\rho^2)$.

Refer to Figure 5.1 for a visual of the relationship between ρ and mutual information. It

is clear that $\lim_{\rho \to 1} -\frac{1}{2} log(1-\rho^2) = +\infty$, $\lim_{\rho \to -1} -\frac{1}{2} log(1-\rho^2) = +\infty$, and

$\lim_{\rho \to 0} -\frac{1}{2} log((1-\rho)^2) = -\frac{1}{2} log(1) = 0$.

In the remainder of the proof, we do not address what happens to $\mathbb{I}_{\mathcal{L}_i}$ if ρ_1 or ρ_2 decreases while the other increases. There is clearly a competing effect on $\mathbb{I}_{\mathcal{L}_i}$ and since the process of interest is 2 dimensional, it is not clear that there is a increase in overall correlation across all directional components unless the correlation of both or at least one increases while the other is fixed.

Since $I_{\mathcal{L}_i}$ is monotonic on $[-1, 0)$ and $I_{\mathcal{L}_i}$ is monotonic on $(0, 1]$, it follows that as $|\rho| \uparrow$, then $I_{\mathcal{L}_i} \uparrow$. If $X = (X_1, X_2)$ and $Y = (Y_1, Y_2)$, then

$\mathbb{I}_{\mathcal{L}_i}(X, Y|\lambda) = \sqrt{I_{\mathcal{L}_i}(X_1, Y_1)^2 + I_{\mathcal{L}_i}(X_2, Y_2)^2} = \sqrt{(-\frac{1}{2} log(1-\rho_1^2))^2 + (-\frac{1}{2} log(1-\rho_2^2))^2}$.

Then if $|\rho_1| \uparrow$ or $|\rho_2| \uparrow$ while the other remains fixed, then $\mathbb{I}_{\mathcal{L}_i}(X, Y|\lambda) \uparrow$. Since $\mathcal{L}_i$ is an arbitrary window within $\mathbb{T}$, then this holds for any $\mathcal{L}_i$ as defined by the pair $(t_i, \mathcal{L}_i)$. □

Although not examined in the proof of Proposition 3, it is important to emphasize that $X \sim N(0, 1)$, $Y \sim N(0, 1)$, and the integration of their respective pdfs assumes continuity when in the actual estimation pdf's empirically, this is computed by discretizing each pdf to a pmf.

Boundary Value Condition:

The most apparent concern with the boundary cases for a bandwidth derived measure is the decreasing size of available samples of position with the bandwidth $\mathcal{L}_i$. If no boundary condition is coerced on $\mathcal{I}(t|\lambda)$, then at t_0, $\mathcal{L}_i = \{t|t \in [t_0, t_{i+\lambda}]\}$ and at t_f, $\mathcal{L}_i = \{t|t \in [t_{i-\lambda}, t_f]\}$ where t_0 and t_f correspond to the first and last position of an animal detected or estimated. In this work, we set $\mathcal{L}_i$ for all *near boundary* t_i according to the following condition. If $t_{i-\lambda} < t_0$, then $\mathcal{L}_i = \{t|t \in [t_0, t_{0+2\lambda}]\}$. If $t_{i+\lambda} > t_f$, then $\mathcal{L}_i = \{t|t \in [t_{f-2\lambda}, t_f]\}$. This boundary condition coerces every time point t_i to have equal size $\mathcal{L}_i$, where any of the *near boundary* t_i all have the same LMI. This is done to ensure that the boundaries of the time domain are well-behaved. A reduction in the sample of observed times will have a direct effect on the computed LMI which is not of direct interest.

For many GPS-derived animal movement applications the sampled locations of an animal are densely recorded over extended time periods, and the number of t_i that this affects is minimal for most considered bandwidths, λ.

Violation of the Distance Metric Properties:

With any measure of dissimilarity, it is important to assess if the measure meets the requirements to be classified as a distance metric. It is known that mutual information is not a distance metric as it violates the triangle inequality $I(X,Z) \leq I(X,Y) + I(Y,Z)$ [28]. However, more simply, a distance metric d must satisfy $d(X,Y) = 0$ when $X = Y$. For mutual information this is clearly violated since $I(X,Y) \neq 0$ when $X = Y$. (In simpler terms, LMI is not equal to zero for two animals when they are the same animal.)

As $I(X,Y)$ unbounded in the positive direction, it would be natural to consider inverting a scaled version of the measure so that a measure of zero identifies two objects that are close and a measure of 1 identifies objects that are far apart. It can also be shown with a few steps of mathematics that taking a measure defined by $d(X,Y) = 1 - I^*(X,Y)$ is not a distance metric (where I^* is the mutual information between X and Y scaled by the maximum possible mutual information defined by $I^*(X,Y) = \frac{I(X,Y)}{I(X,X)}$). Here it is now clear that $d(X,Y) = 0$ when $X = Y$, but we show the violation of the triangle inequality in Appendix A1 7.1.

If the properties of a distance metric are desired, an alternative information theoretic measure of association, referred to as *relative entropy* can be implemented. It does not violate the triangle inequality [28], and as such the entirety of work could be defined and assessed similarly using relative entropy. Going forward, we continue to refer to mutual information as a measure of dissimilarity as opposed to a measure of distance (i.e. a distance metric).

5.2 Simulation Studies

In order to investigate the advantages and disadvantages of the proposed measure, it is instructive to generate simulations with known global mutual information and/or known associative structure over periods of constant behavior and report the LMI computed over these regions and those of transitioning behavior. More specifically, the sensitivity of the measure to the choice of bandwidth, λ, the number of bins (or simply bins) used to discretize a pmf for the movement paths over any $\mathcal{L}_i$, and the signal-to-noise ratio are the parameters of primary interest. The distance between the position of animals is of secondary interest, but is implicitly investigated here as well.

In the construction of simple movement simulations, we consider scenarios where LMI is both ideal and non-ideal, and a discussion of how to handle the non-ideal scenarios follows. Six simulation scenarios are investigated:

1. Simulation 1: A "Dead or Alive" movement model where mutual information is feasibly derived by hand for verification of measure.

2. Simulation 2: A "Shift-Sensitivity" model where global mutual information is known for a period of strong association and a period of lower association.

3. Simulation 3: "Cross-directional Relationship" detection where one animal's latitudinal movement has a strong relationship with the other animal's longitudinal movement while a weak relationship exists between their matching directional movements.

4. Simulation 4: Delayed Onset/Following Behaviors where one animal follows the movement of the other.

5. Simulation 5: "Resolution Challenges" where the bandwidth and pdf discretization parameter sensitivity are examined in the presence of Brownian movement, and low versus high temporal resolution.

6. Simulation 6: A random walk simulation of male-female jaguar relationships [40].

In all simulations, the choice of bandwidth, λ, will be investigated, and in the other simulations, bins, and the signal-to-noise ratio will be examined at an array of values. The relevance of each of the movement behaviors is discussed in more detail in each of the following sections.

5.2.1 Template code for Simulations

All simulations use the same generic format outlined in this section. In the simplest terms, the simulations are performed by generating a uniform time vector and then selecting a function or set of functions for the latitudinal and longitudinal components of each animals movement. Figure 5.2 shows the general pseudo code template used for all simulations. In some of the later simulations minor deviations from this procedure were implemented to induce more complicated attributes such as autocorrelated random errors to induce random walk movement trajectories.

5.2.2 Simulation 1: Analytical Verification of LMI

The objective of our preliminary simulation is to verify and provide further insight into the mechanics of the proposed LMI measure. In this simulation $T_1, T_2,$ and T_3 mark the start, middle, and end of the simulation. In a 2-dimensional space, two of the simplest scenarios that can be examined are when two animals have identical linear movement, or when one animal moves constantly while the other animal is stationary. The sudden halting movement behavior could characterize a resting, critically injured, or deceased animal. The transition in the behavior on one animal will occur at T_2. The simulation visualized and evaluated in this section combines both of these simple scenarios into one to explore the transition properties of LMI.

In Figure 5.3, we outline the analytical checks visually that are performed on LMI for

Pseudo-code for Simulations

Step 1:

- Generate a uniform time vector $\overrightarrow{t}$.
- Instantiate vector of random errors $\epsilon_{lat1}(t)$, $\epsilon_{lon1}(t)$, $\epsilon_{lat2}(t)$, $\epsilon_{lon2}(t)$ for each component with a specified distribution.

Step 2:

- Select $f_{lat1}(t)$, $f_{lon1}(t)$, $f_{lat2}(t)$, $f_{lon2}(t)$.
- Then compute position functions $s_{lat1}(t)$, $s_{lon1}(t)$, $s_{lat2}(t)$, $s_{lon2}(t)$:

$$s_{lat1}\left(\overrightarrow{t}\right) = f_{lat1}\left(\overrightarrow{t}\right) + \epsilon_{lat1}\left(\overrightarrow{t}\right)$$
$$s_{lon1}\left(\overrightarrow{t}\right) = f_{lon1}\left(\overrightarrow{t}\right) + \epsilon_{lon1}\left(\overrightarrow{t}\right)$$
$$s_{lat2}\left(\overrightarrow{t}\right) = f_{lat2}\left(\overrightarrow{t}\right) + \epsilon_{lat2}\left(\overrightarrow{t}\right)$$
$$s_{lon2}\left(\overrightarrow{t}\right) = f_{lon2}\left(\overrightarrow{t}\right) + \epsilon_{lon2}\left(\overrightarrow{t}\right).$$

Step 3: For every $t_i \in \overrightarrow{t}$ the following is computed recursively for each directional component separately:

- (i) Discretize the spatial domain using standard binning procedure: “Equal width”, “Global Equal Width,” or “Equal Frequency” binning.
- (ii) Compute the probabilities of observing a coordinate in each bin.
- (iii) Compute Marginal and joint Shannon’s entropy for each trajectory component:
  Ex: $H(s_{lat1})$, $H(s_{lat2})$, $H(s_{lat1}, s_{lat2})$
- (iv) Compute the directional components of LMI:
  $I_{\mathscr{L}_i}(s_{lat1}, s_{lat2}) = H(s_{lat1}) + H(s_{lat2}) - H(s_{lat1}, s_{lat2})$ and
  $I_{\mathscr{L}_i}(s_{lon1}, s_{lon2}) = H(s_{lon1}) + H(s_{lon2}) - H(s_{lon1}, s_{lon2})$
- (v) and subsequently compute $\mathbb{I}_{\mathscr{L}_i} = \sqrt{I_{\mathscr{L}_i}(s_{lat1}, s_{lat2})^2 + I_{\mathscr{L}_i}(s_{lon1}, s_{lon2})^2}$.

Figure 5.2: Code outline for the simulation generation procedure.

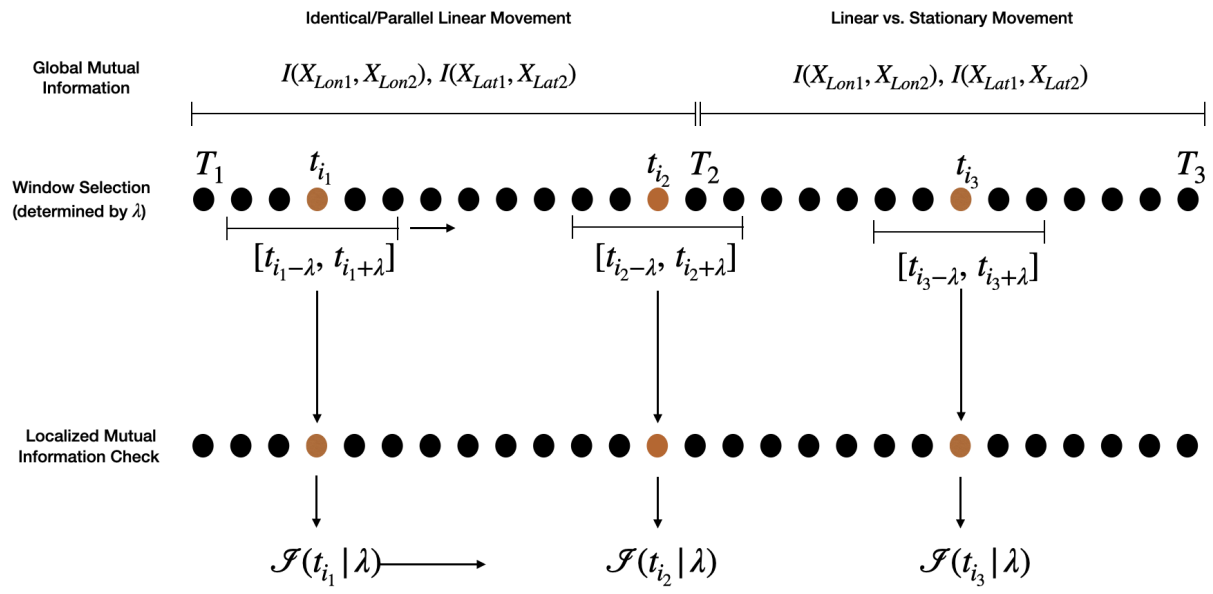

Figure 5.3: Summary of Analytical Verification of LMI Measure. The verification consists of measuring standard/global measure of mutual information from (T_1, T_2) and (T_2, T_3) respectively. LMI is also confirmed for localized regions completely contained with (T_1, T_2) and (T_2, T_3) and also for a localized region containing T_2 where there is at least 1 point on a uniform time grid in both (T_1, T_2) and (T_2, T_3). The trajectories of the animals in (T_1, T_2) are identical/parallel linear movements, and in (T_2, T_3) animal 2 is stationary while the other continues as before.

this simulation. First, we confirm the global/standard mutual information (GMI) for each of the two states of the simulation. Then we compute LMI analytically for three time points: (1) $t_{i_1} = t_i$ with $(t_{i-\lambda}, t_{i+\lambda}) \subset (T_1, T_2)$, (2) $t_{i_2} = t_i$ with $T_2 \in (t_{i-\lambda}, t_{i+\lambda})$, and (3) $t_{i_3} = t_i$ with $(t_{i-\lambda}, t_{i+\lambda}) \subset (T_2, T_3)$.

After manually computing these values for LMI and GMI, we overlay these results with the implemented code of the measure, and discuss why subtle or substantial differences exist.

This simulation model for the first animal is defined by

$$\begin{cases} x(t_i) = t_i - 0.05 + \epsilon_{t_i} & t_i \in [0, 1] \\ y(t_i) = t_i + \epsilon_{t_i} \end{cases},$$

and for the second animal

$$\begin{cases} x(t_i) = t_i + 0.05 + \epsilon_{t_i} & t_i \in [0, 0.5) \\ y(t_i) = t_i + \epsilon_{t_i} & \\ x(t_i) = 0 + x(t_i = 0.5) + \epsilon_{t_i} & t_i \in (0.5, 1.0] \\ y(t_i) = 0 + y(t_i = 0.5) + \epsilon_{t_i} & \end{cases}.$$

To increase the simplicity of this model for analytical verification, the random error term is set to 0. In most simulations following this section, the error term is assumed to be independent and identically distributed. Intuitively, it is expected that if two animals move with the exact same behavior with no noise induced into the process, a perfect association in their movements will be detected. It also follows intuition that there should be no association in the movement of two animals if one animal is motionless and the other is moving with a clearly defined functional behavior.

Computing GMI and LMI

Recall from Equation 3.8 that

$$I(X_1, X_2) = H(X_1) + H(X_2) - H(X_1, X_2). \tag{5.1}$$

Until defined otherwise in this section, X_1 and X_2 denote only the latitudinal movement. Since any LMI component measure with a local neighborhood completely contained in (T_1, T_2) or (T_2, T_3) is identical to the GMI on these intervals (with a subset of points), we only need to compute $I(X_1, X_2)$ at (T_1, T_2), (T_2, T_3) to verify the LMI in these regions. We compute LMI at T_{i_2} by determining the proportion of points in the window $[t_{i-\lambda}, t_{i+\lambda}]$ on either side of T_2.

Computing LMI, which is ultimately a combination of latitudinal and longitudinal movement, is done by each component respectively. Until the end of this section, we only show latitudinal calculations. The combination of latitudinal and longitudinal calculations are

shown as the final step. Since the movement of each animal is constant or stationary, the discretized densities (pmfs) are uniformly distributed across each "bin." Bins, where N is used to denote the number of bins, are the terms used to describe the discretization or "binning" of locations into groups based on proximity. The pmfs are defined by

$$(T_1, T_2) \rightarrow p_{X_1}(x_1) = p_{X_2}(x_2) = 1/N, \quad p_{X_1,X_2}(x_1, x_2) = 1/N \tag{5.2}$$

$$(T_2, T_3) \rightarrow p_{X_1}(x_1) = 1/N, \quad p_{X_2}(x_2) = 1, \quad p_{X_1,X_2}(x_1, x_2) = 1/N \tag{5.3}$$

The simplicity of the marginal and joint pmfs listed above is visualized in Figure 5.4 which illustrates the discretization process of this movement model. In Figure 5.4, blue and red squares identify the discretized location of animal 1 and animal 2 respectively, and the yellow circles mark the starting and end locations for each animal as well as the location where the shift in animal association occurs. The latitudinal behavior modeled here is identical to the constructed models where animal 1's position is uniformly distributed within each blue square and animal 2's position is likewise, but all red squares from $t \in [T_2, T_3]$ are stacked in the same region. When computing the GMI for the time periods $[T_1, T_2]$ and $[T_2, T_3]$, the summation of the pmf's in the entropy components of the equation for mutual information consist of summing $N = 5$ squares (since 5 squares fall in each time period). Since the locations are uniformly distributed into each of the 5 bins shown in this visual, then it is clear that $p_{X_1}(x_1) = p_{X_2}(x_2) = 1/N$ for (T_1, T_2). On (T_2, T_3), it is clear for Animal 2 that all locations are in the same bin, so the pmf is singular $p_{X_2}(x_2) = 1$.

The joint pmfs for longitude can also be visually understood from Figure 5.4. The image is simplified in Figure 5.5 to avoid ambiguity. Although there are N^2 potential bins for the locations to be distributed across, the positions in this simulation fall into only N bins on each time window so the probability of the observing both animals in a single bin is $1/N$.

By Equation 3.8 and following the notation from the Background Section, we compute each of the entropy components at the same time, and then combine the results afterwards

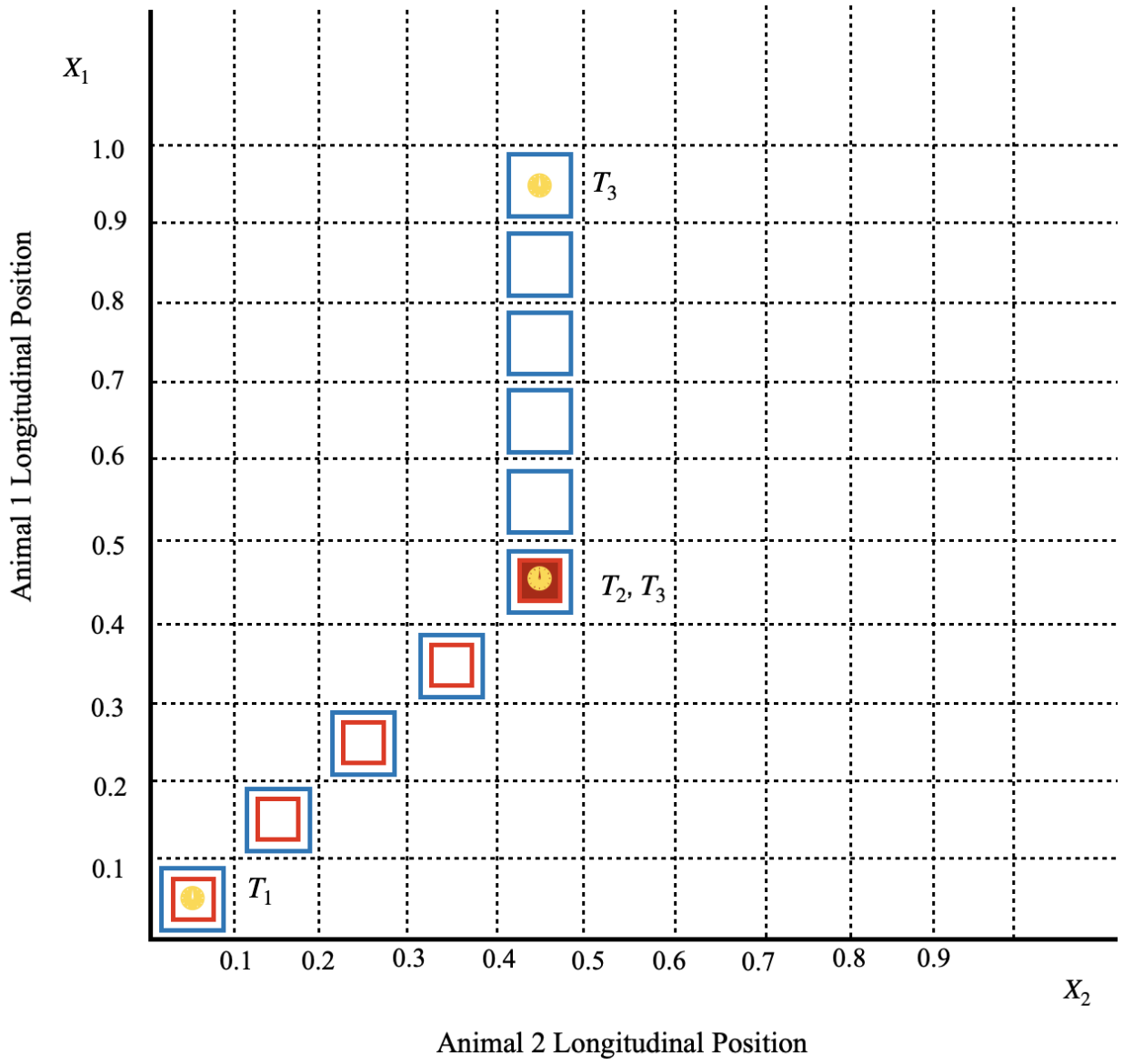

Figure 5.4: Longitudinal Movement of Both Animals discretized on a 0.1 resolution. Yellow circles denote the start and end time locations of the simulation as well as the time of the shift in behavior association.

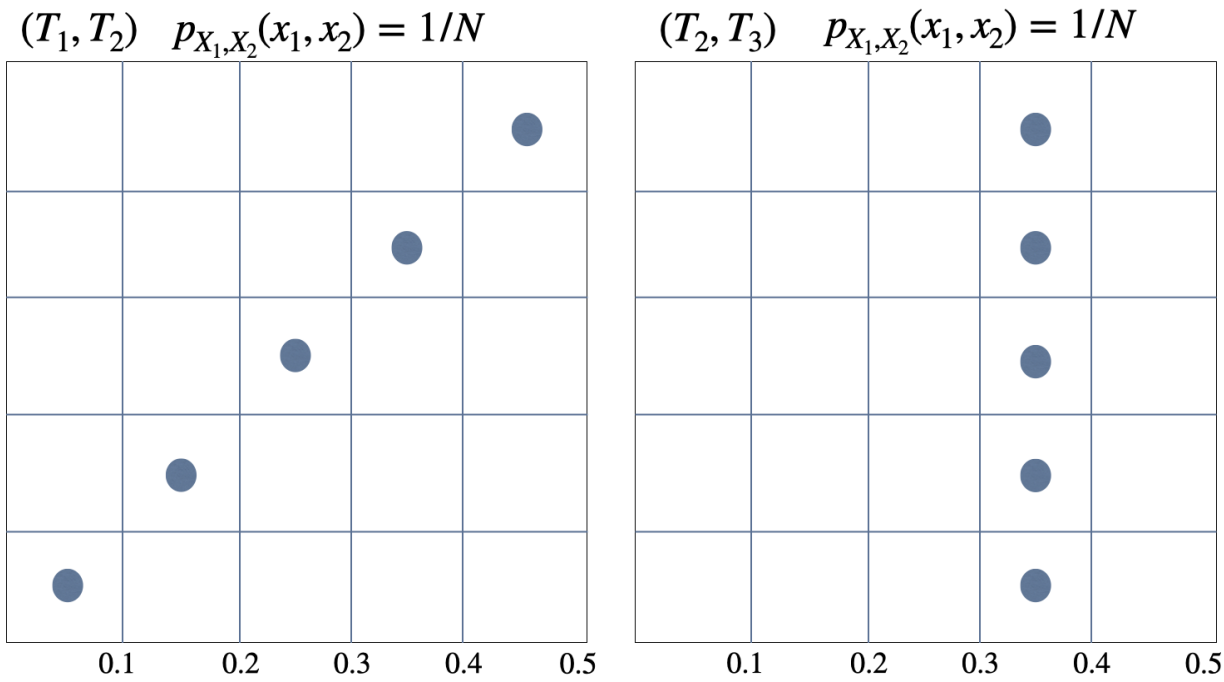

Figure 5.5: Joint Distribution Longitudinal Movement of Both Animals discretized on a 0.1 resolution with $N = 5$. In both time windows, the longitude is uniformly distributed across 5 bins. For simplicity, the vertical axis is not labeled here.

to report mutual information.

$$(T_1, T_2) \qquad H(X_2) = -\sum p_{X_2}(x_2) log\ p_{X_2}(x_2) = -\sum_{i=1}^{N} 1/N\ log(1/N) = log(N) \quad (5.4)$$

$$(T_2, T_3) \qquad H(X_2) = -\sum_{i=1}^{N} 1\ log(1) = 0 \quad (5.5)$$

$$t_{i_2} \qquad H(X_2) = -\left(\sum_{i=1}^{q*N} 1/N\ log(1/N) + \sum_{q*N+1}^{N} 1 log(1)\right) = q\ log(N), \quad (5.6)$$

where q is the proportion of time points that are in the time period (T_1, T_2).

Similarly,

$$(T_1, T_2) \qquad H(X_1) = -\sum p_{X_1}(x_1) log\ p_{X_1}(x_1) = -\sum_{i=1}^{N} 1/N\ log(1/N) = log(N) \quad (5.7)$$

$$(T_2, T_3) \qquad H(X_1) = -\sum_{i=1}^{N} 1/N\ log(1/N) = log(N) \quad (5.8)$$

$$t_{i_2} \qquad H(X_1) = -\sum_{i=1}^{N} 1/N\ log(1/N) = log(N) \quad (5.9)$$

Recall that joint entropy of X_1 and X_2 is expressed by

$$H(X_1, X_2) = -\sum_{x_1 \in \mathcal{X}_1} \sum_{X_2 \in \mathcal{X}_2} p_{X_1,X_2}(x_1, x_2) log(p_{X_1,X_2}(x_1, x_2). \quad (5.10)$$

It follows from Figure 5.5, that half of the bins (of equal width) would be characterized with a joint pmf similar to the left hand image and the other half would be similar to the right hand image. This is shown in Figure 5.6 . It is clear that the joint pmf for a local domain in this region is still $p_{X_1,X_2}(x_1, x_2) = 1/N$. Therefore, the double summation can be simplified to a single summation for each time expressed by

$$(T_1, T_2) \qquad H(X_1, X_2) = -\sum_{i=1}^{N} 1/N log(1/N) = log(N) \quad (5.11)$$

$$(T_2, T_3) \qquad H(X_1, X_2) = -\sum_{i=1}^{N} 1/N\ log(1/N) = log(N) \quad (5.12)$$

$$t_{i_2} \qquad H(X_1, X_2) = -\sum_{i=1}^{N} 1/N\ log(1/N) = log(N) \quad (5.13)$$

Finally, combining all the entropy calculations, we have the following calculations for

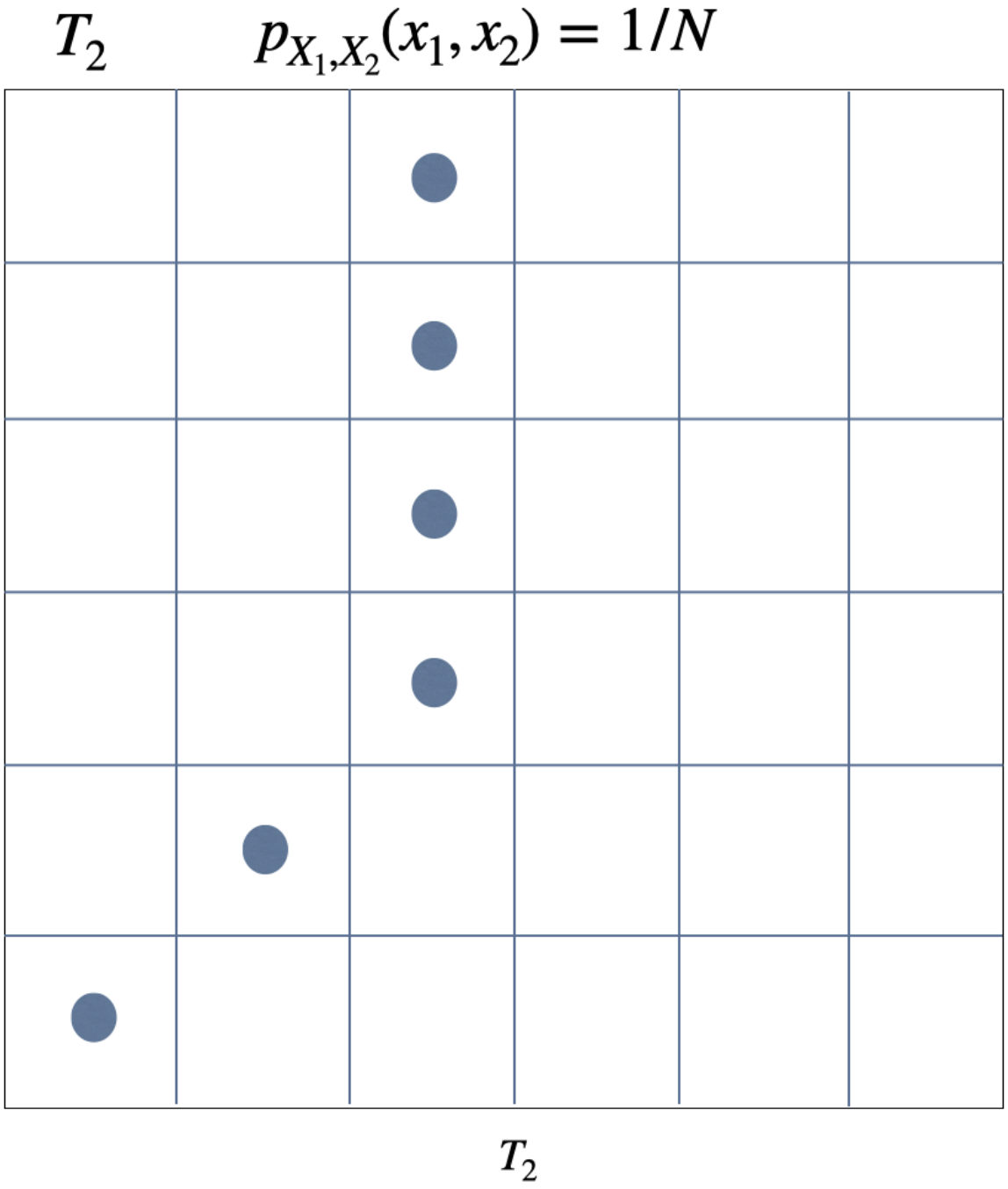

Figure 5.6: Joint Distribution Longitudinal Movement of Both Animals discretized on an undefined resolution with $N = 6$. In both time windows, the longitude is uniformly distributed across 5 bins. For simplicity, the vertical axis is not labeled here, and only the transition time T_2 is labeled on the horizontal axis. The scale of the horizontal axis is dependent on the size of λ.

GMI and LMI:

$$(t_1, t_2) \qquad I(X_{Lat1}, X_{Lat2}) = log(N) + log(N) - log(N) = log(N) \tag{5.14}$$

$$(t_2, t_3) \qquad I(X_{Lat1}, X_{Lat2}) = log(N) + 0 - log(N) = 0 \tag{5.15}$$

$$t_{i_2} \qquad I_{\mathcal{L}_i}(X_{Lat1}, X_{Lat2}) = log(N) + q * log(N) - log(N) = q\ log(N), \tag{5.16}$$

where X_{Lat1} and X_{Lat2} replace X_1 and X_2 as a reminder that this work is only for the latitudinal dimension. Recall that because of the homogeniety of (t_1, t_2) and (t_2, t_3), $I(X_{Lat1}, X_{Lat2}) = I_{\mathcal{L}_i}(X_{Lat1}, X_{Lat2})$ in both intervals.

These analytical results identify that identical movement is equivalent to the entropy of the shared movement vector. This is clearly the maximum attainable mutual information. It follows our intuition that linear and stationary movement have zero-valued association (as measured by mutual information), and, at the exact value of the shift from linear to stationary movement for animal 2, the LMI is equal to half of the maximum attainable mutual information. A small modification to the prior work reveals that $I_{\mathcal{L}_i}(X_{Lat1}, X_{Lat2}) = 1/2\ log(N)$ at exactly T_2 since $q = 1/2$ at this location.

Note that as shown in these equations, mutual information is theoretically unbounded as the number of bins, N, increases. However, the gains in mutual information by increasing N in our simulation are penalized logarithmically, and the interpretability of mutual information is jeopardized as N approaches and surpasses the number of sampling points in the movement vectors. Increasing N to equaling or surpassing the number of sampling points defeats the purpose of discretization.

In Figure 5.7, the latitude-longitude movement trajectories from this simulation are shown as a reference for the remainder of this section. In Figure 5.8, the analytical calculations for the latitude component are plotted over the computed localized mutual information using several combinations of *bandwidth (bw)* and *bins*. An arbitrary time domain of $[0, 1]$ is used. The upper and central plots of Figure 5.8 provide largely harmonious results with a few

nuances regarding boundary/end-point precision and the binning procedure implemented in the code. In the implemented code, we use a computationally faster binning procedure referred to as *equal frequency binning* as opposed to *uniform or equal width binning*. The equal frequency binning procedure reduces the number of bins input if it is not possible to assign a value to every bin. The details of this procedure and end-point binning decision rules are not the primary focus in this work, and more information can be found in the following source [48]. For the bottom-left plots of Figure 5.8, the large discrepancies are a result of the mentioned binning-reduction which lowers the $log(N)$ to $log(N-m)$ where m is the amount of bins removed. In the bottom-right plots of Figure 5.8, the large discrepancies are caused by the large bandwidth relative to grid-resolution choice and the end-point LMI condition chosen in the General Properties Section of this work. In brief, as the bandwidth increases to spanning the full time grid, LMI simply converges to the GMI from (t_1, t_3) which has a value of $1/2\ log(N)$. The work to show this is identical to our calculation for LMI at t_2, and is therefore not shown. For the lowest row of plots in Figure 5.8, with $bw = 32$, we have not evaluated the full analytic solution since the extremely large bandwidth requires additional boundary condition considerations that are not the main focus of this section.

The binning procedure implemented computationally in this sections and all remaining section has several differences which are dominantly attributed to *equal frequency binning*, as opposed to *equal width binning*, and the machine learning bin reduction strategies have been studied further in [48]. These differences result in discrepancies in the grouping/discretizing of locations which account for differences in the timing of the drop in LMI, the maximum potential LMI Equal width binning is shown in Appendix 7.2

Now, we bring together the longitudinal and latitudinal LMI components to derive the final LMI measure plots. Recall that $\mathbb{I}_{\mathcal{L}_i} = \sqrt{I_{\mathcal{L}_i}(X_{Lon1}, X_{Lon2})^2 + I_{\mathcal{L}_i}(X_{Lat1}, X_{Lat2})^2}$. Then it follows that

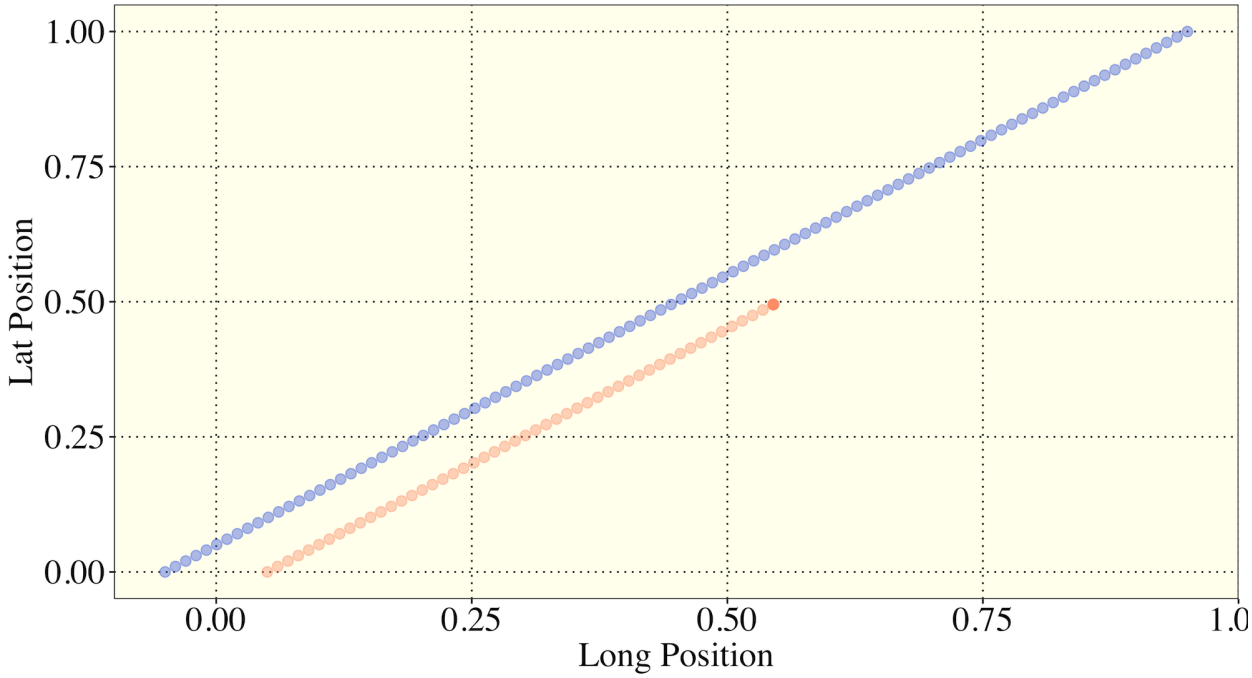

Figure 5.7: Simulated animals move in unison until the terminal halt of the second animal marked by a denser colored dot.

$$(T_1, T_2) \qquad \mathbb{I}_{\mathcal{L}_i} = \sqrt{(log(N))^2 + (log(N))^2} = \sqrt{2}\, log(N) \tag{5.17}$$

$$(T_2, T_3) \qquad \mathbb{I}_{\mathcal{L}_i} = \sqrt{0^2 + 0^2} = 0 \tag{5.18}$$

$$t_{i2} \qquad \mathbb{I}_{\mathcal{L}_i} = \sqrt{q^2(log(N))^2 + q^2(log(N))^2} = q\sqrt{2}\, log(N). \tag{5.19}$$

For $t_{i2} = T_2$, it can be shown that $\mathbb{I}_{\mathcal{L}_i} = \sqrt{2}/2\ log(N)$ which is half of the LMI on the interval (T_1, T_2).

In Figure 5.9, the final analytical LMI calculations are plotted over the computed LMI function. The same observations made for a single component (as in Figure 5.8) can be said here. We add to our comments from before by stating that it is advisable to have a bandwidth that is at least double the number of bins. This is examined further in later sections. Additionally, this simulation oversimplifies the reality of movement trajectories by assuming that movements of a given behavior are perfectly homogeneous. In reality, the

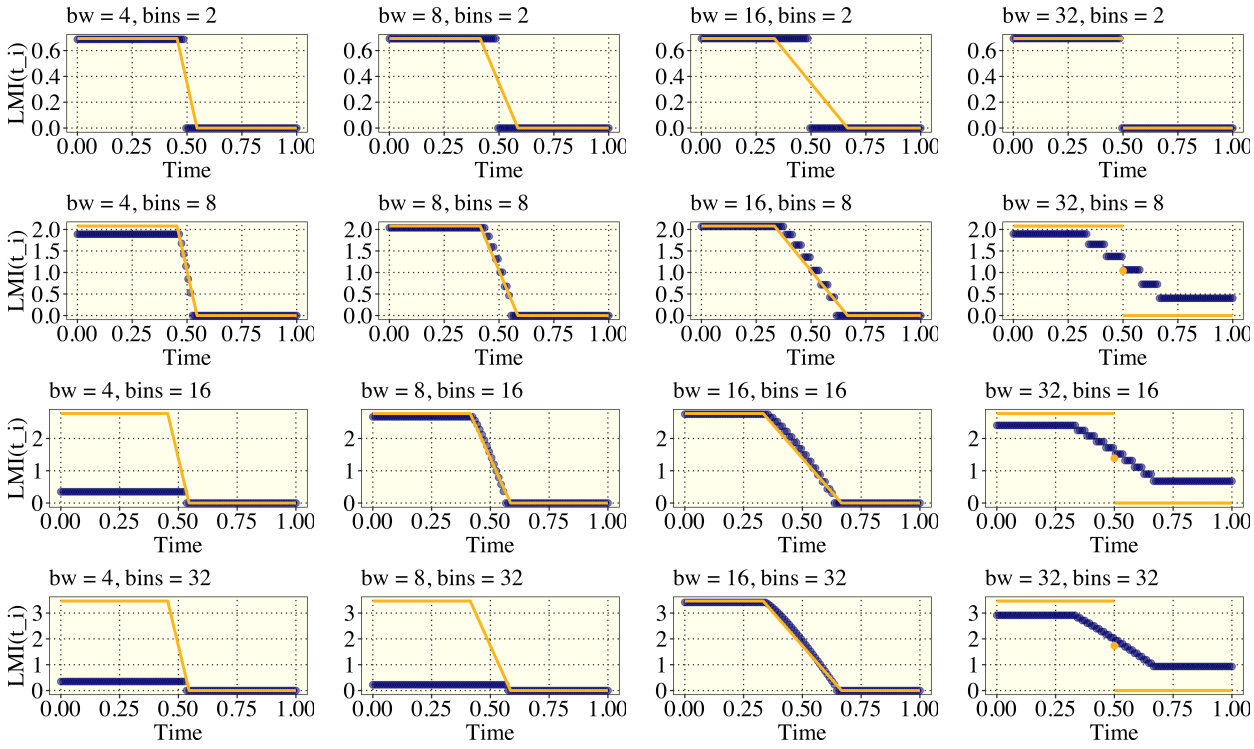

Figure 5.8: The localized mutual information latitude component based on the movement in Figure 5.7. The golden lines represent the LMI latitudinal component computed analytically disregarding the cases where the LMI window crosses the behavior transition. The upper line in at $ln(N)$ (which is the logarithm used in the implemented code) where N is the number of bins. The golden dot is the LMI analytically evaluated at T_2 which was shown to be $1/2\ log(N)$. The vertical axis is labeled as "LMI," but for this plot is only the longitudinal component of LMI. Note that for plots with $bins > bw$, the large difference between the analytical and the computed LMI values is a result of the use of a more efficient binning procedure which drops excessive bins which lowers the maximum measurable entropy. Refer to Appendix 7.2 for an example of a more similar binning procedure [48]. Note that for $bw = 32$, we have not evaluated the full analytic solution since the extremely large bandwidth requires additional boundary condition considerations that are not the main focus of this section. Instead, we have only plotted the LMI latitude component at $t_{i_2} = T_2$, and we have plotted the maximum and minimum potential LMI as reference lines.

entropy of a movement trajectory can be subject to variation which, as shown in this section, is directly related to the maximum value for mutual information. Various strategies can be proposed to appropriately visual LMI. Going forward in this work, we scale every value of LMI by the maximum attainable LMI in its localized window of time. This is expressed by

$$\mathbb{I}^*_{\mathcal{L}_i} = \frac{\mathbb{I}_{\mathcal{L}_i}(X_1, X_2)}{\mathbb{I}_{\mathcal{L}_i}(X_1, X_1)},$$

where the denominator represents the maximum mutual information for a given window $\mathcal{L}_i$ which is simply the mutual information of one of the animal's movement with respect to itself.

In Figure 5.10, the scaled LMI is shown for four considered bandwidths. It is noted here that the largest bandwidth considered overlaps the behavior transition for almost all time points on the defined time grid. In these first simulations, random measurement error/noise is not induced into the process since the purpose of this simulation was to confirm agreeing LMI results from the analytic solution and the simulation.

In all cases the drop in association is clearly detected, and all of them contain valid information about the shift in association. Given the prior knowledge of the abruptness of the shift in behavior association, some researchers may prefer the upward and leftward plots of Figure 5.10 that show a steep drop in LMI to reflect the true nature of this correlatory shift. However, the gradual decline in LMI in the downward and rightward plots of Figure 5.10 which are using larger bandwidths indicates a constantly increasing number of time points that are in the zero-association region of the time domain. The larger bandwidth, however, do not depict the perfect association as well since they are unable to avoid spanning the region of the behavior shift for animal 2.

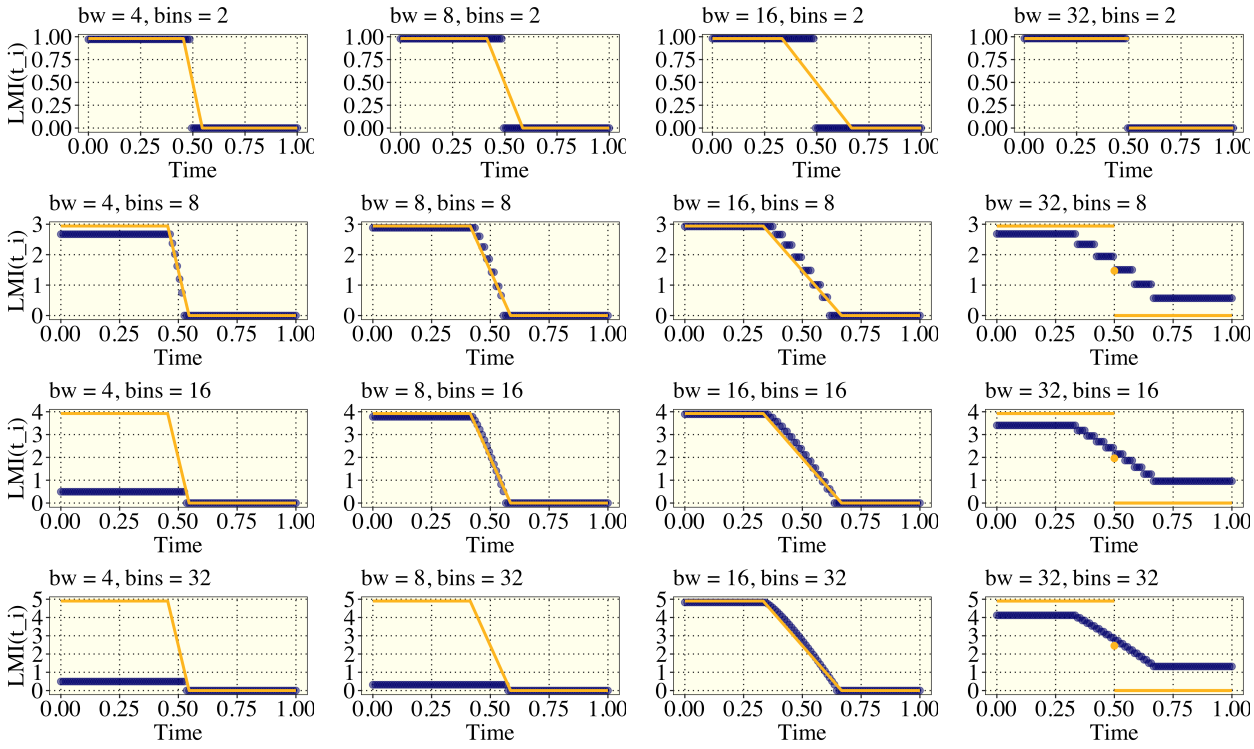

Figure 5.9: The localized mutual information based on the movement in Figure 5.7. The golden lines represent the LMI longitudinal component computed analytically disregarding the cases where the LMI window crosses the behavior transition. The upper line in at $\sqrt{2}\ ln(N)$ (which is the logarithm used in the implemented code) where N is the number of bins. The golden dot is the LMI analytically evaluated at t_2 which was shown to be $\sqrt{2}/2\ log(N)$. Note that for plots with $bins > bw$, the large difference between the analytical and the computed LMI values is a result of the use of a more efficient binning procedure which drops excessive bins which lowers the maximum measurable entropy. Refer to Appendix7.2 for an example of a more similar binning procedure [48]. Note that for $bw = 32$, we have not evaluated the full analytic solution since the extremely large bandwidth requires additional boundary condition considerations that are not the main focus of this section. Instead, we have only plotted the LMI at $t_{i_2} = t_2$, and we have plotted the maximum and minimum potential LMI as reference lines.

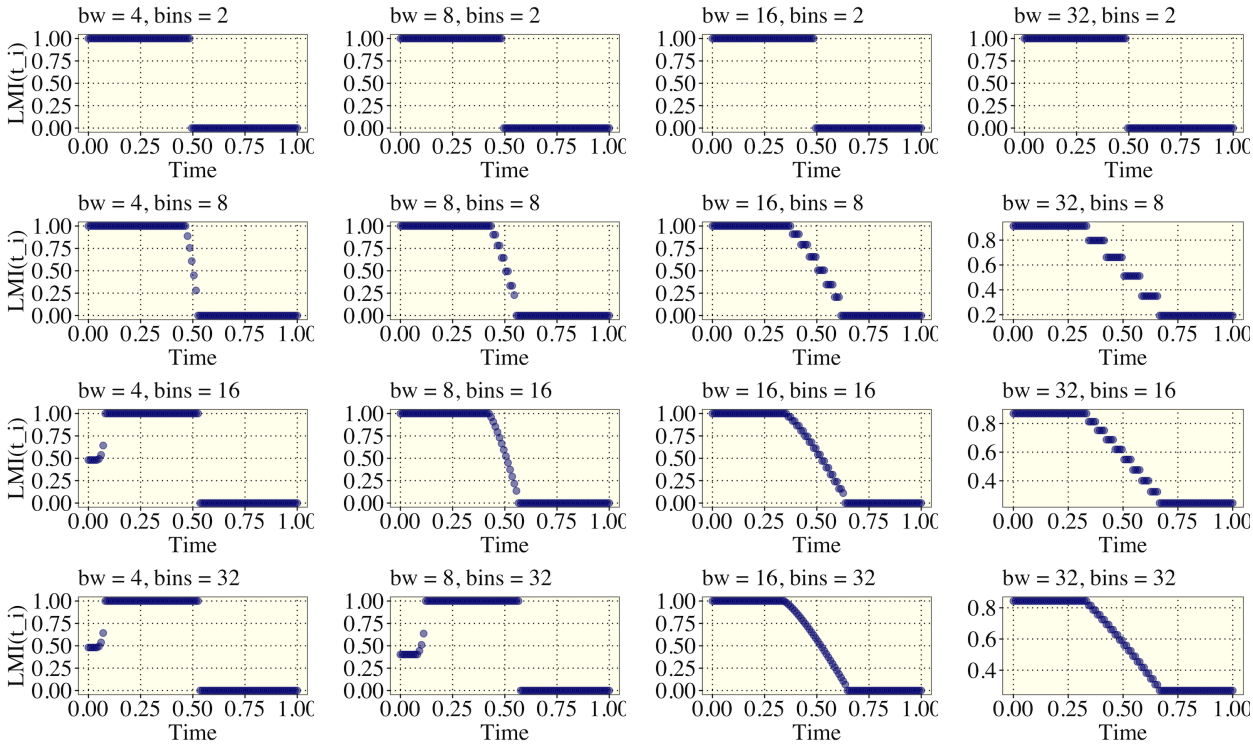

Figure 5.10: The localized mutual information functions for an array of bandwidths for the simulation show in Figure 5.7. Note that using too many bins with too few sample points (as determined by bw) is discouraged. It is clear that a good discretization should involve trying to reduce the behavior found in the sampled points into fewer bins than there are points. The intial dip in LMI in the lower left plots is a results of the unnecessarily large choice of bins and the bin reduction procedure for the longitudinal component. More details about the binning and bin reduction prodcedure can be found in the following source [48]

5.2.3 Simulation 2: Association Shift Sensitivity

Similar to the first simulation, where in the first half of the time domain both animals move linearly at the same speed, another simulation is constructed to assess the measure's ability to detect shifts in movement association that are similar functionally, but marked by a clear change in the relationship of two animals. The linear movement characterizing the animals in the first half of the time domains would be similar to herd/pack behavior or cooperative hunting in the case of solitary apex predators if the animals are close in proximity. If they are far apart from each other, this could characterize migratory movement induced by a similar climate dependent or seasonal shift in behavior.

The generation of independent and identically distributed noise with no propagated/auto-correlated error is important as a part of this simulation in order to ensure that the underlying movement generated is preserved, but at the same time partially confounded. Error defined in this way characterizes standard instrumentation error for GPS tracking devices where measurement error of some magnitude is inherent, and it is important that the LMI measure can still detect a shift in behavior in a simple movement scenario.

The generated movement of the first animal is defined by

$$\begin{cases} x(t_i) = t_i + a_{x1} + \epsilon_{t_i} & t_i \in [0, 30] \\ y(t_i) = t_i + a_{y1} + \epsilon_{t_i} \end{cases},$$

and for the second animal

$$\begin{cases} x(t_i) = t_i + a_{x2} + \epsilon_{t_i} & t_i \in [0, 15) \\ y(t_i) = t_i + a_{y2} + \epsilon_{t_i} & \\ x(t_i) = b_{x2}(t_i - 15)^2 + x(t_i = 15) + \epsilon_{t_i} & t_i \in (15, 30] \\ y(t_i) = -b_{y2} * (t_i - 15) + y(t_i = 15) + \epsilon_{t_i} & \end{cases},$$

In our simulation, the coefficients are selected with an effort to generate movement where one animal returns to the same region as the beginning of the simulation ($a_{x1} = -1, a_{y1} = 0, a_{x2} = 1, a_{y2} = 1, b_{x2} = -1/15, b_{y2} = -1.15$). The time domain is scaled to give an example when position is monitored hourly for a 30 day period, with a shift in behavior occurring at Day 15. The generated process characterizes perfectly associated movement from $t_i \in [0, 15]$, as shown in the prior simulation, with a subsequent drop in movement association as the second animal turns sharply and moves with a different relationship between latitudinal and longitudinal movement. It has been confirmed that the scaled global mutual information from $t \in [0, 15]$ is perfect/maximized ($rel\ GMI = 1.00$), and the global mutual information from $t \in (15, 30]$ drops notably with the shift in behavior ($rel\ GMI = 0.93$).

The challenge of interest is that the shift in movement association is stark, but the movement trajectories in the second time window are only subtly different. In brief, quadratic and linear functions are similar functionally, especially in small monotonic regions of the time domain for quadratic functions. As a result, the relatively high association between the two animals in the latter time window is expected since the strictly linear movement of Animal 1 can still sufficiently explain the quadratic movement of Animal 2. It is our objective in this first simulation to assess if the LMI measure proposed successfully detects this shift and when it fails to effectively do so.

In Figure 5.11, the first round of simulations is performed with 4 different bandwidths, and zero error induced into the generated movement model. In this case, all bandwidths successfully detect the drop in movement association between the two animals, but smaller and larger bandwidths are detecting different but equally interesting features. The lower bandwidths of $bw = 2, 4$, identify the largest drop in association on the $[0, 1]$ scale for LMI, but the larger bandwidth clearly mark the lowest point of association at the exact location of the shift. The reason for this is because time windows (centered on some t_i) that overlap the behavior shift are more disparate than time windows that don't overlap the transition. More specifically Animal 2's movement is not monotonic in the neighborhood surrounding

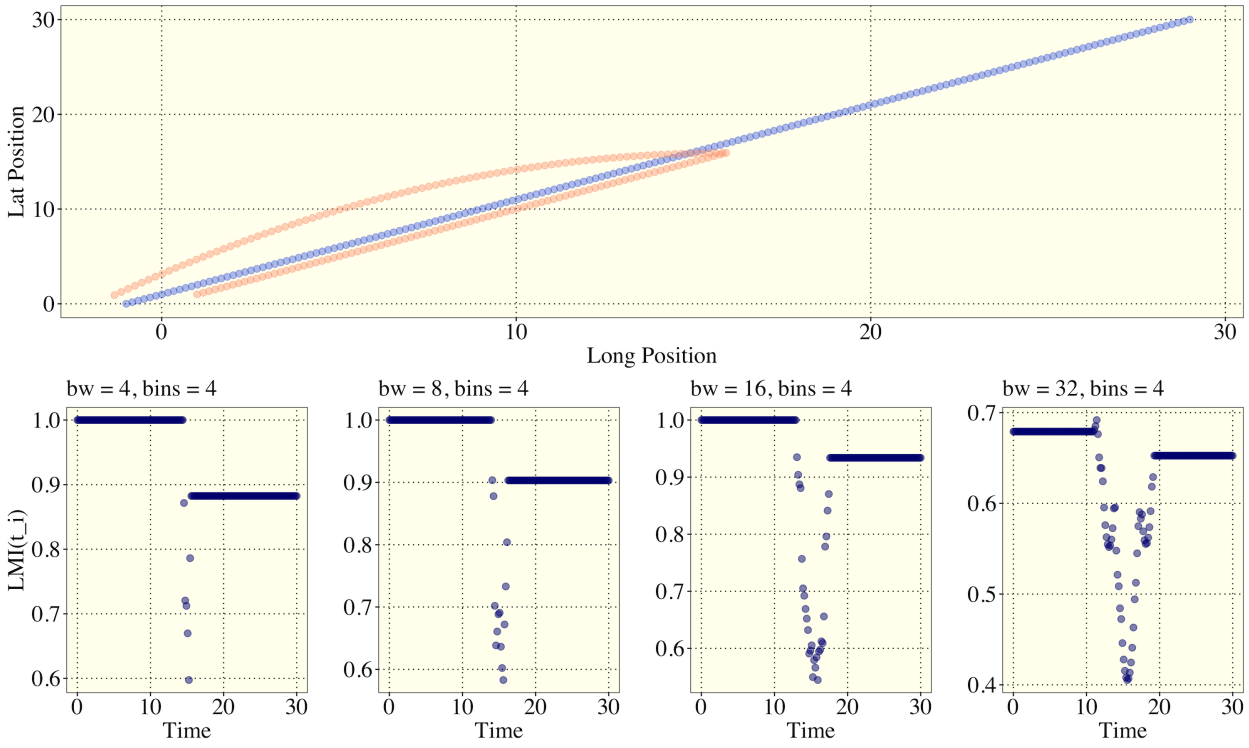

Figure 5.11: Simulation 2 movement with $\epsilon_{t_i} = 1.0$. (Lower) LMI functions with various bandwidths (bw) and number of bins (bins) set to 4 for the discretized estimation of the pmf for each time window surrounding t_i.

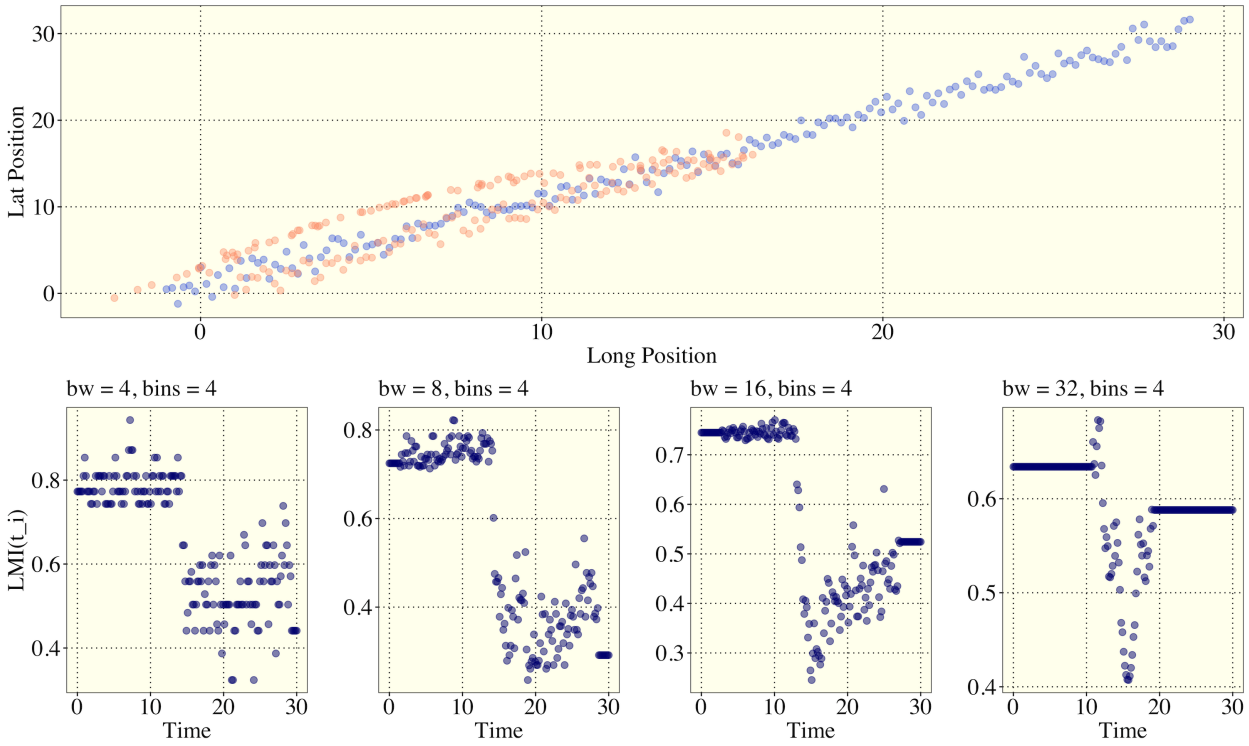

Figure 5.12: (Upper) Simulation 2 movement with $\epsilon_{t_i} = 0$. (Lower) LMI functions with various bandwidths (bw) and number of bins (bins) set to 4 for the discretized estimation of the pmf for each time window surrounding t_i.

the behavior shift, and LMI will record higher associations for regions where both animals have monotonic movement.

In this movement scenario another two rounds of simulations are performed in which the iid error is increased from $\epsilon \sim N(0, 0)$ to $\epsilon \sim N(0, 1.00)$. In Figure 5.12, the each set of simulations are shown with the same bandwidth parameters considers previously. All bandwidths satisfactorily detect a shift to lower association where the smaller bandwidths identify the shift as a stepwise/abrupt behavior shift. Bandwidth selection is studied in more detail in the Simulation 5 Section. It is apparent that substantial increases to noise do not inhibit the LMI measure's ability to detect shifts in behavior association, although the induced error prevents the model from detecting perfect association in the first half of the time domain. Three important conclusions from this simulation are summarized:

1. Increasing random measurement error (which is assumed to be iid for each time point)

marginally decreases the LMI measure's ability to detect an underlying process and association of animal movements. Any increase in the independence of a process will, by definition, lower the mutual information between two animals. If the errors have related/autocorrelated error terms then this issue would be clearly reduced. This is not shown since it is not the primary focus here, but the autocorrelation of error is possible if both animals are moving in a same region with poorer GPS signal. However, even in the presence of high iid error at each time, the measure still detects the shift and preserves the clear decline in association surrounding the time of the behavior shift.

2. Because of 1., it is important to note that it is advisable to smooth a process prior to using the proposed LMI measure. Smoothing splines, as an example, can be used to filter noise out of process that is known to be continuous, and the process is then represented by a Fourier or B-spline (polynomial) model which both have exceptional properties (such as differentiability) [44, 45, 46]. This was done in prior work with the LMI measure [40].

3. The proposed measure is highly sensitive to transition-states between behaviors. The LMI measure in all cases indicates that the time of lowest association between animals is in the direct neighborhood of the behavior shift as opposed to the entire last half of the time domain. This is attributed to the inability of linear movement to adequately contain information about an abrupt turning motion. As such, LMI shows evidence of being an exceptional measure for shift detection in the association of animal movements.

5.2.4 Simulation 3: Cross-dimensional/Cross-directional Movement Association

In this simulation, we highlight a nuance of LMI, as defined in this work, that can be addressed when necessary, with a modification to the LMI measure. It has already been shown in Simulation 1 that, at any time t_i, if one animal is not moving while the other is moving, then we expect $\mathcal{I}(t = t_i; \lambda) = 0$. In the first simulation, this was true in the case where one animal was simulated to be stationary *in both* the latitude and longitude

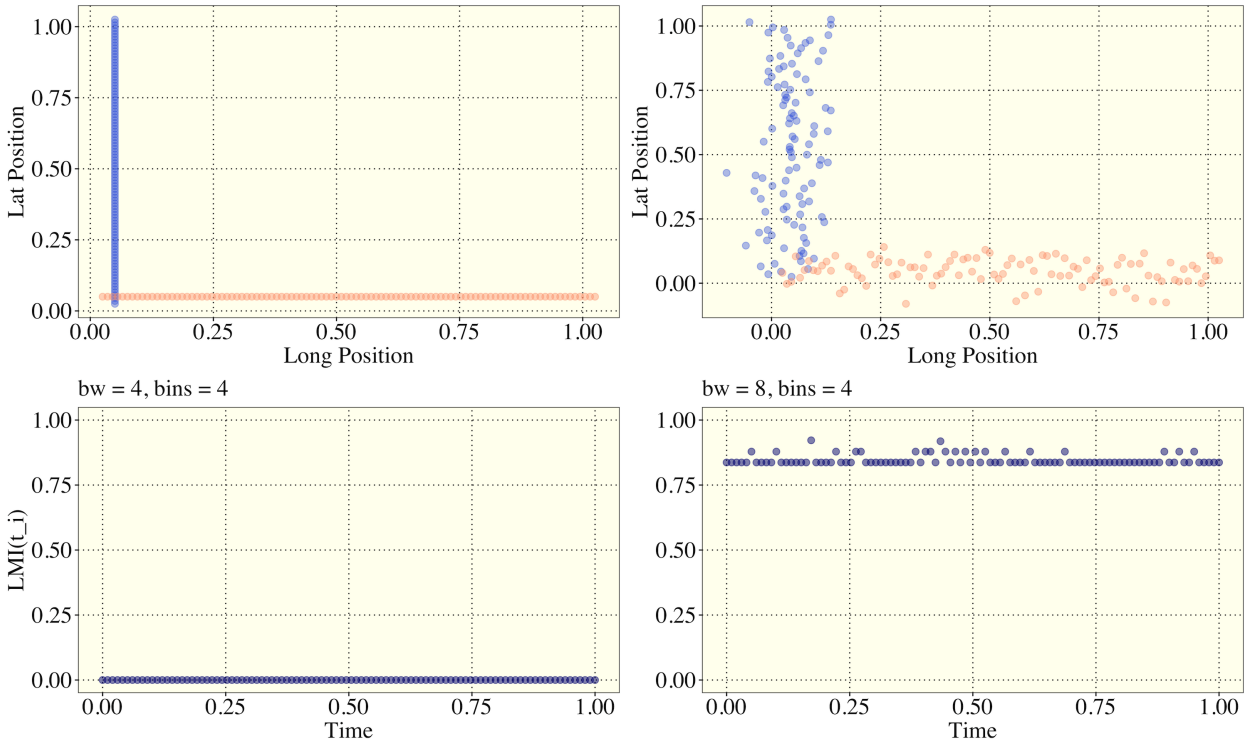

Figure 5.13: (Upper) Simulation 3 movement paths for strict cardinal movement generated with $\epsilon_{t_i} = 0$ and 0.05 respectively. (Lower) The LMI Functions for the corresponding movement paths from the upper plots.

directions.

We propose another simple movement model where one animal moves due north, and the other animal moves due east. Animal 1 and Animal 2's movements are defined by

$$\begin{cases} x(t_i) = t_i + a_x + \epsilon_{t_i} & t_i \in [0,1] \\ y(t_i) = 0 + a_y + \epsilon_{t_i} \end{cases},$$

and

$$\begin{cases} x(t_i) = 0 + a_x + \epsilon_{t_i} & t_i \in [0,1] \\ y(t_i) = t_i + a_y + \epsilon_{t_i} \end{cases}.$$

Figure 5.13 presents the resulting LMI from $t \in [0,1]$, and we only consider zero random error and some arbitrarily induced random error $\epsilon \sim N(0, 0.05)$. Although perhaps a nuance, the results of this simulation indicate a clear weakness in the proposed measure of LMI. Since

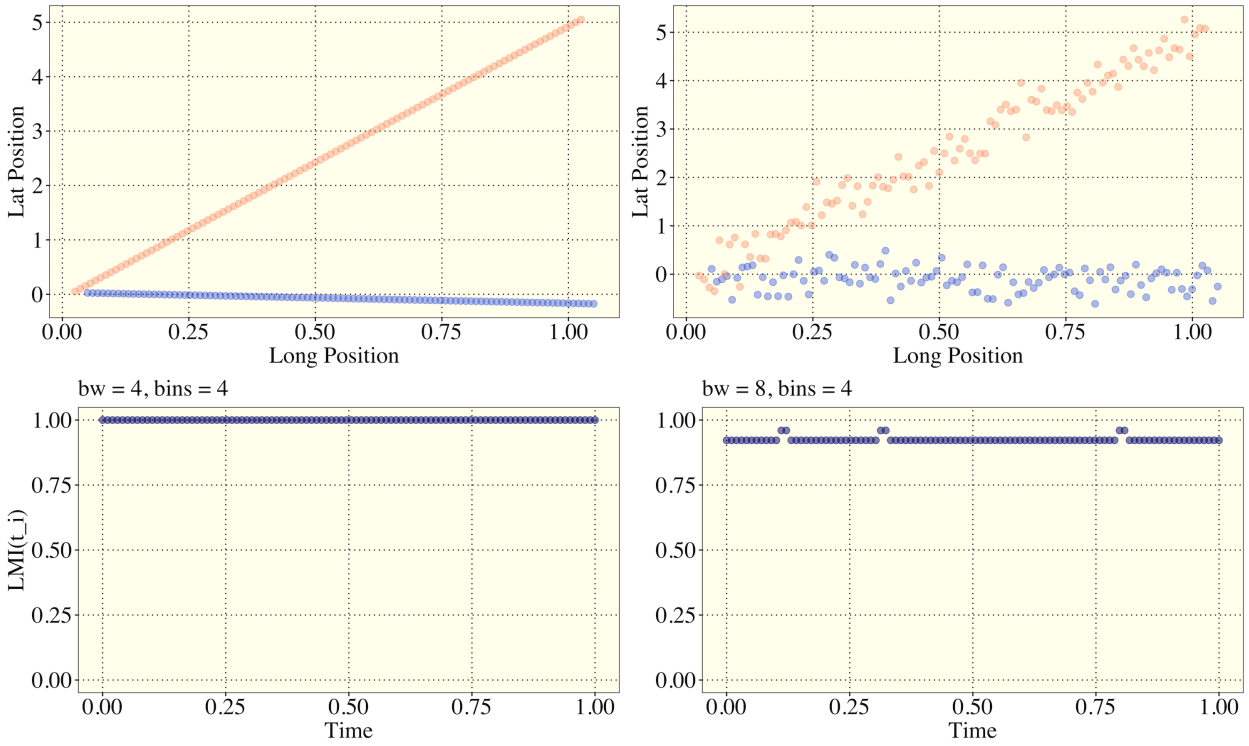

Figure 5.14: (Upper) Simulation 3 movement paths generated with $\epsilon_{t_i} = 0$ and 0.05 respectively with rotation off the cardinal axes. (Lower) The LMI Functions for the corresponding movement paths from the upper plots.

the joint (latitudinal and longitudinal) LMI measures only sums the association of a pair of animal movements by *matching directional components*, the measure is not detecting the strong *cross-directional* association. Ironically, in this extreme situation, inducing error into the process marks the animal movement behaviors as highly associative, although not perfectly associated as would be desirable.

Another similar movement model is proposed where the same movement is rotated off-parallel with the Longitude and Latitude axes. We now define Animal 1 and Animal 2's movements by

$$\begin{cases} x(t_i) = t_i + a_x + \epsilon_{t_i} & t_i \in [0,1] \\ y(t_i) = -0.20 * t_i + a_y + \epsilon_{t_i} \end{cases},$$

and

$$\begin{cases} x(t_i) = t_i + a_x + \epsilon_{t_i} & t_i \in [0,1] \\ y(t_i) = 5 * t_i + a_y + \epsilon_{t_i} \end{cases}.$$

These movement path's are perpendicular in $\mathbb{R}^2$ since both animals move at the same speed in the longitude-direction while Animal 1 and Animal 2's latitudes changes at a rate of -0.20 and +5 the rate of change in longitude. In Figure 5.14, the LMI measure is assessed with the same bandwidths and error terms.

The rotation of movement yields a strong association which in comparison to the prior simulation marks an interpretation challenge for our measure of LMI that must be addressed. In Figure 5.14, the LMI measure is assessed with the same bandwidths and error terms. This is shown in Figure 5.14. For empirically observed or estimated movement trajectories, it is clear that witnessing a two animals movement exactly parallel to lines longitude and latitude is unrealistic, and so this measure is robust for most animal movement modeling problems.

However, this simulation still identifies an intriguing issue that stems from the definition of our current measure of LMI, which does not account for cross-directional movement association. We propose examples of where a better measure of LMI should be considered:

1. Landscape structure at two distant sites: Consider two animals of the same species that reside along two different rivers. The first river runs approximately north-south and the second river runs approximately east-west. If the animals both move similarly along these rivers then the strongest relationship in their movement is expected to be cross-directional. This would be realistic for jaguars that hunt along similar waterways and may be located in disjoint habitats.

2. The example laid out in (1) would also hold for other land features. In Figure 5.15, an elevation map of the San Francisco Peaks of Northern Arizona is depicted. In this image, it is clear that the highest ridge is geographically curved, almost completing a full circle. If animals in this ecosystem have a tendency to move on the steep slopes of this range in the

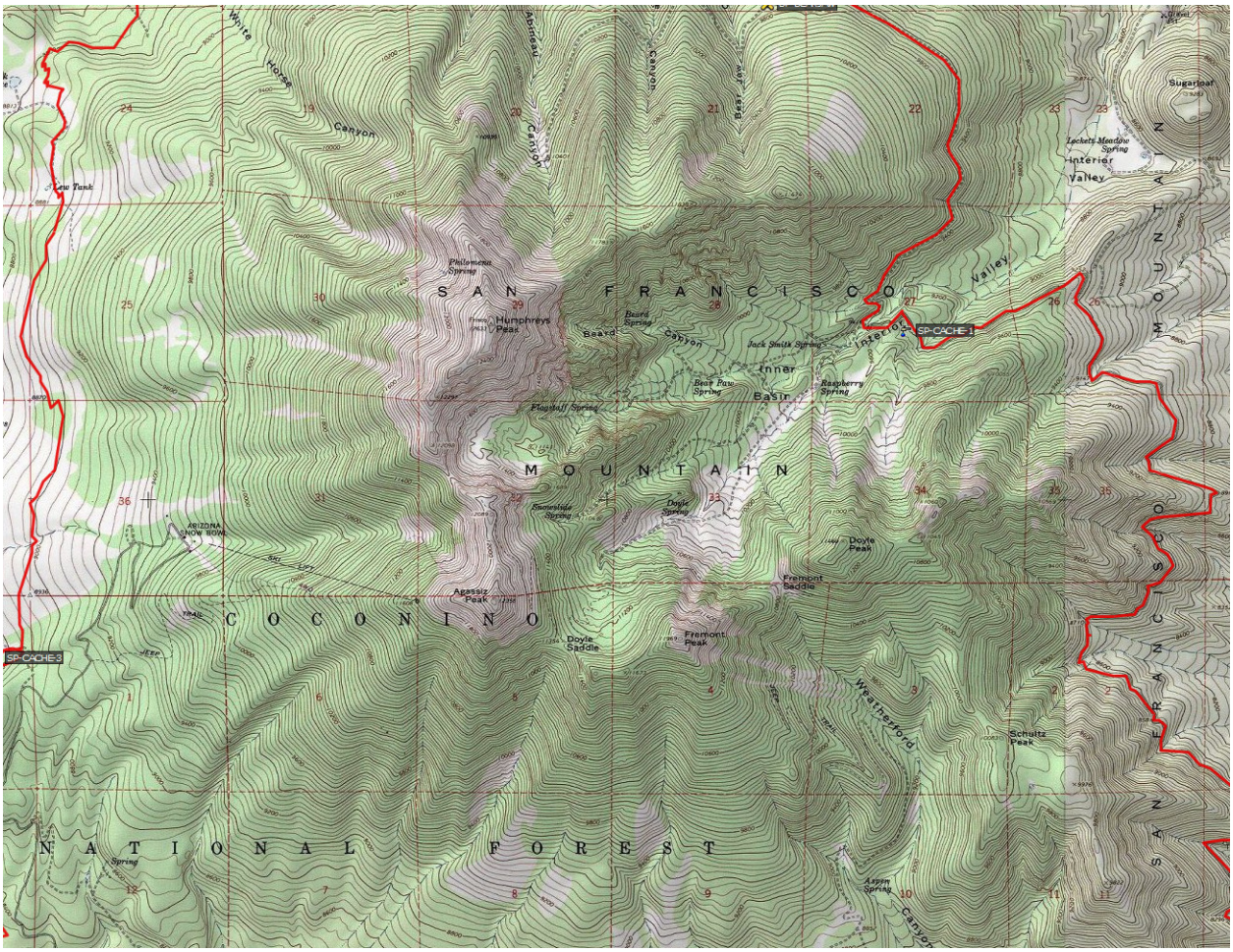

Figure 5.15: Topographic Map of the San Fransico Peaks and the surrounding section of the Coconino National Forest near Flagstaff, Arizona. The intent of presenting this figure is to draw attention to the natural C-shaped or bowl-shaped curvature of this mountain range.

same way, then it is expected that two animals could have strong cross-directional association in their movements. Although, it would be highly unlikely to observe zero LMI (as in our simulation), if their movement associations are largely cross-directional, then a lower LMI would be reported than if they were on identically oriented terrain.

3. Transportation data. Although not tied as closely to the field of movement ecology, the movement of planes, passenger vehicles, and trains etc. may be marked by cross-directionally related behavior, since the behavior of human transportation is largely more predictable. As an example, cars and trains will almost always follow roadways, railways, and air-routes, and many examples could be contrived to justify the presence of cross-directional association

similar to (1) and (2). However, the integration of human and animal telemetry data has been considered in recent years which may mark an important future integrating human and animal movement and the detection of associations between such movements [41]. In the Discussion section, we propose a simple modification to our current measure of LMI to handle cross-directional association.

Another alternative would be to consider a different information theoretic measure. *Total Correlation*, also referred to as the *Multiinformation* is an extension of mutual information to quantify the dependency among a set of n random variables [48]. This measure is a logical and simple approach to addressing this issue, but there may be reason for still considering an component-wise measure of association as defined in this work. As an example, a researcher may be primarily interested in latitudinal association, and the approach considered in this work retrieves this information directly. Although no definition of Localized Total Correlation (LTC) is considered, the R code provided in the coding LMI section could be quickly reconstructed for the user to choose between computing LMI and LTC. The R code is provided in Appendix 7.4.

5.2.5 Simulation 4: Delayed Onset/Tracking Movement Association

In the first two simulations, animals that traveled alongside each other with the same behavior were shown to have perfect association as measured by the LMI measure. It becomes instructive to identify if the LMI measure identifies perfect association between animals that exhibit the same behavior but not at the same time. There are multiple scenarios where this would be important to consider in animal movement applications: Broadly, examples of this behavior would include, hunting/tracking behavior, scat/scent marking, commensalism (such as bison plowing paths in deep snow for pronghorns), scavenging, herd behavior, mating behaviour, and migratory behavior. In each of these cases, it would be of interest to researchers to identify how much time in a week, month, or season is marked by strong association between a subjects within predator and prey populations in an ecosystem. Two

examples are elaborated on further. Delayed regional migration of birds, such as arctic terns, could also be characterized in this manner. Recent literature has provided evidence that arctic tern colonies across the Northern Hemisphere share common migratory routes, and as such, the movements of some colonies along similar routes may be delayed by several days or weeks [49]. Although not explored in this work, in the neotropical apex predator application that follows, jaguars, like many large cats, use scent and scrape marking strategies to passively communicate with each other [50, 51]. If predators are following similar routes to marked sites, then this could classified as a type of following behavior. The same may apply for males that are in search of females during a mating season.

In this simulation, the movement pattern complexity is increased to explore nonlinear movement. A simple example using "line drill/gym suicides" motion is shown first. I model Animal 1's and 2's movements by

$$\begin{cases} x(t_i) = a_{xj} sin(t_i) + \epsilon_{t_i x} \\ y(t_i) = a_{yj} sin(t_i) + \epsilon_{ty}, \end{cases}$$

and

$$\begin{cases} x(t_i) = a_{xj} sin(t_i - \varphi) + \epsilon_{t_i x} \\ y(t_i) = a_{yj} sin(t_i - \varphi) + \epsilon_{t_i y}. \end{cases}$$

For both animals, this movement is characterized by path retracing where additional time is spent at the ends of the path. In Figure 5.16, their movement is modeled to be identical except for a phase shift of $\varphi = \pi/2$. We consider two scenarios with $\epsilon = 0, 0.2$. Although clearly simplified, this movement characterizes a simple staggered migration between two locations, where an animal (such as a migratory bird) spends more time at the far ends of the route, and less time at any given position in between destinations.

In both cases, the LMI identifies perfect association in the animal movement paths with short periodic drops in their association, occurring at $t = \pi/2,\ \pi,\ 3\pi/2$. Over the domain of $t \in [0, 2\pi]$, these are the locations where the animals are briefly at points where one animal

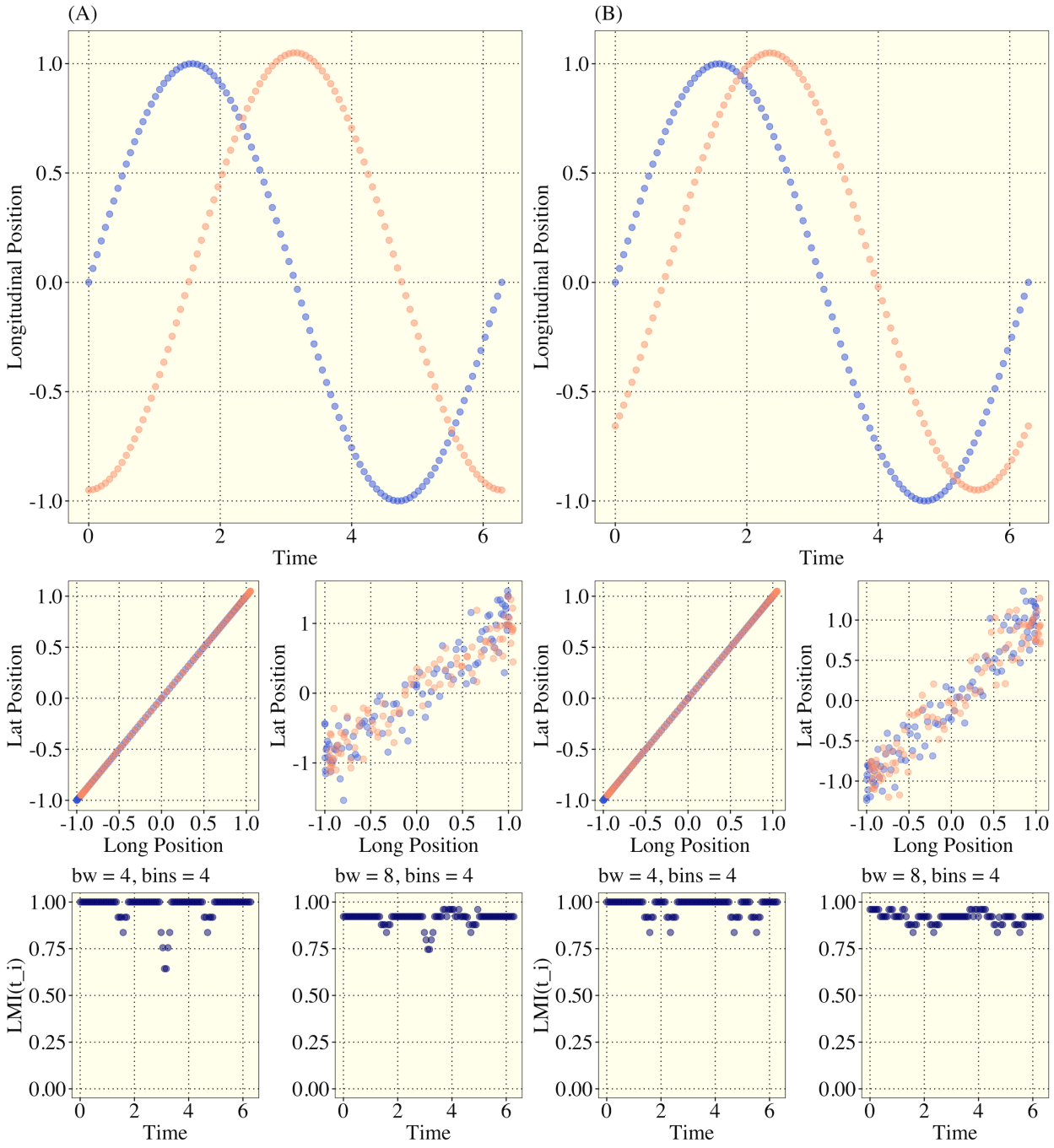

Figure 5.16: Simulation 4 Linear Tracing Movement Paths. (A) [Upper] plot show the induced temporal phase shift of $\varphi = \pi/2$ for the Longitudinal component. [Center] The generated movement paths in $\mathbb{R}^2$ with $\epsilon = 0, 0.2$. [Lower] The LMI functions for each of the respective errors. (B) Same as detailed for (A) but with $\varphi = \pi/4$.

is either at an inflection point or a critical values on the sine function while the other animal is at the opposite. The magnitude of the drop in LMI computed during these short windows is dependent on the bandwidth, and the number of bins used in the discretization process although this is not shown in these simulations. The strong association is also well-captured in the presence of iid error.

In the second scenario, we consider the exact same movement behavior, but with a phase shift of $\varphi = \pi/4$. In the right column of plots in Figure 5.16, the periodicity of the drop from perfect association in LMI changes to $t = \pi/2, 3\pi/4, 3\pi/2, 7\pi/4$. At $t = \pi/2, 3\pi/2$, animal 1 is experiencing a direction change while the other animal continues to move in the same direction. At $3\pi/2, 7\pi/4$, animal 2 is experiencing the same (but delayed) direction change.

In both scenarios shown in Figure 5.16, the change in direction of either animal marks the dip in LMI. In essence, this is an identical phenomena to the drop in LMI shown at the behavioral shift in the Simulation 2 section; at an inflection point, the temporal neighborhood is monotonic, and at the critical values, the temporal neighborhood is not monotonic. More specifically, on a small window surrounding a direction change at a critical value, the surrounding time points characterized an even function (symmetric about t_i; $f(t) = -f(t)$). On a small time window at any other location, the surrounding time points characterize either an odd function ($f(t) = f(-t)$) in the case where the other animal is at an inflection point on the sine curve or the function is neither even nor odd.

Two more scenarios are considered for a more complicated moving pattern where two animals follow each other in a circle with some phase shift. Animal 1 and 2's movements are modeled by

$$\begin{cases} x(t_i) = a_{xj} sin(t_i) + \epsilon_{t_i x} \\ y(t_i) = a_{yj} cos(t_i) + \epsilon_{ty}, \end{cases}$$

and

$$\begin{cases} x(t_i) = a_{xj} sin(t_i - \varphi) + \epsilon_{t_i x} \\ y(t_i) = a_{yj} cos(t_i - \varphi) + \epsilon_{t_i y}. \end{cases}$$

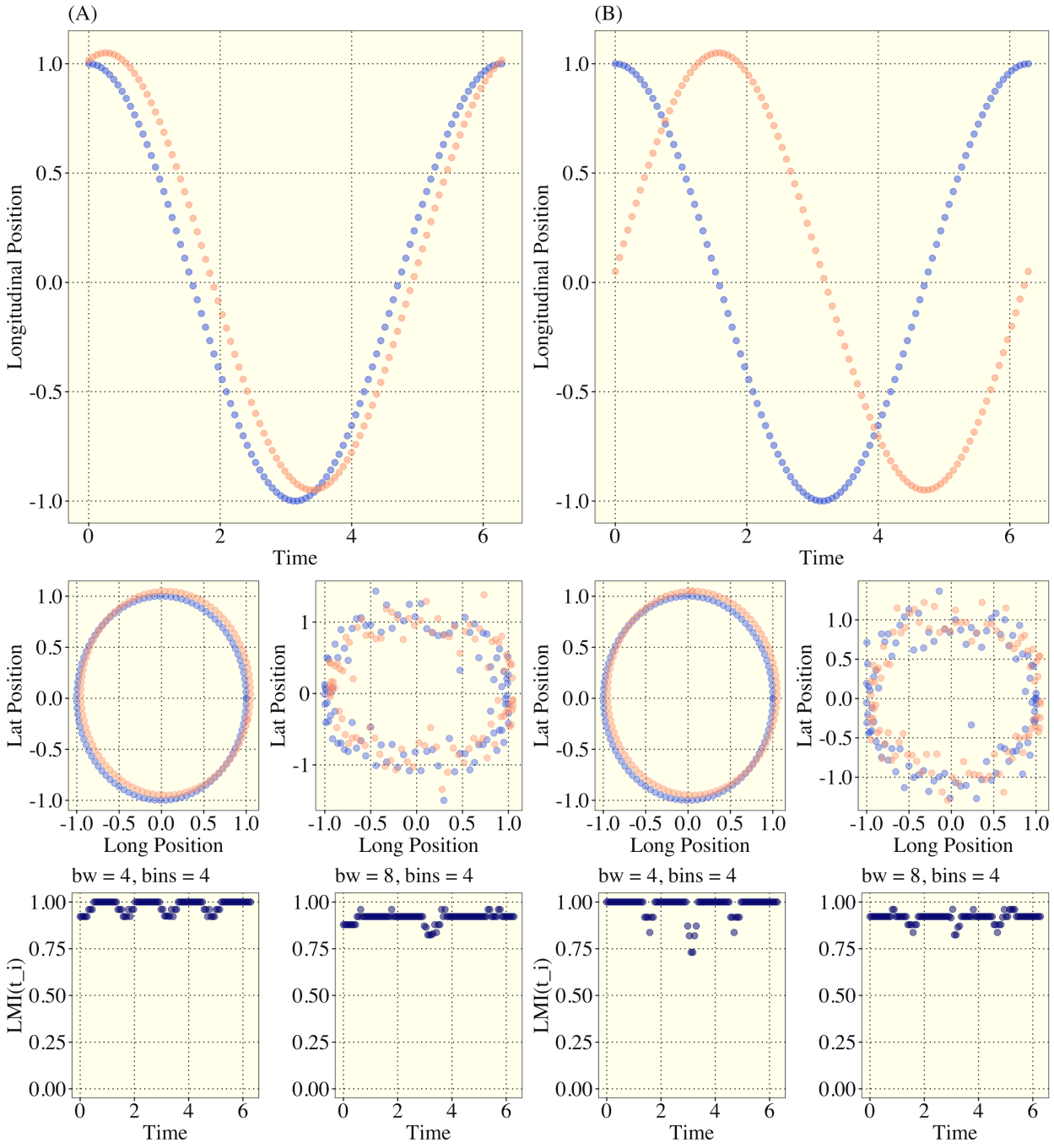

Figure 5.17: Simulation 4 Circular Tracing Movement Paths. (A) [Upper] plot show the induced temporal phase shift of $\varphi = \pi/2$ for the Longitudinal component. [Center] The generated movement paths in $\mathbb{R}^2$ with $\epsilon = 0, 0.2$. [Lower] The LMI functions for each of the respective errors. (B) Same as detailed for (A) but with $\varphi = \pi/4$.

In these two scenarios, shown in the Figure 5.17, $\varphi = \pi/12$ and $\varphi = \pi/2$ respectively. The same conclusions from the prior scenarios are achieved here, where perfect association is detected except for at critical values in position for either animal, and in the presence of substantial iid random error, the same association is clearly detected. It is clear from the simulations in this section that proposed LMI measure is an exceptional tool for detecting following/tracking behavior. In order to eliminate the dips in LMI that would occur when either animal changes direction while the other continues along a monotonic trajectory, curve registration or warping would be required to align the curves. However, in many scenarios it is clear that this small dip may not occur biologically since tracing patterns may not resemble those shown in these simple simulations. Further, the instances where one animal changes direction while the other remains on a steady course may be important landmark features that should not be filtered out. As a result, this measure does not explicitly require curve alignment models to detect strong by delayed associative movements.

5.2.6 Simulation 5: Implications of Parameter Selection for Bandwidth and Bins

In the Simulation 1 and Simulation 2 sections, there are clear (asymptotic) trends in the shape of the computed LMI function as the bandwidth and the number of bins used to construct the pmfs for each animal increases. There is also the question of what time resolution is required to uphold the integrity of the LMI measure. In the two sets of simulations in this section, I examine two distinct types of movement in a unit square. The first movement model simulates Brownian particle movement for both animals, and the second simulates identical but phase shifted cyclic movement for both animals similar to prior simulations in this work.

The Brownian movement models are both defined by

$$\begin{cases} x(t_i) = \epsilon_{t_i x} & t \in [0,1] \\ y(t_i) = \epsilon_{t_i y} & \\ \epsilon_{t_i x}, \epsilon_{t_i y} \sim Unif(0,1). & \end{cases}$$

For this movement model, characterized by jittered/random movement in the square $[0,1] \times [0,1]$, it is expected that no association should exist in the movements of two animals generated by this process. We measure LMI for a time resolution of 2, 4, 8, 16, 64, and 512 time points (including boundary times). We also consider bandwidths ranging from $bw \in [1,8]$ and number of bins ranging of 2, 3, and 4. The large collections of simulations described here are depicted in Figure 5.18.

For a small number of points, high and moderately-high LMI is detected at most or all time points, and in the case of only having two points for each animal, the LMI measure always reports perfect association. As the time resolution (number of points) increases, the LMI is gradually driven to zero. Further, increasing the number of bins increases the LMI measure for all simulations where the time resolution permitted for an increase in bins. As an example, it would not make sense to discretize a movement path with only 4 observed locations using 8 bins, and the same concept applies for a local time window. The increases in LMI for increasing number of bins can be offset by increasing the bandwidth parameter. This is shown clearly in the final two rows of 5.18.

The second set of simulations are intended to juxtapose the Brownian particle motion simulation. Animal 1 and 2 have movement defined by

$$\begin{cases} x(t_i) = a_{xj} sin(t_i) + \epsilon_{t_i x} \\ y(t_i) = a_{yj} sin(t_i) + \epsilon_{t_i y}, \end{cases}$$

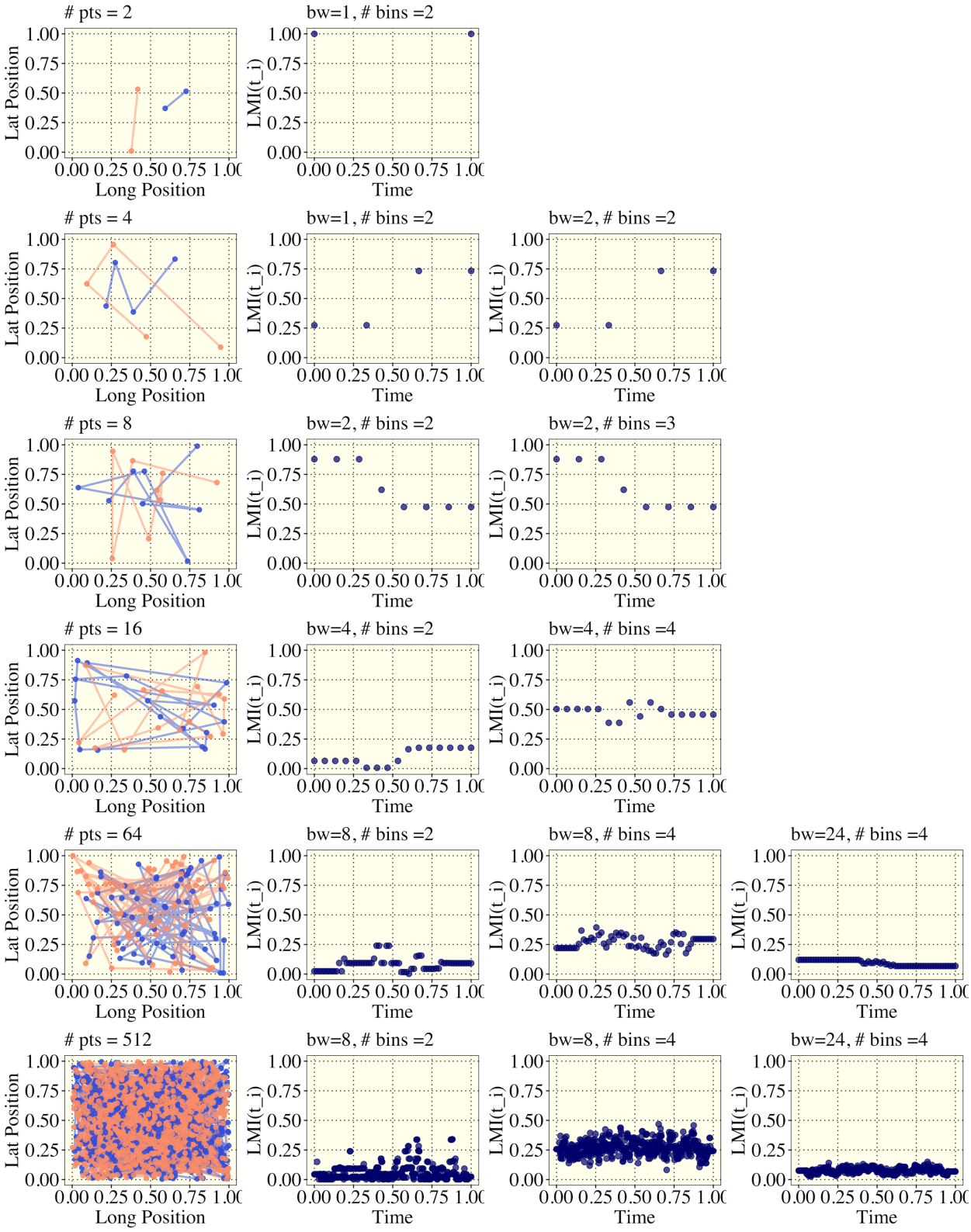

Figure 5.18: LMI Sensitivity to low temporal resolution for Brownian particle movement. The first column is the animal movement path in $\mathbb{R}^2$, and the remaining columns are the computed LMI functions for an array of bandwidths and bins.

and

$$\begin{cases} x(t_i) = a_{xj} sin(t_i - \epsilon_\varphi) + \epsilon_{t_i x} \\ y(t_i) = a_{yj} sin(t_i - \epsilon_\varphi) + \epsilon_{t_i y}. \end{cases}$$

On the unit square, $\epsilon_{t_i x}, \epsilon_{t_i y} \sim N(0, 0.025)$, and $\epsilon_\varphi \sim N(0, \pi/12)$. The random phase shift, ϵ_φ, allows for the animal to follow farther or closer that a fixed phase shift as shown in previous simulations.

In Figure 5.19, the same parameters for bandwidth and number of bins are examined, and it is clear that the same problem exists for extremely low temporal resolutions where perfect or near perfect association is computed. However, as the temporal resolution increases the association between the animals stabilizes with clearer structure that is not trending towards zero like the Brownian motion simulation. This section motivates guidelines for the use of this measure pertaining to required temporal resolution and tuning the bandwidth, and number of bins parameters. These guidelines are provided in the Discussion Section.

5.2.7 Simulation 6: Simulating Male-female Neotropical Predator Movement Association

The final set of simulations are motivated by the first implementation of this measure on monitoring male-female and male-male jaguar movement associations [40]. In one case detailed in this work, a male jaguar (Jaguar 18) relocated to the same region as a similar aged female (Jaguar 12). There were several periods of high co-occurrence potential which were finally followed by Jaguar 12 removing herself by approximately 30km before returning to the same location two months later. At the end of the time window of high co-occurrence potential, the proposed LMI measure detected a sharp decline to nearly zero using a bandwidth of 48 hours (or 4 days) [40]. This section aims to explore this specific behavior in a controlled simulation.

In the construction of an appropriate advanced animal movement simulation, it is best

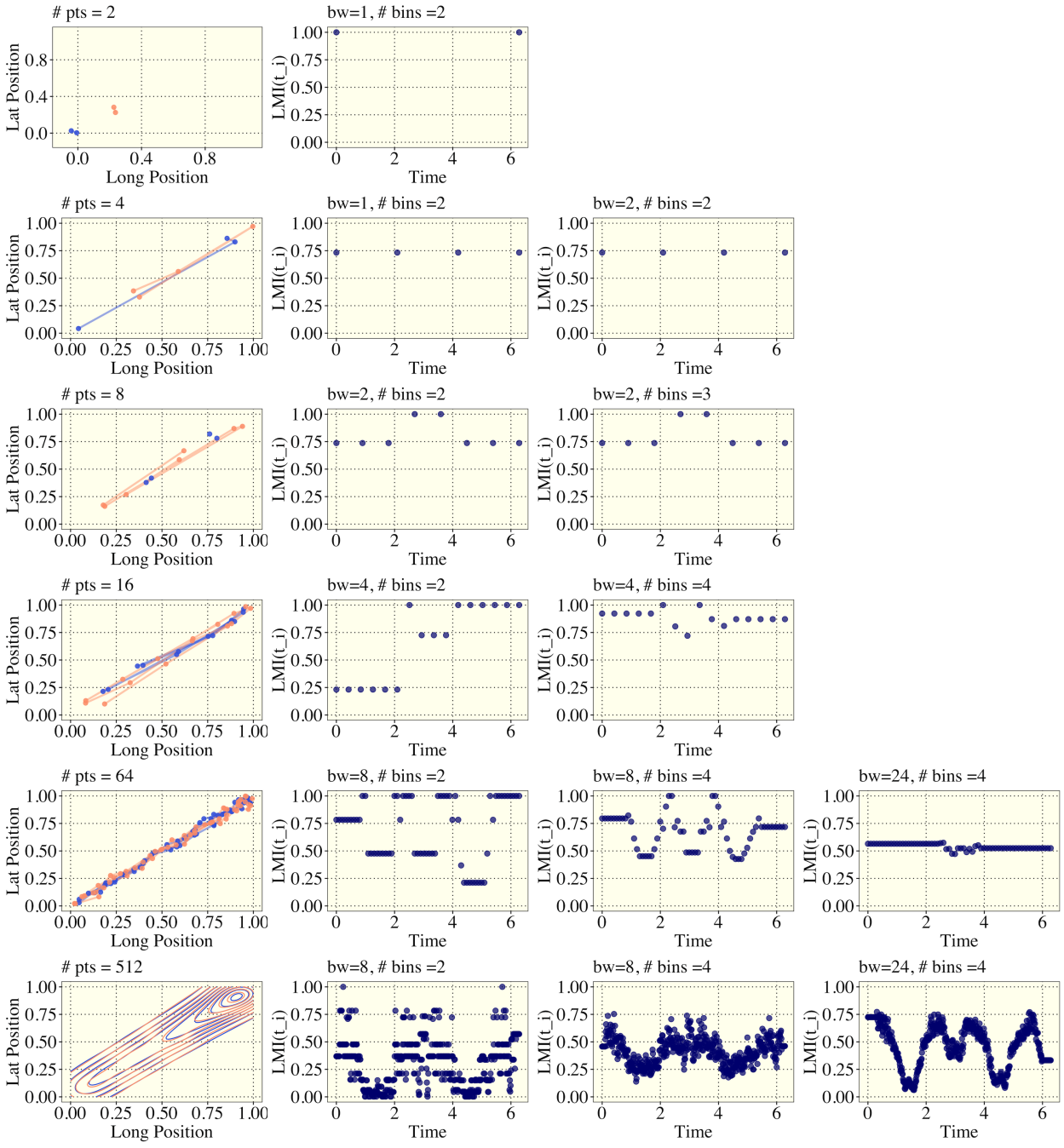

Figure 5.19: LMI Sensitivity to low temporal resolution for cyclical movement association. The first column is the animal movement path in $\mathbb{R}^{\not\perp}$, and the remaining columns are the computed LMI functions for an array of bandwidths and bins.

to consider 3 primary objectives: (1) the simulated movement must mimic the complexity of animal movement in residential/courtship and migratory states, (2) the simulated movement should also be simplified to a single transition period to clearly illustrate shifts in the implemented LMI measure, and (3) the proximity of the male-female pairs must be reasonably captured in the residential/courtship and migratory state. For the residential/courtship state, the following random walk model is proposed for both male and female jaguars:

$$\begin{cases} x(t_i) = sin(t_i) + \epsilon_{t_i x} & t \in [0, 30) \\ y(t_i) = cos(t_i) + \epsilon_{ty} \\ \epsilon_{t_i x} = \epsilon_{t_{i-1} x} + \omega_{t_i x} \\ \epsilon_{t_i y} = \epsilon_{t_{i-1} y} + \omega_{t_i y} \\ \omega_{t_i x} \text{ and } \omega_{t_i y} \underset{iid}{\sim} N(0, \sigma^2) \end{cases}$$

where $x(t_i)$ and $y(t_i)$ are the longitudinal and latitudinal position of the animal at time i, and ϵ is an autocorrelated error term associated with an animals movement at time i and $i-1$.

This is a simplification of the solitary, but often related, non-stationary movements of male and female jaguars during courtship. This period of time is marked by frequent periods of high co-occurrence potential with regular periods of separation. The modeled movement is circular by definition, but "drifting" movement is induced through the autocorrelated error terms ϵ_{t_i} which is an important consideration in modeling animal movement since deviations in foraging behavior may result in temporary or permanent shifts in movement trajectories. The initial condition/position of each jaguar is randomly instantiated within some arbitrary distance of the origin. As the movements of two jaguars under this simulated process will be marked by similar characteristics, the measure of LMI over this section of the time domain is expected to be high regardless of proximity.

In the following female migration state, the male jaguar will be set to continue his pre-

scribed territorial movement as detailed previously. The female's movement behavior, however, will immediately transition to a migratory state modeled by

$$\begin{cases} x_f(t_i) = x_f(t_{i-1}) + \alpha\epsilon_{t_ix} + \beta|x_m(t_i)| + \xi_{t_ix} \quad t \in [30, 60] \\ x_f(t_i) = y_f(t_{i-1}) + \alpha\epsilon_{t_iy} + \beta|y_m(t_i)| + \xi_{t_iy} \\ \epsilon_{t_ix} = \epsilon_{t_{i-1}x} + \omega_{t_ix} \\ \epsilon_{t_iy} = \epsilon_{t_{i-1}y} + \omega_{t_iy} \\ \omega_{t_ix} \text{ and } \omega_{t_iy} \underset{iid}{\sim} N(0, \sigma^2) \\ \xi_{t_ix} \text{ and } \xi_{t_iy} \underset{iid}{\sim} N(0, \sigma^2) \end{cases}$$

where x_f and y_f are the female's longitudinal and lateral position, and x_m and y_m are the male's longitudinal and lateral position which was generated from the first simulation model. This migratory model induces a repelling dependency between the male and female pair where the movement of the female is propelled based on the position of the male. The terms $\alpha, \beta = 0.01$ are scalars used to weight the value of the autocorrelated error term and the male position term to provide a realistic migration of the female that is not strictly linear since resource distribution and land cover may cause deviations from a direct straight-line migration away from her previous home range shared by the male. The initial condition for the female in this second time window, t_0, is set equal to the final position from the simulation generated for the first time window for the female to ensure that the generated path is a piecewise continuous process.

In Figure 5.20, the generated male and female movement models are shown in the three rightmost plots, and the autocorrelated error term progression is shown in the 2 leftmost plots. Both the male and female jaguar move in "drifting circles", and then the behavior transition of the female is stark and enduring for the remainder of the time domain. In the 60 day time period simulated, positions are generated every hour which yields 1440 points on the resulting time grid. In Figure 5.21, the LMI for their movement vectors

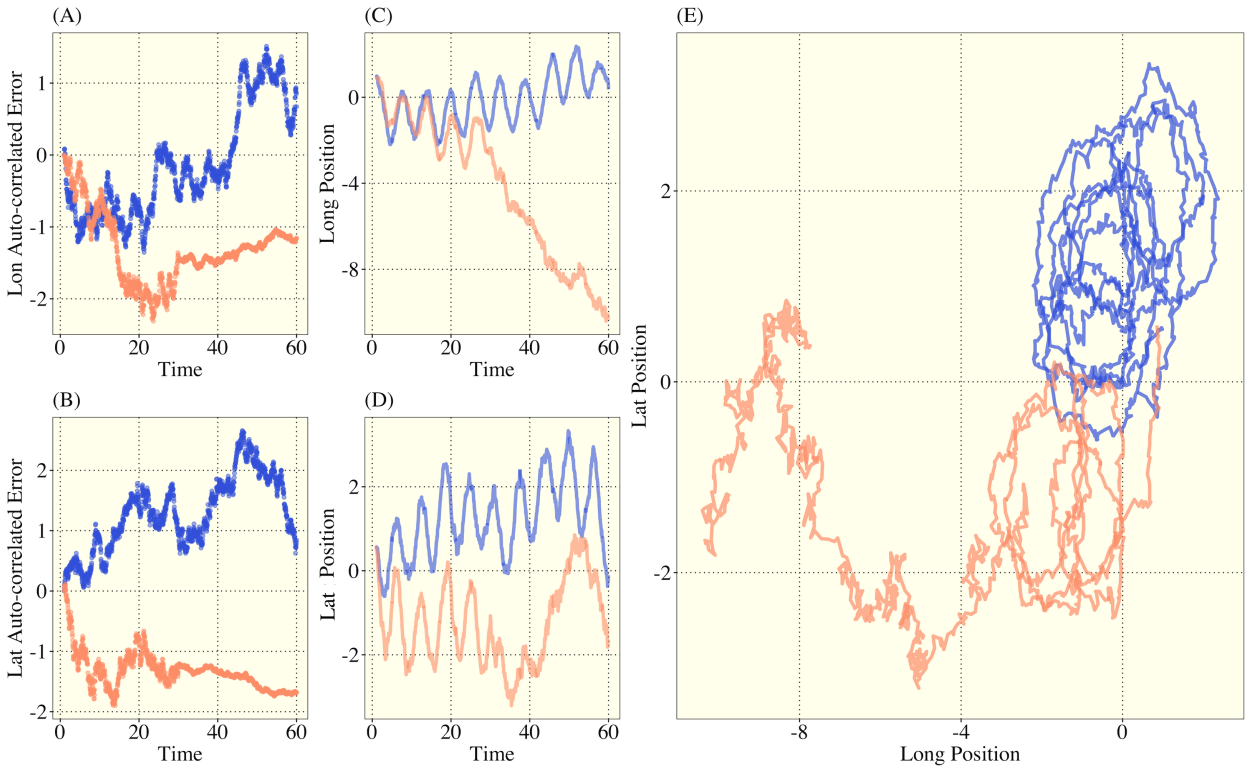

Figure 5.20: Simulated movement path for male (blue) and female (orange) jaguars with a behavior shift induced into the females movement at $t = 30$

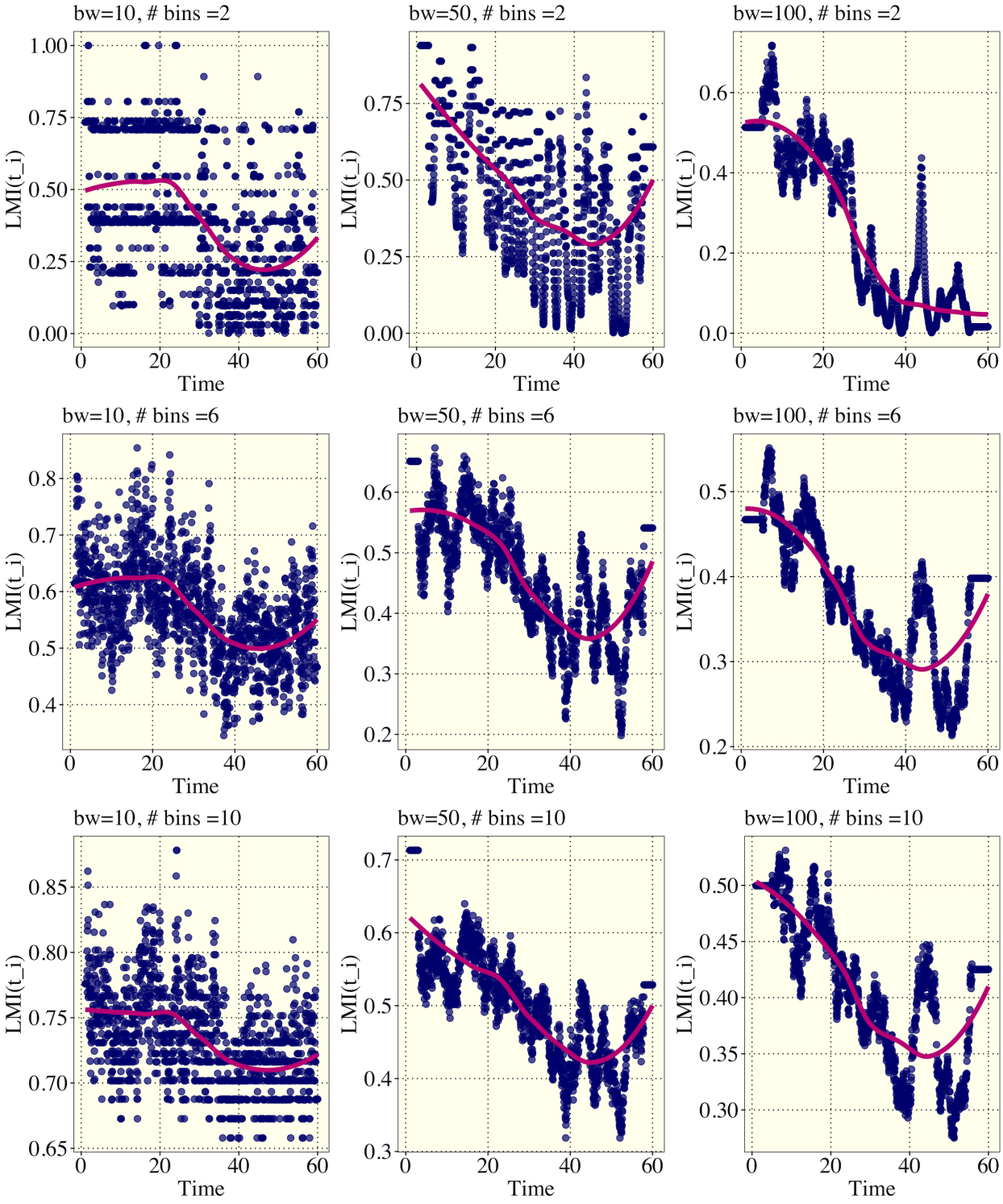

Figure 5.21: LMI function computed for an array of bandwidths and number of bins. The overlaid magenta line in each plot is a LOESS trend line.

is computed with $bw = 10, 50, 100$, and $bins = 2, 6, 10$. Recall that at any given time point t_i the maximum attainable LMI is computed, and then the joint LMI measure is then scaled with respect to the maximum potential LMI, where $LMI(t_i) = 0.00$ identifies that no information about the movement of one jaguar is detectable from the other, and $LMI(t_i) = 1.00$ identifies that all information contained in one jaguar's movement is detectable from the other. The final LMI functions have 1440 points which are all depicted with a locally estimated scatterplot smoothing (LOESS) overlay to discern trends in cases where over-plotting of points in apparent.

For all combinations of bandwidths and number of bins, the LMI measure successfully identifies strong association between the male-female pair during the time where both are in a residential state even though they are both subject to independently autocorrelated error terms. The LMI measure also successfully detects the shift in movement association. The detected shift in behavior is most apparent when increasing bandwidth and number bins, and the functional structure of the computed LMI functions is refined/de-noised. Of particular interest is the upper-right plot with $bw = 100$ and $bins = 2$. In this scenario, the drop in LMI is abrupt and bottoms out at exactly $t = 30$, where there is a "cusp-like" shift in behavior. With our prior knowledge of the abruptness of the induced shift in behavior, the LMI measure, with this choice of parameters, does an exceptional job at locating the sharp drop in movement association. As a reminder, $bw = 100$ indicates that the time window for each local measure of LMI is 200 hours, equivalently 8.3 days. All of the plots in the right most column shown declining association in 200 hour window LMI measures. There is a peculiar spike in LMI shown in these plots which can be attributed to the similar latitudinal behavior of both animals for approximately $t \in [40, 50]$. This can be seen in the bottom-center plot of Figure 5.20, where both the male and female have repeated instances where their latitudinal position is increasing in unison.

5.3 Summary of LMI Measure Characteristics

This work details a rigorous process of evaluating a new measure of association between GPS detected movement paths or estimated trajectories. I summarize the important details of this work with commentary when necessary.

1. Non-negativity, Symmetry: the LMI measure is shown by proof to be semi-positive definite and symmetric.

2. Monotonic relationship with ρ. Although shown for only normally distributed random variables, it is shown that increases in correlation between two variables also indicates an increase in the LMI measure. This would need to be shown for other distributions more generally in future work to confirm that this is true for a wider range of distributions from the exponential family.

3. Shift Detection: The LMI measure is an effective tool for detecting a shift in the association of animal movements even if the shift is functionally subtle. Shifts from monotonic to non-monotonic movement for only one of the animals yield large drops in movement association in the neighborhood surrounding such behavior.

4. Cross-directional association: Perhaps the primary disadvantage of the presently evaluated measure of LMI is the absence of cross-directional association detection. I propose a simple modification to the current measure that would address this disadvantage. The new measure is expressed by

$$\begin{cases} \mathcal{I}(t;\lambda) = \mathbb{I}_{\mathcal{L}_i}(X,Y|\lambda) \ \text{ with } \ \mathcal{L}_i = \{t|t \in [t_i - \lambda, t_i + \lambda]\}, \\ \text{where } \ \mathbb{I}_{\mathcal{L}_i}(X,Y) = \nu_i \times (I_{\mathcal{L}_i}(X_1,Y_1) + I_{\mathcal{L}_i}(X_2,Y_2)) + (1-\nu_i)(I_{\mathcal{L}_i}(X_1,Y_2) + I_{\mathcal{L}_i}(X_2,Y_1)), \\ \nu_i \in [0,1] \\ I(X_j,Y_j) = \int\limits_{\mathcal{X}\times\mathcal{Y}} \int p_{(X,Y)} log \frac{p_{(X,Y)}}{p_X(x)p_Y(y)} dxdy \ \text{ for } \ j = 1,2. \end{cases}$$

The terms in this model are not squared or square-rooted as in the measure of LMI defined in this project, which is not necessarily needed since the mutual information components used to compute LMI are shown to be non-negative. The critical modifications in this proposed measure are the incorporation of two additional cross-directional measures of mutual information for the relationship between animal 1 and animal 2's longitude and latitude respectively and vice versa. An important question of the value of cross-directional versus standard mutual information on a time window $\mathcal{L}_i$ is more important to detect and visual in the final outputted LMI function visualizations. The parameter ν could be defined uniformly across the full time domain to value cross-directional and standard LMI equally with $\nu = 0.5$ or with $\nu = 0, 1$ the standard or cross-directional LMI would be completely disregarded. The ν_i, corresponding to a specific time window $\mathcal{L}_i$, could be specifically set for certain portions of the time domain to up-weight cross-directional mutual information when (as an example) the aspect of the slope that two animals are on are estimated to be near perpendicular.

5. Delayed Onset tracking movement: The LMI measure is an appropriate tool for detecting following or path-tracing/tracking behavior. This attribute of the measure will have practical uses in monitoring larger volumes of animal migration data and predator-prey dynamics, as well as human-animal interaction applications in cases, where human movement/transportation can be tracked over the same time period.

6. Tuning Parameters: Giving the user parameters to subjectively tune could be considered a disadvantage, but we argue against this notion as it is an opportunity for the researchers, implementing such a measure, to use field expertise to adjust the measure to the application or behavior of interest. A researcher may be particularly interested in *short-time correlations* (correlations measured over a few days or weeks) or *long-time correlations* (perhaps measured over months, seasons, or even years). Our approach allows researchers to consider either with minor adjustments to the input parameters

for the measure The parameters are not abstract: *bandwidth* controls the size of the temporal neighborhood used to measure correlation between animals at a given time, and *number of bins* controls the complexity of discretized movement over that same neighborhood. As mention in (4), locally adaptive parameters would be an interesting extensions of this measure.

As a whole, this work justifies the use of bandwidth derived correlation functions. Mutual information is a highly flexible measure of association that can handle violations of monotonicity that challenge the use of Pearson and Spearman correlation measures. I return to our ultimate proposed question: What does correlation mean in animal movement? Correlation is ultimately a measure of dissimilarity of two processes or observational units. In movement ecology, any characteristics that make the movements of animals more similar should be detectable by some dissimilarity metric. Correlation in movement paths or trajectories should be a flexible idea, and there should be several types of movement behaviors that are identifiable prior to a full statistical modeling process. In any standard regression analysis it is common practice to examine a correlation matrix of predictor and response variables and the variance inflation factor. We should model this process in movement ecology by considering metrics that detect association between movement trajectories of all animals in the study. I emphasize that this notion of dissimilarity is a means as opposed to an end objective. Dissimilarity measures are a vital tool in modern statistical modeling, especially unsupervised machine learning and spatial statistics.

I encourage the prescribed use of this measure, and more importantly, I encourage others to challenge the understanding of movement association in telemetric data analysis laid out in this work.

6 Smoothing Splines of Apex Predator Movement: Functional Modeling Strategies for Exploring Animal Behavior and Social Interactions

The work in this section has largely been published in *Ecology and Evolution*, and ideally the work in this section should be referenced using the following citation:
Whetten A.B. (2021). Smoothing Splines of Apex Predator Movement: Functional Modeling Strategies for Exploring Animal Behavior and Social Interactions. *Ecology and Evolution*. Vol 20 (Issue 11). DOI: 10.1002/ece3.8294

6.1 Summary/Abstract

The collection of animal position data via GPS tracking devices has increased in quality and usage in recent years. Animal position and movement, although measured discretely, follows the same principles of kinematic motion, and as such, the process is inherently continuous and differentiable. I demonstrate the functionality and visual elegance of smoothing spline models. I discuss the challenges and benefits of implementing such an approach, and I provide an analysis of movement and social interaction of seven jaguars inhabiting the Taiamã Ecological Station, Pantanal, Brazil, a region with the highest known density of jaguars. In the analysis, I derive measures for pairwise distance, co-occurrence, and spatiotemporal association between jaguars, borrowing ideas from density estimation and information theory. These measures are feasible as a result of spline model estimation, and they provide a critical tool for a deeper investigation of co-occurrence duration, frequency, and localized spatio-temporal relationships between animals. In this work, I characterize a variety of interactive relationships between pairs of jaguars, and I particularly emphasize the relationships in movement of two male-female and two male-male jaguar pairs exhibiting highly associative relationships.

6.2 Introduction

Technological advancements in remote sensing of animal movement, referred to as animal telemetry, have revolutionized the discipline of movement ecology. Animal movement data provides critical information about ecological processes, and it can be a vital asset to conservation efforts of species and ecosystems. The increased feasibility of tracking and collecting animal movement information has yielded large reservoirs of fine-scale spatio-temporal data, and the challenges of meaningfully modeling animal behavior have resulted in the expansion of holistic machine learning methodology that appropriately considers animal psychology and cognition [7, 5, 2].

The analysis of animal telemetry data has a number of challenges. (1) Spatial and temporal density of measurements is subject to extreme variation. Animal behaviors may shift phenologically between migratory and residency states, and even for non-migratory species, this problem can present itself in a smaller scale region as animals shift between resting, foraging, or transit states. Temporal density variation may be caused by loss of connection, malfunctioning, and damage of the device over time. (2) Even with advancements in precision and reliability of animal tracking, the datasets are inherently discrete, and any analysis of such data requires a conscious choice between modeling such processes discretely or attempting to model them continuously. (3) Animal behavior cannot be univariately characterized. Animal movement is characterized by position, rate of change of position, and co-occurrence with other animals, all of which may suddenly shift under interactions with an array of environmental factors that alter the allocation of critical resources for survival [5, 2].

Discrete time methods have had steady use in the field [8, 9, 10, 11], but recent literature has provided significant progress in continuous-time modeling [12, 13, 14, 15]. Animal movement is explicitly continuous, like any kinematic process, and continuous-time models celebrate and take advantage of this continuity in the modeling process. These models are

exceptional and flexible tools for modeling the complexity of animal movement. However, I emphasize that we should more fully embrace animal movement as a kinematic process. We must acknowledge that projectile movement in a real space $\mathbb{R}^d$ is smooth, and I propose that we further consider modeling strategies and methodological developments that account for the 1st and 2nd order differentiation of a animal movement processes.

I present a philosophically different approach for analyzing animal telemetry in which the unit of analysis is a curve (or function) as opposed to single site measurements. This approach, widely referred to as functional data analysis (FDA) roots in the assumption that measurements vary over some continuum such as space or time, and that there is an underlying smoothness inherent to the process of interest [44, 45, 52]. The assembly of an entire smooth curve of an animal's movement is accomplished using linear combinations basis functions which are the foundation of smoothing spline models. They are widely acclaimed for their ability to model complex and noisy data [44].

Animal movement is a visual spectacle, and the statistical visualization of animal movement is greatly aided using smoothing splines. FDA methods provide a viable and accessible option for examining an estimated complete path and the speed and acceleration (and deceleration) along this path, which are vital in the classification of various types of animal behavior. There have been recent basis function models proposed to model animal movement [7, 53, 54, 55, 56], but there is great need to incorporate a wide array of strategies for an appropriate and application-specific exploration using smoothed spline models.

In this project, I analyze and visualize the movement of seven Jaguars inhabiting the Taiamã Ecological Station, Pantanal, Brazil and the associative and co-occurrence relationships between them. Fine-scale movement of jaguars in this region has recently been explored using association rule mining algorithms to study their behavior and social interaction. Identifying behavioral changes and social interactions are crucial aspects of species ecology, and this recent work has added to literature of jaguar territory sharing [19]. Jaguars are generally solitary and territorial apex predators, but in areas with high primary productivity, the

overlap of territory and its effects on mating, cooperation, and competition yield a complex system of interdependent subjects that can directly or passively interact [19, 57, 58].

I construct smoothing spline models to continuously and differentiably characterize the movement, resting, and migratory behavior of these 7 jaguars. These smoothing spline models provide exceptional fit, and they provide the means to feasibly measure animal association using a measure of mutual information from the discipline of information theory. Further, I introduce the concept of a *Co-occurrence Potential Plots* which are smooth density functions derived from the distance between pairs of jaguars on the refined and unified grid. The refinement and unification of the time-grid is an inherent and advantageous by-product of spline models.

In efforts to improve upon the previous work in Fontes et. al., this analysis accomplishes two primary objectives: (1) An estimation of co-occurrence potential which has a conservative theoretical standing in the presence of measurement error for lower raw time resolution and allows for inferences to be made between observations on the raw time grid, (2) A derivation of a correlation function based on animal movement, which captures shifts in the associations between individuals. In (1), the conservative theoretical nature of this measure refers to the difference between co-occurrence potential and co-occurrence frequency, where co-occurrence frequency is a count of the amount of times that two animals occur within a certain spatial and temporal radius, and co-occurrence potential is a measure of the density of time values on a time grid where two animals are within a radius where there is high probability of co-occurrence based on the ability of the animals to interact in between time observations. The use of a density measure, such as co-occurrence potential, can be more conservative since the constructed probability density function identifies time periods where interaction is more likely as opposed to a simple count of time points. This application of FDA methods to animal movement showcases the plausibility of studying animal movement with the theoretical backing of the laws of kinematic motion, and most importantly, the approach provides an increased set of tools to improve the study animal movement in relation

to dynamic social and environmental factors.

In this project, it is important to acknowledge that measurement error is not considered since this attribute was not recorded in the public version of the data product. The exact specifications of the utilized GPS tracking devices and a disclaimer regarding the data quality are detailed in the following section. FDA methods exists to address measurement error for various disciplines [7, 59, 60], and I leave this important and interesting aspect of animal telemetry to future work.

6.3 Methods

Fitting smoothed spline models, provides a number of advantages for irregularly and sparsely measured data that is known to vary over some continuum, but it is important to note that some sacrifice of position is made in a model that aims to smooth a function through a series of measurements [44]. More specifically, smoothing spline models differ from interpolation models since the objective of interpolation is to fit a function that crosses through all recorded measurements of a process with an error of zero, where as for smoothing splines, the objective is to fit a simpler function that captures the main features of the process while minimizes the error between the optimal function and the recorded measurements. Generally, smoothing splines are more informative as they prevent over-fitting to noise in the raw data which can obscure critical features of a process. Since GPS positioning systems have known measurement error (even though measurement error is not reported in this data product), I aim to show that this sacrifice is worth the benefits of this approach, and further that modifications to the model can be instated to adapt and improve this approach.

6.3.1 Fitting Smoothed Spline Models to Jaguar Movement

For a collection of raw hourly recordings of a single jaguar's position, denoted by $Y_{lat} = [y_{lat\,1} \dots y_{lat\,n}]$ and $Y_{lon} = [y_{lon\,1} \dots y_{lon\,n}]$, I estimate $\hat{x}_{lat}(t) = \sum_{k=1}^{K} c_{lat\,k}\phi_k(t)$ and $\hat{x}_{lon}(t) =$

$\sum_{k=1}^{K} c_{lon\ k}\phi_k(t)$ subject to a roughness penalty on the second derivative of the basis expansion $\Phi = [\phi_1(t) \dots \phi_K(t)]$ where c_k are the coefficients of the terms of the basis expansion denoted by ϕ_k, which in this project is constructed using a B-spline basis expansion [44, 46]. Both latitude and longitudinal movement can be individually expressed as an unconstrained minimization defined by

$$\underset{\overrightarrow{c}}{min} \| \overrightarrow{y} - \Phi \overrightarrow{c} \|^2 + \lambda c^T R c \quad for \ \ \lambda \geq 0, \tag{6.1}$$

where $R_{jk} = \sum_{l=1}^{M} \phi_j''(\tilde{t}_l)\phi_k''(\tilde{t}_l)h$ for $h = \tilde{t}_l - \tilde{t}_{l-1}$ and the value M is the number or time points on a fine time grid $t_1, \dots, t_M$. [44].

We select an appropriate value for λ using the optimal lambda for a single site determined by the generalized cross-validation criteria, $GCV = \frac{MSE(\lambda)}{(1-\frac{df_\lambda}{M})}$ where $df_\lambda = trace(S)$. The GCV criterion is derived from the mean-squared error penalization criterion for the spline model defined by

$$MSE(\lambda) = \frac{\| \overrightarrow{y} - \Phi \overrightarrow{c} \|^2}{M - df_\lambda} \tag{6.2}$$

For jaguar movement, I have fitted the spline models with low or negligible roughness penalization, since the precision of movement is of high priority. The roughness of the movement can also be restricted by latitude and longitude separately which may be on interest if we seek to model movement with substantial differences in between latitudinal and longitudinal behavior (such as long distance ungulate or bird migration), but for this work the roughness is penalized equally for both dimensions. The resulting smoothed jaguar movement curves have the form

$$\hat{x}_{lat} = \Phi(\Phi^T\Phi + \lambda_{lat}R)^{-1}\Phi^T \overrightarrow{y} = S_{lat}\, \overrightarrow{y}_{lat}. \tag{6.3}$$

$$\hat{x}_{lon} = \Phi(\Phi^T\Phi + \lambda_{lon}R)^{-1}\Phi^T \overrightarrow{y} = S_{lon}\, \overrightarrow{y}_{lon}. \tag{6.4}$$

The jaguar's 2-dimensional movement is then characterized by coordinates on the path $(\hat{x}_{lon}(t), \hat{x}_{lat}(t))$ which has been done similarly in recent work [7, 61]. I note that Equations (2) and (3) jointly characterize a two-parameter search for λ_{lat} and λ_{lon}. In all cases, although an optimal GCV criterion can be detected, some additional tuning by visual inspection was performed, and this is a common practice when constructing spline models to ensure that critical shifts in animal position are being correctly captured by the model. With a GPS tracking device of sufficient resolution, critical shifts in behavior should be discernible in the presence of measurement error, and because of this it is important to not rely solely on an optimization criteria when fitting such a model. Over-fitting permits too much roughness in the model which ascribes measurement error to ecological behavior, and under-fitting ascribes actual movement to measurement error.

In order to meaningfully estimate jaguar position across highly disparate densities of raw time recordings, careful placement of knots is advised. Let $(t_1, \ldots, t_n)$ be independently and identically distributed time samples from an unknown distribution f_h. We estimate the density of sampled times for a given jaguar using kernel density estimation defined by $\hat{f}_h(t) = \frac{1}{nh} \sum_{i=1}^{n} K(\frac{t-t_i}{h})$, where K is gaussian kernel function and h is a smoothing bandwidth parameter where higher values of h yield a smooth estimate of the density [62]. Let $k = \hat{f}_h(t^*)$ be selected as a threshold where t_i with $\hat{f}(t_i) > k$ define the collection of high density times $\{t_i | \hat{f}_h(t_i) > k\} = (\tau_1, \ldots, \tau_m)$ where $\tau_1 < \ldots < \tau_m$. This selection of knots is carefully placed to avoid over fitting regions of the time domains that are barren or extremely sparse. This is desirable for periods where GPS tracking devices are out-of-operation for an extended period, but it is still desirable to fit regions with dense recordings with high precision.

As a part of this dissertation, we assess the sensitivity of the (automatic) density-based knot placement method described above. The assessment of this method was done for 2 of the jaguars used in the remainder of this work (Jaguar 12 and Jaguar 81). This can be found in Appendix 7.3.

Continuous-time estimation of distance and speed has been developed for standard con-

tinuous time models [63]. In the next two sections, I outline a derivation of speed and distance measures for animal movement in the FDA paradigm.

6.3.2 Differentiation of the Smoothed Position Functions and Derivation of Rest Period Density Functions

Differentiation of the smoothed position paths is then conveniently estimated using the same collection of coefficients, $\overrightarrow{c}_{lat}$ and $\overrightarrow{c}_{lon}$, and the derivation functions are defined by

$$\hat{x}'_{lat}(t) = \sum_{k=1}^{K} c_{lat\,k}\phi'_k(t), \quad \hat{x}'_{lon}(t) = \sum_{k=1}^{K} c_{lon\,k}\phi'_k(t) \tag{6.5}$$

where $\phi'_k(t)$ is the derivative of the basis expansion [7, 44, 64].

The estimated speed of jaguar position can then be defined by $\hat{x}'(t) = \sqrt{(\hat{x}'_{lat}(t))^2 + (\hat{x}'_{lon}(t))^2}$. Behavioral states of animal movement are generally characterized by different speed of movement. As an example a resting state should be characterized by lower estimated speeds while migratory, foraging, and other transitory states are characterized by faster speeds. For this project, I used a speed of 0.25 meters/second as a cutoff between resting and transit states. Clearly, a literal resting state should have a derivative value of zero, so in this application resting state has a looser interpretation that characterized by stationary and exceptionally small changes in position. Similar to before, I subset "resting state" times and derive a kernel density function for the distribution of resting times, $\hat{f}_h(t) = \frac{1}{nh}\sum_{i=1}^{n} K(\frac{t-t_i}{h})$, where K is Gaussian kernel function and h is a smoothing bandwidth parameter where $t_1, \ldots, t_n$ are restricted to the set $\{t_i |\, \hat{x}'(t) < 1\}$.

6.3.3 Pairwise Jaguars Distance Functions and Derivation of co-occurrence Potential Plots

For any pairs of jaguars, J_1 and J_2, with geographic position monitored on the domain $[a, b]$ and $[c, d]$, respectively, with $a < c < b < d$, a distance measure can be defined between pairwise estimations of position on the refined regular time grid $t_1, \ldots t_p$ where $c = t_1$ and $b = t_p$, and the distance metric in this work is the WGS84 ellipsoidal distance [65]. This regular time grid is subsetted from the refined global time grid used to smooth jaguar position; in this work the refined grid provides an estimate of position every 60 minutes. Although not finer than the raw grid, this grid resolution was chosen since already provides extensive interpolation of missing hours, and the smoothed spline model are smaller in size. The choice of time grid is arbitrary in the FDA paradigm, and it can be readily refined to a desired resolution. As an example, the smoothed spline models implemented in this project could be refined to provide 1 minute estimations, and they would still follow the same smoothed path defined on the selected resolution. There may be clear advantages to estimating movement on this resolution, but this is a question that will be left to future work.

co-occurrence potential in this work is defined as a density function of times from the refined and unified time grid where the distance between a 2 or more jaguars is within a certain threshold. This work only examines pairwise co-occurrence potential, but I discuss the extension to greater than two jaguars in the Discussion Section. More specifically, I define the co-occurrence potential function by $\hat{C}_h(t) = \frac{1}{nh} \sum_{i=1}^{n} K(\frac{t-t_i}{h})$, where K is Gaussian kernel function and h is a smoothing bandwidth parameter where $t_1, \ldots, t_n$ are restricted to the set $\{t_i |\ dist(\hat{x}_{J1}(t_i), \hat{x}_{J2}(t_i)) < \delta\}$. The parameter δ is a distance threshold, and co-occurrence potential for this application is set to $\delta = 1800m$. This indicates that times where a pair of jaguars are estimated to be within this threshold have a high probability of (either passive or direct) interaction [66]. This threshold is chosen with the intent to only capture time periods where a high probability of interaction is possible. Higher co-occurrence potential implies

that there is a larger volume of times on the refined time grid where a pair of jaguars are in close proximity indicating that there is the potential for an interaction. In previous work, co-occurrence frequency is defined on the raw time grid for times where a pair of jaguars were within 200m to 400m of each other. The raw time grid in this work records positions of jaguars at a maximum of every hour. Within an hour time-window, it is apparent that jaguars can travel far beyond 200m to 400m since an animal walking slowly at 4 kilometers per hour in a straight-line can cover 10 times the distance of 400m in an hour.A threshold distance of 1800m is too far to imply direct interaction at a given time, however, there is a probability that two jaguars can interact with each other in between known or estimated positions. For this reason, it is still instructive to compute the density of times where jaguars fall within a larger radius than 400m.

6.3.4 Mutual Information of Jaguar Movement

Mutual information is a measure of mutual dependence between two random variables, or more simply, the amount of information gained about one variable by observing the other [28]. Let (X, Y) be a pair of random variables with values spanning the space $(\mathcal{X} \times \mathcal{Y})$. The mutual information between two jointly continuous random variables X and Y is defined by

$$I(X;Y) = \int_{\mathcal{Y}} \int_{\mathcal{X}} p_{(X,Y)}(x,y)\ log \frac{p_{(X,Y)}(x,y)}{p_X(x)p_Y(y)} dxdy \tag{6.6}$$

where $p_{(X,Y)}$ is the joint probability density function of X and Y, and p_X and p_Y are the respective marginal density functions. It is clear that if X and Y are independent then information gained from observing one of the random variables does not provide information about the other, and recall that for independent random variables, $p_{(X,Y)}(x,y) = p_X(x)p_Y(y)$, which implies from Equation (4) that $I(X;Y) = 0$ [28].

To measure dependence or strength of association between pairs of jaguar movements, it is clear that a global measure of mutual information is insufficient to measure correlation

between jaguars since their relationships may be dynamic and shifting. I propose the use of the localized mutual information measure $I_{\mathcal{L}}$. Other localized mutual information measures have been derived for various applications [30, 38, 39]. In this work, $I_{\mathcal{L}}$ is defined by

$$I_{\mathcal{L}}(X;Y) = \int_{\mathcal{Y}_{\mathcal{L}}} \int_{\mathcal{X}_{\mathcal{L}}} p_{(X_{\mathcal{L}},Y_{\mathcal{L}})}(x,y)\ log \frac{p_{(X_{\mathcal{L}},Y_{\mathcal{L}})}(x,y)}{p_{X_{\mathcal{L}}}(x) p_{Y_{\mathcal{L}}}(y)} dxdy \tag{6.7}$$

where $\mathcal{X}_{\mathcal{L}}$ and $\mathcal{Y}_{\mathcal{L}}$ are restrictions of the random variable to the domain defined by the set $\mathcal{L} = \{t | t \in [t_i - \lambda, t_i + \lambda]\}$. The parameter λ defines the bandwidth or radius over which local mutual information is measured.

Ultimately, the advantage of this approach is to construct a bivariate measure of mutual information, and finally to generate a mutual information function with respect to time. For two bivariate random vectors $X = (X_{lat}, X_{lon})$ and $Y = (Y_{lat}, Y_{lon})$, I define joint local mutual information by

$$\mathbb{I}_{\mathcal{L}}(X,Y|\lambda) = \sqrt{I_{\mathcal{L}}(X_{lat};Y_{lat})^2 + I_{\mathcal{L}}(X_{lon};Y_{lon})^2}. \tag{6.8}$$

Clearly, various weighting schemes for combining local mutual information for latitude and longitude could be derived. (Also, since the measure of mutual information is measured from the center of a interval, it may be advantageous to weight the contribution of realizations of a random variable in the mutual information computation based on their proximity to the center of the interval although this is not explored here.) Finally, I define the joint local mutual information function with respect to time by

$$\mathcal{I}(t;\lambda) = \mathbb{I}_{\mathcal{L}_i}(X,Y|\lambda). \tag{6.9}$$

where $i = 1, \ldots, dim(\overrightarrow{t})$ and $\overrightarrow{t}$ is the vector of times from the refined time grid. It is important to note that in this application the values of t are limited to the defined resolution of the spline model. So each time t_i is associated with a given $\mathcal{L}_i$, and as such, the pair $(t_i, \mathcal{L}_i)$ defines a centered window $\mathcal{L}_i$ over which $\mathcal{I}$ is evaluated at a given time t_i.

This derived result can be used to monitor periods of time where high and low correlation between a pair of jaguars is observed, and it provides a tool for monitoring if periodicity in the strength of their relationships exists. An example we might look for would be strength of relationships in movement between a male-female pair of jaguars during and between potential mating periods. Ecologically, higher mutual information indicates that there is a stronger association of movement since more information about the movement of one jaguar is explained by the movement of the other.

I also note other methods that have been developed in recent years to model social interactions within the movement model as opposed to the post-hoc measures of distance, co-occurrence potential, and correlation of movement (as measured by mutual information) [67, 68]. Although several advantages exist in the use of such methods which rely on continuous-time and non-parametric smoothing models, there remain important advantages of the use of semi-parametric smoothing models (as are used in this paper) [69].

6.3.5 Data: Taiama Ecological Station Jaguar Movement Data

I add to the the previous investigation of movement and social interaction of a collection of jaguars in the Taiamã Ecological Station, Pantanal, Brazil. The majority of jaguars examined in this project were fitted with Lotek GPS Iridium satellite collars and monitored for periods of 60 to 591 days [71]. The movement of Jaguar 88 was monitored using a Lotek GPS GlobalStar satellite collar. The authors of the study have made it public and freely available at DOI: 10.1002/ecy.2379 and also at Dryad Digital Repository (https://doi.org/10.5061/dryad.2dh0223). In this project, I utilized data from the full monitoring periods on 7 jaguars from this region, and Table 6.1 presents the number of recordings

and the length of the monitoring period. The finest temporal resolution of the data is on hourly intervals, however there are frequent gaps in recordings where missing measurements may be present for 2 hours to several days. It is important to disclaim that the authors of this data did not provide an estimated or empirically computed measure of error radius associated with each position. Instead, they have reported a dilution of precision of less than 10 which provides moderate to good levels of confidence in animal position. Dilution of precision refers to the quantification of error propagation in satellite navigation on the precision of estimated position [70]. Previous work using this data product has also not incorporated the use of measurement error [19, 71, 72]. Animal movement data with an unreported measurement error is not ideal, but the aim of this project expand on previous analysis in an effort to provide further understanding of jaguar behavior and interaction. Their findings on jaguars in this region were accomplished by measuring and studying the co-occurrence and correlation between several pairs of jaguars. Using trajectories and association rule mining algorithms and a distance radii of 200m and 400m, they were able to estimate co-occurrence frequency and a single correlation metric for each jaguar pair [19]. Following the results section, I discuss the differences between this analysis and previous work which primarily pertain to the differences between coocurence frequency and co-occurrence potential and quantifying the correlation between pairs of animals.

The jaguars examined in this project were selected on the condition that they shared an overlapping monitoring period with at least one jaguar from the monitoring period with the highest activity monitoring period from December 2014 to the summer of 2015. The final and more detailed investigation of social interactions is performed for Jaguars 12, 13, 18, 41, and 81.

For all visualizations used in this work, I numerically transform to time in days from the earliest available date 10/9/13 for Jaguar 88. As such $t = 0$ is the first day recorded for Jaguar 88, and the final day on this scale is $t = 591$ when the final measurement on Jaguar 13 is recorded, 08/24/15. This is particularly useful for monitoring periodicity and duration

Table 6.1: Monitoring statistics of Jaguars from the Taiamã Ecological Station

Jaguar Local ID	Frequency	Monitoring Period
12	2681	12/5/14 to 4/18/15
13	5040	12/7/14 to 8/24/15
18	2314	11/29/14 to 4/13/15
22	4709	9/11/14 to 5/21/15
41	4952	12/5/14 to 8/17/15
81	10988	10/15/13 to 5/29/15
88	1296	10/9/13 to 4/20/14

of events, since it is difficult to quickly understand the number of days or weeks between two dates.

6.4 Results

The primary challenge in mapping and analyzing relationships between Jaguars at the Taiama Ecological Station is the staggered time windows that each Jaguar is monitored coupled with the inconsistent temporal resolution of GPS readings. To reach our final selection of 7 jaguars, we removed two jaguars with less the 100 GPS recordings and two jaguars (Jaguar 91 and 92) that were monitored many months after the remaining jaguars (Jaguar 116 and 117). There are 3 females (Jaguars 12, 41, and 88) and 4 males (Jaguars 13, 18, 22, 81). I visualize the remaining 7 jaguars in Figure 6.1. Across the three plots provided, we can develop a short narrative of a few major movement characteristics. Within their respective time domains, most of the 7 jaguars have stable fluctuations in position within their territories (with some clear overlap in territories)[19, 75]. However, Jaguar 81 (male, age=4yrs), the jaguar with the longest monitoring window, makes a significant territorial transition from residing in the same region as Jaguar 88 (female, age=5yrs) to the territory of Jaguar 12 (female, age=4yrs). There appears to be a period of interaction between Jaguar 12 and Jaguar 81, and then Jaguar 12 makes a temporary but significant migration south for approximately 3 months before returning to the same region again as Jaguar 81. There are other male-female interactions that not as easily discernible, and more investigation is clearly required.

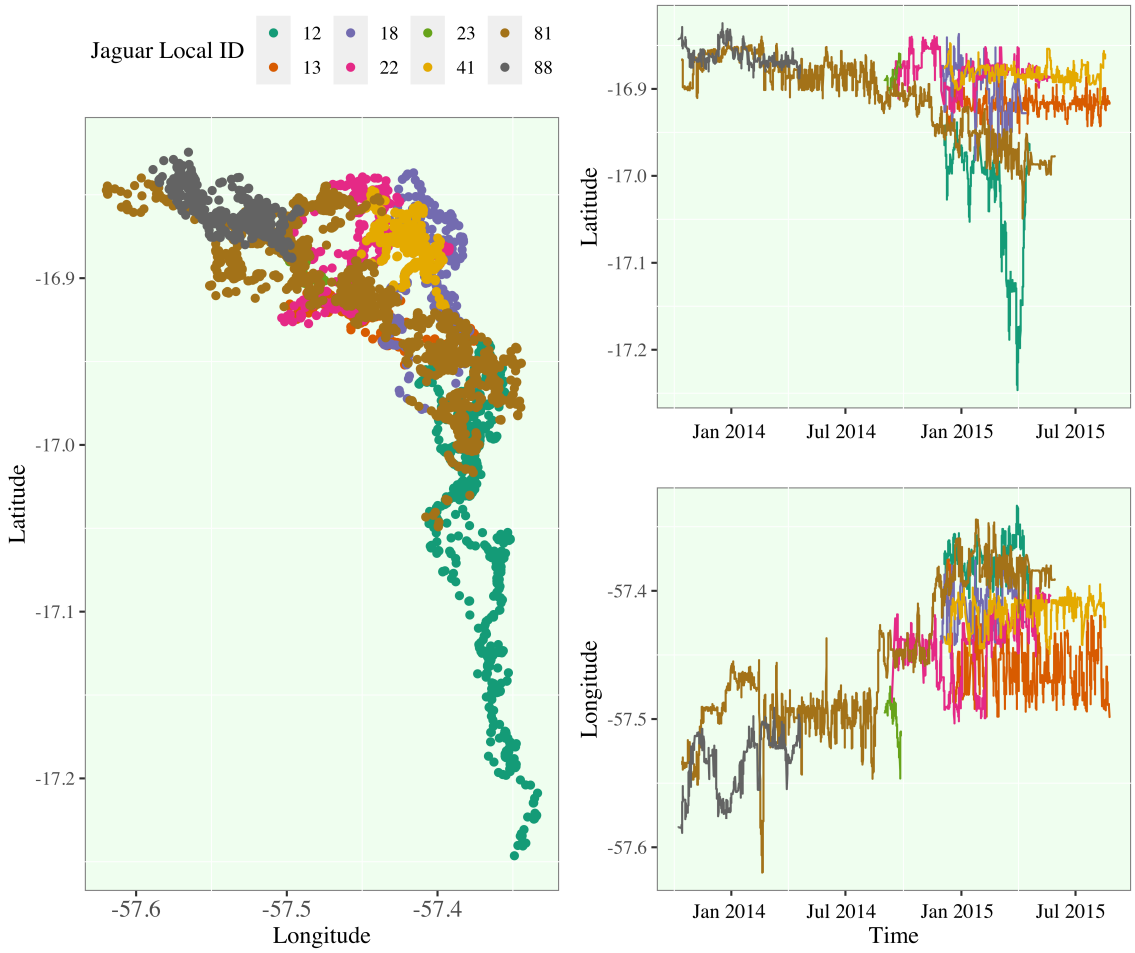

Figure 6.1: Visualization of Jaguar Movement in the Taiamã Ecological Station. (Left) The spatial distribution of GPS recordings is plotted and colored by Jaguar ID. (Right) The temporal change in each Jaguar's latitudinal and longitudinal position [73, 74]. A terrain map of this region is provided in the published work [40]

In Figure 6.2, I present a detailed visualization of the smoothing of Jaguar 12's residential to migratory transition. As a can be seen visually, the fit of this spline model is exceptional and only a small selection of points are not well fit to the estimated path. This is an acknowledged sacrifice of information, in exchange for a number of benefits, primarily the refinement of the time resolution and consistency to a uniform time grid shared by all jaguars. In Figure 6.3, I present the smoothed spline models for the remaining seven jaguars. Further tuning of the model for Jaguar 41 and 88 should be considered as some raw locations are not well-estimated, but Jaguars 13, 18, 22, and 81 have exceptionally well fit models. A well-fit model loosely refers to a spline model that captures the raw movement path with reasonable accuracy from a visual inspection, and few positions are poorly estimated. The remaining jaguars have some points that the spline models did not fit as well under the general temporal density distribution procedure for knot placement documented in the methods section. There are some cases where it appears that the spline model "overshot" the path when an animal changed direction suddenly, or where there were a couple outlier points that the algorithm did not prioritize fitting. When optimizing a spline model overall minimization of the error is prioritized as opposed to local minimization of the error. Improvements to the models could be achieved by increasing knot densities in regions where it appears that the model is not fitting as well as other regions or deriving a localized spline modeling procedure that performs piecewise error minimization; these options are left to future work. We will use these models as is, since the deviations from the raw movement path are still limited, and most of movement profiles from these jaguars are well captured, meaning that the model is estimating a smoothed path through the majority of raw positions while avoiding overfitting to the exact positions in the raw data. All smoothing spline models have been smoothed to estimate behavior on a 1 hour resolution.

In Figures 6.4 and 6.5, I present the first derivative functions of the each jaguar's movement, as well as, the density of rest periods. Rest periods are defined (with some level of arbitration that is worthy of discussion) as times when the estimated speed of a given

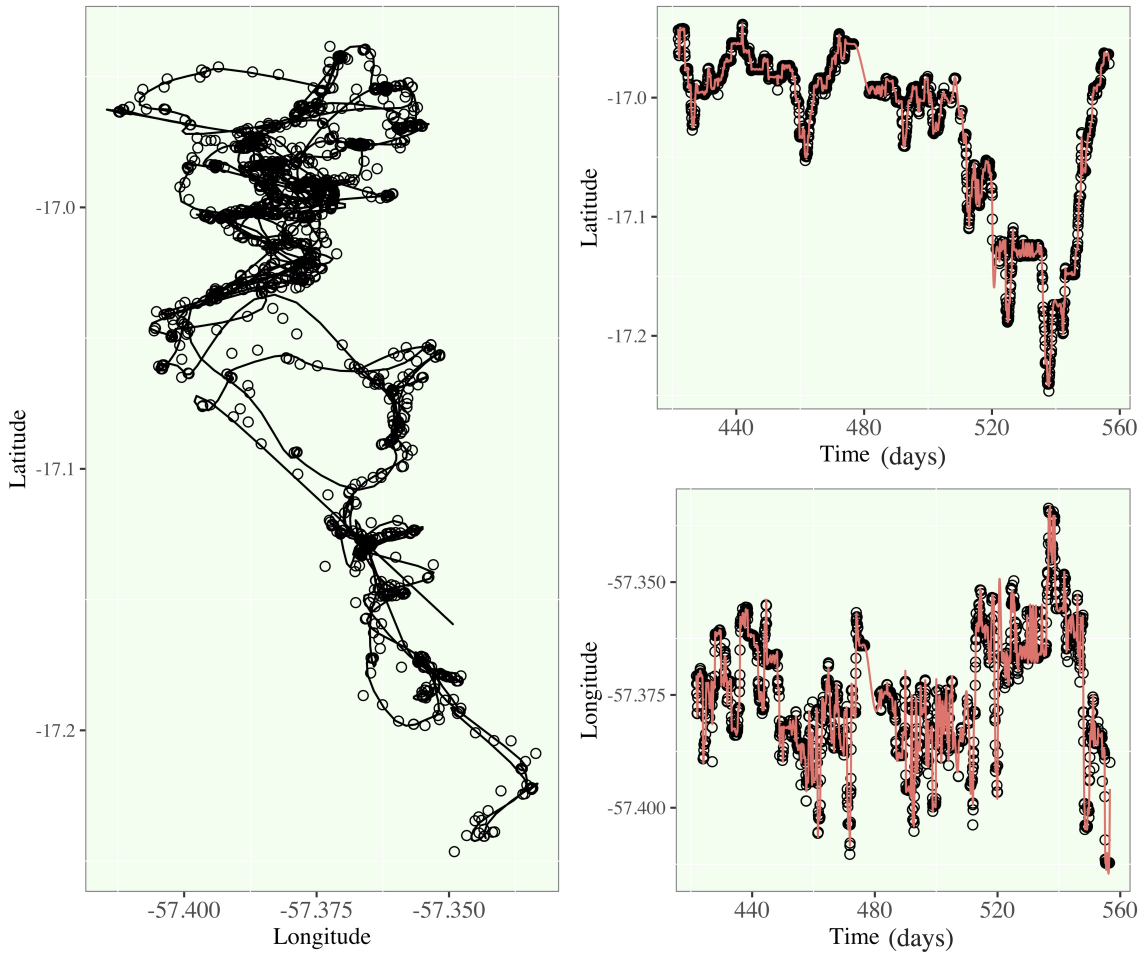

Figure 6.2: Smoothing Spline Model for Jaguar 12 (female, age=4). (Left) The raw latitude-by-longitude position and spline model estimations are overlaid. (Right) The raw and smoothed components (latitude and longitude) are plotted with respect to time in days where $t = 0$ identifies the beginning of the study period in this region.

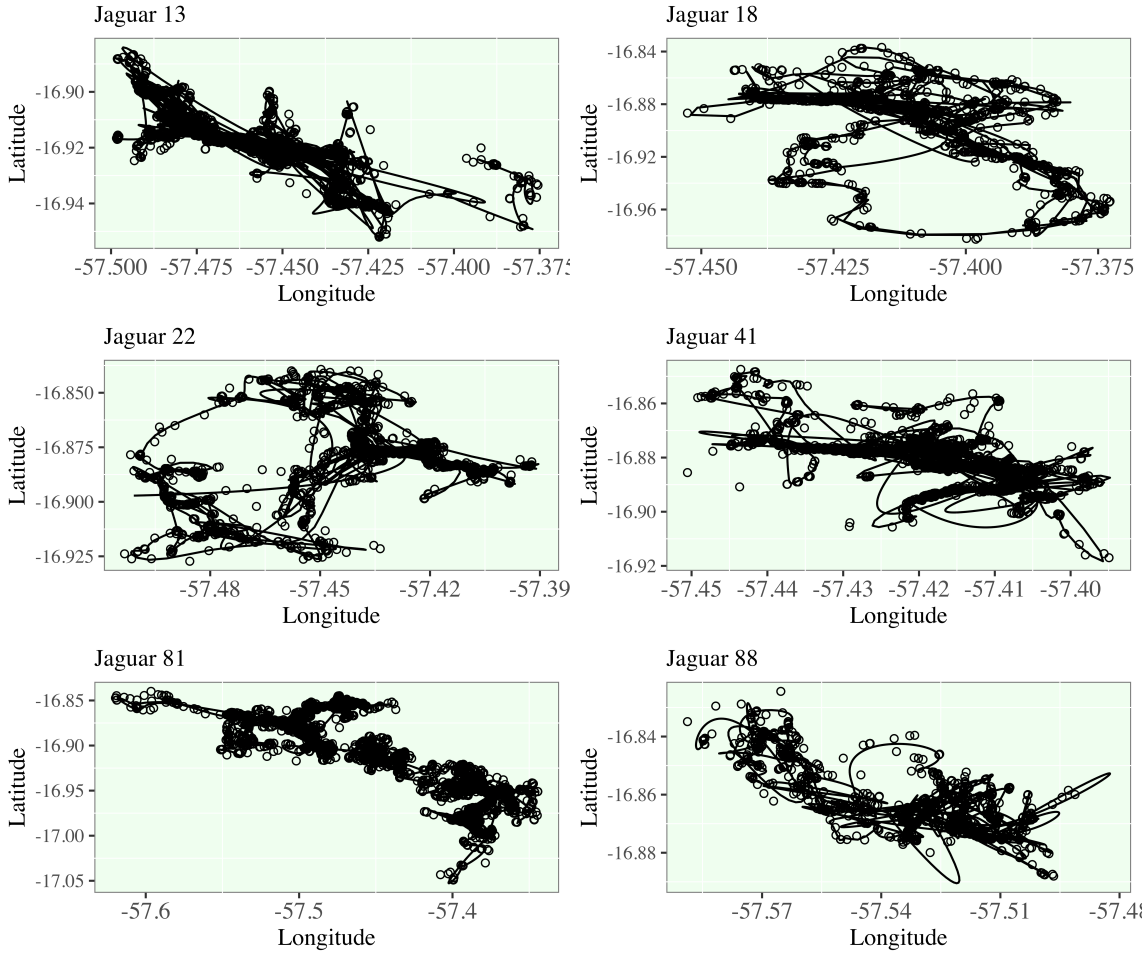

Figure 6.3: Smoothing Spline Model for Jaguars 13,18,22,41,81, and 88. For brevity, the decomposition of the spline models to latitude and longitude is not shown.

jaguar is less than 0.25 meters per second. Any times where this condition is satisfied are found below the orange line. My working definition of a jaguar rest period is inherently a binary classification of movement, and the times that satisfy this condition are subsetted to derive rest-period densities. I emphasize the substantial shift in the rest-period density structure of Jaguar 12. Jaguar 12 in the first half of her tracked time domain has higher rest period density, meaning that she is estimated to have more rest periods or periods of slower movement. In the latter half, her rest period density drastically drops to below a third of previous levels. No other jaguars show this trends as drastically; Jaguar 81 has a drop in rest period density during a migratory period prior to entering the initial territory of Jaguar 12. In all of the remaining density plots, however, there is an apparent cyclic nature to rest period density that is approximately weekly to bi-weekly for most jaguars.

In Figure 6.6, I present the pair-wise distance relationships between several jaguar pairs, and their respective co-occurrence potential measures [76]. The four selected pairs are chosen deliberately as many jaguars had zero or near zero co-occurrence potential. The male-female pairs are Jaguar 12 and 81 and Jaguar 18 and 41, and the male-male pairs are Jaguar 18 and 81 and Jaguar 13 and 81. In the distance function plots, which are all identically scaled on the vertical axis from 0 to 30,000 meters, we note the significant differences in distance functions across all chosen pairs. For Jaguar 12 and 81, there is a first encounter with the highest co-occurrence potential, and then there is an extended period of zero co-occurrence potential. Following this hiatus, there is an extended period of regularly occurring bursts of high co-occurrence potential, which is then followed by the long migration of Jaguar 12 away from Jaguar 18. At the end of their shared time domain Jaguar 12 returns and there is a short period of moderate co-occurrence potential that is evidence of some final return to territory sharing before we lose sight of their movement. The other male-female pair (Jaguars 18 and 41) on the other hand, has regular intervals of high co-occurrence, but we note that in a similar seasonal time window (at approximately Day 500) Jaguar 41 distances herself from Jaguar 18, but at a much lower magnitude than Jaguar 12.

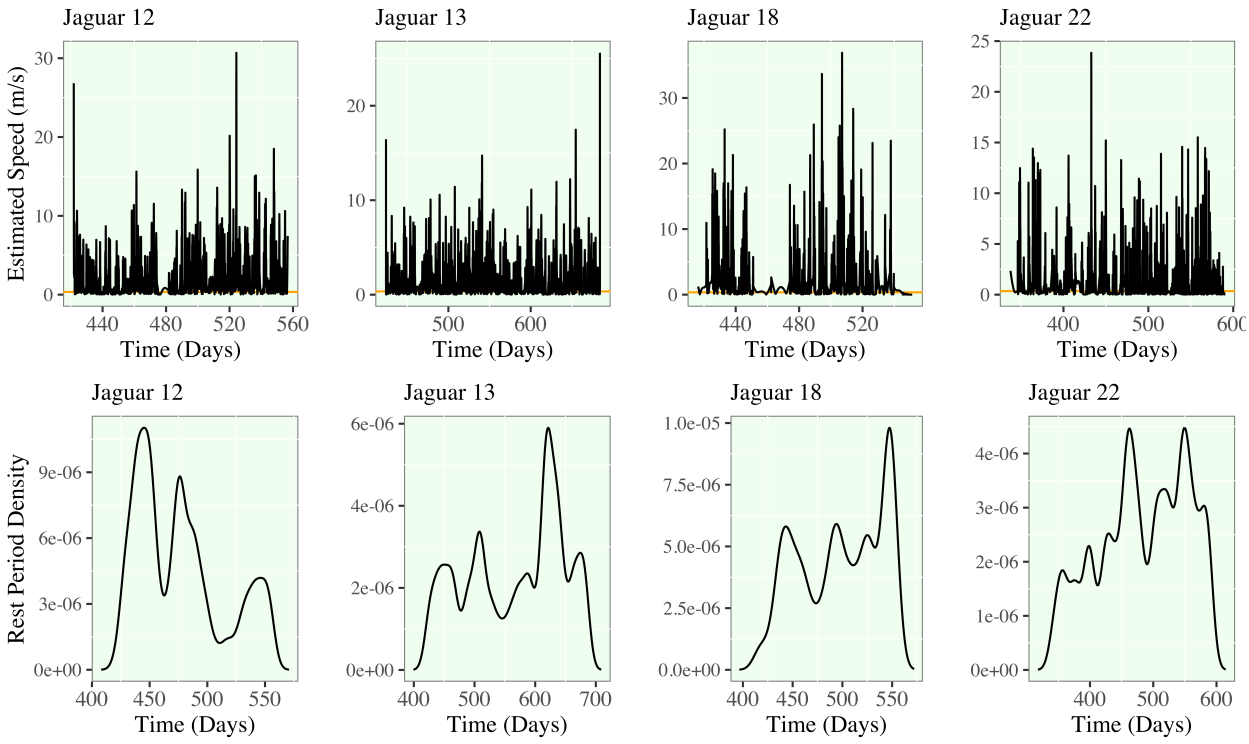

Figure 6.4: Spline model estimation of speed and rest period density for Jaguars 12,13,18,22. (Upper) A horizontal orange line is plotted at a speed of 0.25 m/s. (Lower) All hours in the spline model that are estimated to have speeds lower than this line are subsetted as a new vector to compute the density of rest periods. The selected bandwidth for estimation varies by jaguar and they range from approximately 4 to 12 days. As a result, a detected shift in the density of rest periods over time would indicate a shift to lower or higher density of rest periods occurring in a 4 to 12 day window.

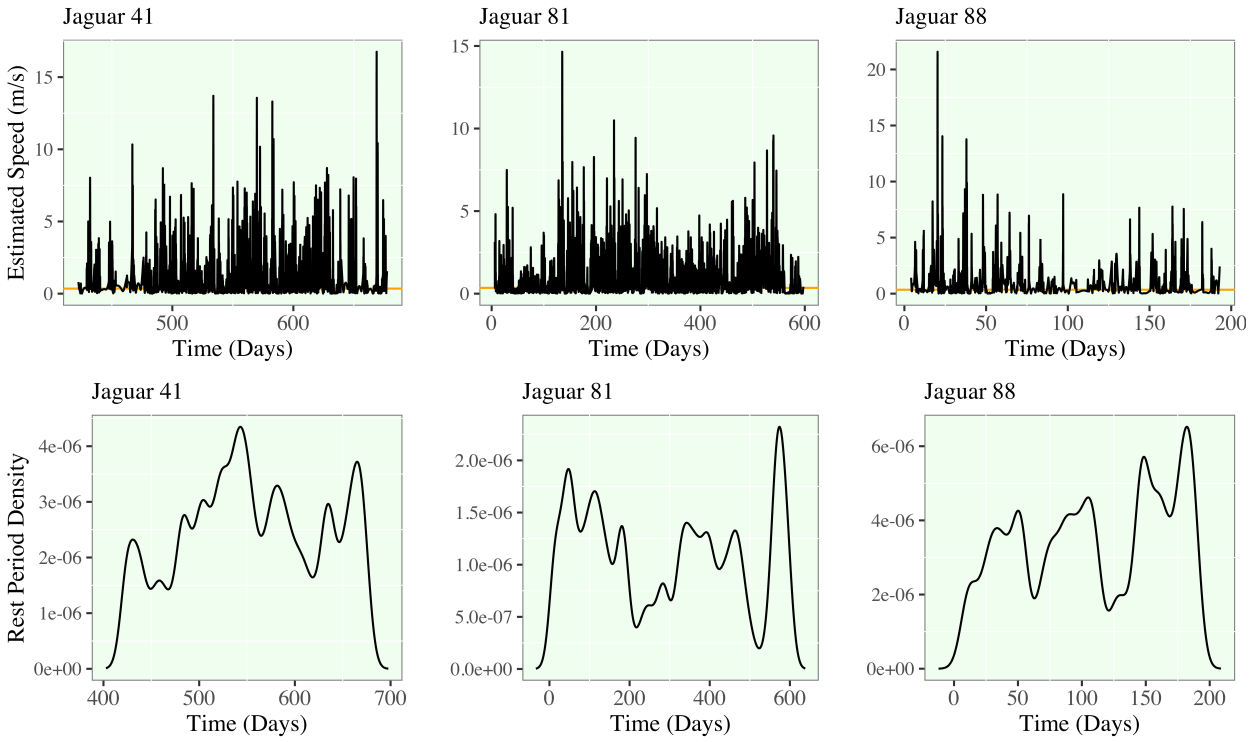

Figure 6.5: Spline model estimation of speed and rest period density for Jaguars 41,81,88. Refer to the caption of 6.4 for the interpretation.

For the male-male pairs, Jaguar 13 and 81 only have high co-occurrence for a small time-window while Jaguar 81 is still migrating to new territory. Jaguar 18 (M) and Jaguar 81's (M) relationship is particularly interesting as there is an early period of high co-occurrence, and then, during the period of high co-occurrence between Jaguar 12 (F) and 81 (M), there is a hiatus in their co-occurrence. High co-occurrence between these two males is then resumed once Jaguar 12 (F) leaves the territory and they move within short distances of each other for an extended period which ends before the return of Jaguar 12.

I present the localized mutual information profiles for the same four pairs jaguars in Figure 6.7 using a bandwidth of $\lambda = 48$ hours. This bandwidth identifies that the measure of localized mutual information is computed for a 4 day period centered on a given time. For Jaguar 12 (F) and 81 (M), there is a cyclical spike in the strength of association (i.e. local mutual information) immediately prior to and during most of the periods of high co-occurrence potential. The times of strongest association in movement occur during the second and longest period of high co-occurrence from approximately Day 475 to Day 510, and when Jaguar 12 returns at the end of the study period. On the other hand, Jaguars 18 and 41, although regularly experiencing period of high co-occurrence, do not show a similar associative trends. There movement has the strongest association early in the study period and then it gradually decline in the following weeks.

For the male-male pairs of jaguars, there are repeated periods of high mutual association that do not show clear trends with co-occurrence potential. For Jaguar 13 (M) and 18 (M), there is a drop in the strength of association in their movement in the final weeks of the study and this is when these two jaguars are consistently the furthest apart. Interestingly, Jaguar 18 and 81 (male-male pair) have the strongest association in their movement at a similar time to the peak in association between Jaguar 12 and 81 (female-male pair). The female-male pair have a peak in association at Day 478, and the male-male pair have a peak in association at Day 471. These two associations are characterized by a zero-level co-occurrence between the male pairs of jaguars, and increasing co-occurrence potential between the female-male

Table 6.2: Peak association in between Jaguar Pairs. Distance and localized mutual information are summarized by quantiles for pairs 12 vs. 81, 18 vs. 81, and 18 vs 41 for a time window of interest surrounding a peak in association of movement as measured by localized mutual information.

Jaguar Pair	Time Window	Metric	Min	Q1	Q2	Q3	Max
12 (F) vs 18 (M)	Day 476 to 479	Dist (m)	118.4	591.1	1212.0	2299.0	2874.1
		Mut Info	0.385	0.447	0.499	0.612	0.667
18 (M) vs 81 (M)	Day 469 to 471	Dist (m)	7069.5	9174.9	10641.1	11562	12537
		Mut Info	0.316	0.416	0.519	0.637	0.744
18 (M) vs 41 (F)	Day 455 to 477	Dist (m)	156.0	1736.0	2071.2	2922.6	4039.1
		Mut Info	0.266	0.406	0.515	0.634	0.999

pair.

In order to further investigate the cause of these spikes and drops in mutual information, it becomes highly instructive to summarize the pairwise distance and localized mutual information for these pairs of jaguars in addition to the pair of Jaguars 18 (M) and 41 (F). This is shown in Table 6.2. Between Days 476 to 479, Jaguars 12 (F) and 81 (M) are in close proximity with an estimated median hourly distance of 1212m apart and a minimum estimated distance of 118.4m apart. The spike in their correlatory movement peaks in this window marks that their relationship in this time is characterized by periods of direct interaction. Jaguars 18 (M) and 81 (M) during their peak in movement association in the time window from Day 469 to 471 is not direct as the minimum estimated distance between these jaguars is 7069m. However, in the time window from Day 455 to 477 (which overlaps this time), Jaguars 18 (M) and 41 (F) have an estimated median distance of 2071m and a minimum distance of 156.0 meters with extended periods of high co-occurrence potential. *What is especially interesting about these observations is that the peak in association between the two male jaguars is that it characterized by a periods when both male jaguars have close interaction with females.* The comparison of localized mutual information plots for Jaguar's 12, 18, 41, and 81, provides a clear characterization of interaction on a local male and female jaguar behaviors.

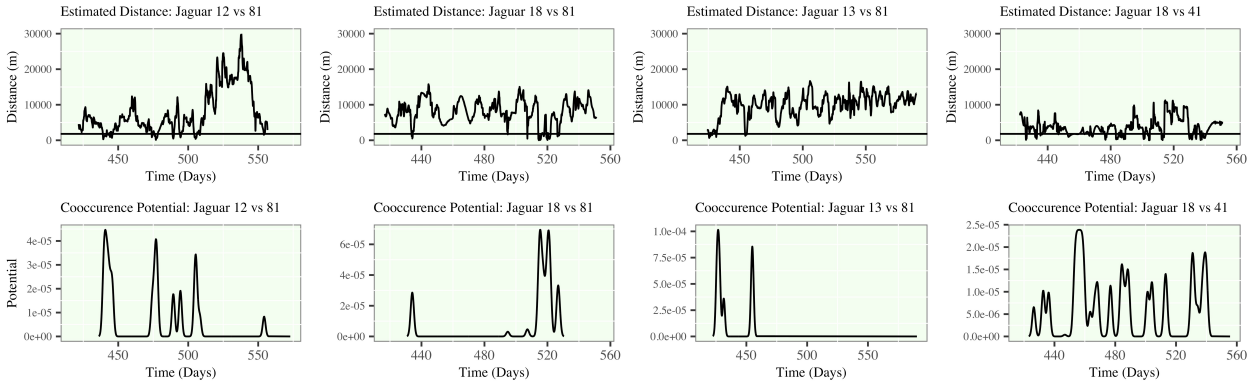

Figure 6.6: (Upper) Distance plots for Jaguars 12-81, 18-81, 13-81, and 18-41. Distance is derived from pairs of smoothed spline models. A horizontal line at Distance=1800m is placed to mark the defined threshold of co-occurrence. (Lower) All times that distance between a pairs of jaguars are subsetted to derive the density of times where jaguars fall within this threshold. The spacing and duration of close proximity is accentuated and this measure of co-occurrence provides easy access to measures of duration and frequency of co-occurrence or gaps in co-occurrence.

6.5 Discussion:

The apparent complexity of jaguar movement and interaction in the Taiamã Ecological Station is driven by the high density of jaguars [19, 57]. Monitoring the complex fine-scale movement of multiple animal with shifts in territorial and social nature differs from previous examinations of animal movement using smoothing spline models [7, 53, 54, 55]. This work provides a preliminary strategies for monitoring movement, behavior, social interactions, and the strength of association between animal movement, all of which are best explored on a refined and unified time grid smoothed using spline models.

The Taiama Ecological Station is a crucial conservation region for jaguars, and it is the region with the largest known density of jaguars, and further, this region provides insights into the needs of an ecosystem to sustain a large volume of neotropical apex predators [57, 78, 79]. Recent work has shown that the size of this conservation region is insufficient to protect this specific feline population. The study of space-use and animal interaction is a crucial step to assessing the conservation needs for this species[80, 81].

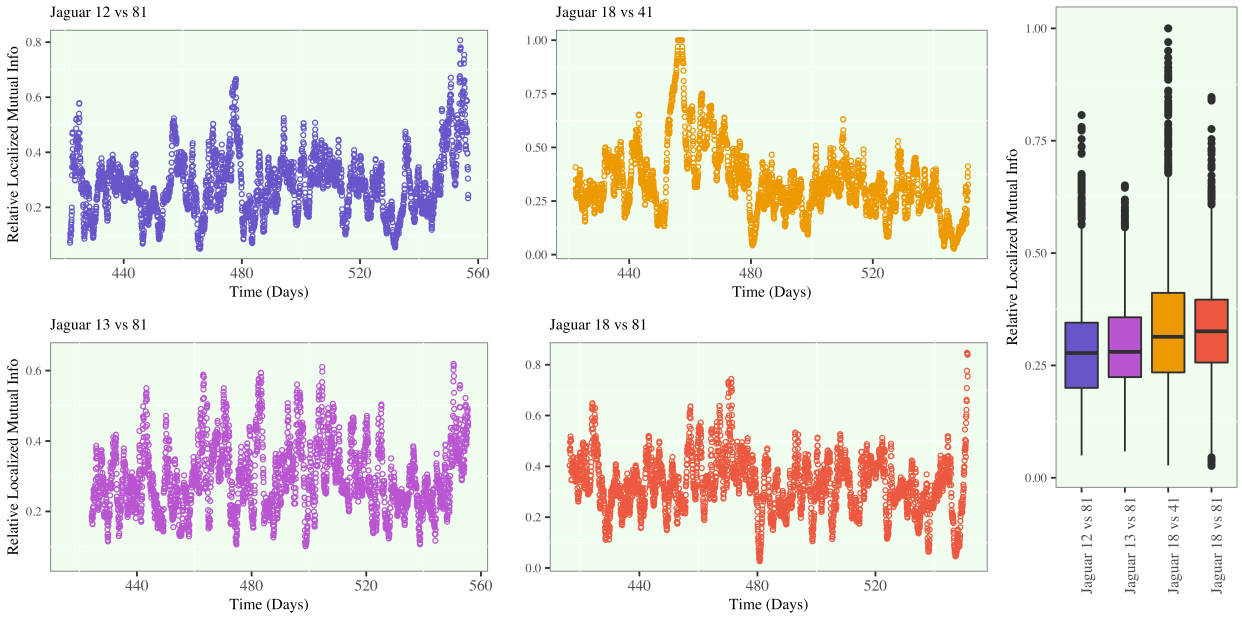

Figure 6.7: Localized mutual information plots. (Left) The localized mutual information with a bandwidth of $\lambda = 48$ hours for each time point in the refined time grid is plotted by each pair of Jaguars. The y-axis is scaled by the maximum localized mutual information at each time point and as a result the range of the y-axis is from 0.00 to 1.00. As a result, the scaled localized mutual information can be handle similarly to a measure of correlation, where 0.00 denotes no correlation between the movements and 1.00 defines a perfect unity in movement. (Right) The overall spread of localized mutual information measures across the time grid is summarized using boxplots.

As the objective of this work is comparative to the recent work on pairwise jaguar interactions, I compare the primary differences and potential advantages over Fontes et. al. 2021.

1. *co-occurrence potential vs. co-occurrence frequency*: Although measurement error is not considered in either analysis, it is crucial to acknowledge error in position and choose a metric for examining distance between animals that accounts for movements that may occur between known positions. co-occurrence frequency is defined in previous work on a very close proximity of 200m and 400m which can be advantageous in the sense that jaguars within this range are almost surely aware of each other. However, simply counting the instances of co-occurrence in this way does not provide a tool for measuring and visualizing periods where co-occurrences are realized in high or low densities. It is clear that a period with a high density of co-occurrences is more likely to contain interaction since there are more opportunities for an interaction to take place. Given that the raw recordings are at best defined on a 1 hour resolution, it is evident that even over dense or difficult terrain, jaguars have the potential to cover a distance many magnitudes farther than 400m. Additionally, loud mating calls are used by the species to attract mates far beyond this range, and scent and scrape markings are other methods of communication by this largely solitary predator [50]. co-occurrence potential in this work is a simple extension of co-occurrence frequency where a larger distance is used for measuring frequency, and the densities of these frequencies is used to derive a probability density function that identifies time windows where there is a greater probability of an interaction. The visualization of co-occurrence in this way provides a convenient tool for examining complex patterns in co-occurrence between animals or differences between pairs of animals.

2. *Localized Mutual Information Functions vs Trajectory and Association Rule Mining Correlation Metric*: The derivation of a single correlation coefficient as laid out in Fontes et. al. 2021, it is attractive in its simplicity and use of interpretable association

rules. However, as is evident in the relationship between Jaguar 12 and Jaguar 81, shifts in behavior states over time result in shifts in the association of movement. This is apparent for most pairs of jaguars. There is always some level of associations between animals of the same species in the same local ecosystem, even if there is no direct interaction. As an example, as shown in the state matrices in Fontes et. al., there are overlapping times of day where Jaguars are resting or in other transitory states [19]. It follows that some mutual information between jaguars is evident as movements in the region may be connected through animal gender, daylight, and shifts in weather or climate. In the localized mutual information functions derived in this work, spikes or periods of relatively higher correlation denote stronger relationships between a pair of jaguars. More simply, local mutual information functions can be thought of as a time-dependent measure of correlation or association of animal movement. The ability for this method to captures association of movement regardless of direct proximity is a critical advantage in adapting correlation analysis of animal movement beyond co-occurrence studies. This is most clearly illustrated in the ability of the proposed localized mutual information measure to detect a spike in similarity of movement between two males (Jaguar 18 and 81) when they are both interacting (or in close proximity of a female. It is only after this spike that they move closer to each other and observe a spike in co-occurrence potential. *It is important to note that the proposed LMI measure and movement associations driven by scent and scrape marking patterns should be explored further via simulation studies.* The integration of GPS tracking data and geographical distribution of scent and scrape marking patterns would permit for the testing of the influence of scent and scrape marking behavior on animal movement [51]. This would provide crucial insight since scent and scrape marking data would represent the true population of jaguars of a region which may assist in explaining behaviors of observed jaguars in the presence of unobserved jaguars. The spike in the Jaguar 18 and 81's coocccurence potential following provides evidence of increased male-male interaction

only once females have distanced themselves from each respective male.

3. *Extension to higher-order interactions*: Although not shown in this work, the methods implemented have the ability to be extended to monitor three way interaction. co-occurrence potential for any given jaguar, in relation to two or more other jaguars, would be the density function of time recordings on the refined time grid where any jaguar is within a set radius (such as 1800m). The localized mutual information measure could be readily adapted to measure partial mutual information [82], where the association between two jaguars is measured while controlling for another jaguar. It is important to note, that in both this work and Fontes et. al., the interpretations are based solely on observed individuals, and there are still challenges present in interpreting interactions detecting between pairs of jaguars when there are likely other interactions with unobserved individuals.

As mentioned briefly above, jaguar social interaction, although primarily characterized by direct (or close-proximity) interaction, is not the only form of social interaction that exists and should be detectable. Like many apex predators, territorial marking, is a common form of passive communication. Jaguars may deliberately avoid or follow these routes which should be characterized by higher associations between animals. Young male have a tendency to be nomadic and older jaguars tend to have established territory with minimal overlap (where overlap is typically shared with females in the region). Female jaguars behavior is also generally characterized by a temporary associations with a male, and then they avoid male interactions when caring for cubs[58, 83, 66, 84, 85].

All of these characteristics of jaguar movement and interaction are detectable in this analysis. Jaguar 12 (female; age = 4) and Jaguar 81 are detected to have strong but temporary associations which *increase in frequency* as time progresses, and then there is a rapid distancing between the pair and the association in their movement drops for over two months. The ability to detect an increase in frequency in high co-occurrence is visually inconclusive without the use of co-occurrence potential plots. Finally, their association and co-occurrence

potential increase at the end of the study as she returns to her baseline territory at the beginning of the study. Jaguar 12's resting behavior also shows distinct shifts from the period of high co-occurrence potential with Jaguar 81 to the farthest point in her migration south. It is suspect that Jaguar 12's sudden drop in rest period densities suggests a shift between mating and cub rearing movement behaviors where she is depended on to make successful hunts to provide for her young. Females are generally considered to have smaller home ranges, but the seasonal shifts in this Jaguar 12's behavior for months of this year show evidence that some females have multiple or shifting home ranges during mating and cub-raising periods [57]. That fact that some female jaguars make longer temporary migrations proceeding interactions with male should be considered when defining an appropriate conservation region for the species since the time spent away from males is a critical time for survival of the next generation of cubs.

The nomadic behavior of Jaguar 81, which is recorded at a fine-scale for almost two years, provides particular insights regarding male-male relationships between established and nomadic male interactions. Jaguar 13 and 81 only seem to interact for a brief time in passing, and Jaguar 81 continues to move past Jaguar 13's territory. However, Jaguar 18 and 81 show evidence of coexisting in a similar region with distinct shifts in behavior. Jaguar 18 and 81 have the strong associations in movement in the presence of a local female. Jaguar 18 keeps at a farther distance from Jaguar 81 once high co-occurrence between Jaguar 12 and 81 begin, and Jaguar 18 is not shown to near Jaguar 81 until Jaguar 12 has initiated a prompt departure from the region.

The migrations of Jaguar 12 and 81 provide evidence that interacting with high co-occurrence potential in regions of high population density utilize expansive regions of land (upwards of 30km) [57]. This is critical to understand as conservation efforts demand estimations of the required conservation area for endangered species [78, 79]. With any region of higher jaguar density, this work confirms that increasing conservation land for jaguar's will only aid their ability to coexist in higher abundance [80], since longer migration's (greater

than 30km) of a terrestrial predator could easily span outside of protected areas with a radius of less than 60km. As the movement of all jaguars in this region are not observed, it would be hypothesized and left to future work to examine how often migrations of this level take place in regions with high densities of apex neotropical predators.

Smooth spline modeling of jaguar movement, as demonstrated in this study, is not without some caveats that should demand further attention in future work. As mentioned earlier, smoothing of paths requires some sacrifice of the exactness of position, and some particular movements are more difficult to catch than others. For animal telemetry, spline models are subject to over- and under-fitting challenges which can be observed in Fig 6.3. Some paths are clearly more variable than the smoothed model suggests, and depending on the density of time measurements in some region, the model may tend to overshoot or undershoot a sharp change in direction. As in recent developments in standard continuous time models, there are opportunities to improve the fit of the model by accounting for geographic features/barriers, social encounters, atmospheric conditions etc [86]. Random walk schematics have shown great potential improving the modeling of animal movement, and these methods should be adapted to the FDA paradigm.

In this analysis, there is no accounting of measurement error, which is a significant element of most animal telemetry data. The data used in this study did not publicly provide measurement error to pair with GPS point estimates of position. As mentioned previously, some recent work has provided possible methods for accounting for measurement error in spline models, and these should be adaptable to many applications in animal movement.

The use of information theory in animal telemetry is sparse, but this work demonstrates the value of adapting measures of entropy and mutual information to animal telemetry. The derived measure of localized mutual information, verifies that although the distance between jaguars has a tendency to yield higher associations in their movement, this is not uniformly true and there are strong associative movements between male-male and male female pairs that can occur far beyond the co-occurrence potential threshold that I have defined in this

work.

In overview, the approach used in this work effectively handles the challenges of spatial and temporal density, modeling continuity and differentiability of spatial movement, and multivariate characterization of animal behavior. To elaborate on the latter, the spline models that I construct in this work retain information about animal position and rate of change of position while refining the movement uniformly with other animals which ultimately allows for a unique and visual-friendly characterization of shifts in interaction and social behavior.

I commend past work in the study and modeling of animal telemetry, social interaction monitoring, and I encourage further work in modeling of these complex processes and relationships.

6.6 Data Accessibility:

Jaguar movement database: a GPS-based movement dataset of an apex predator in the Neotropics. [71, 72]

The authors of the study own the data set and made it public and freely available at the Dryad Digital Repository with the following DOI accession number- DOI: 10.1002/ecy.2379. It can also be accessed via the following link: https://doi.org/10.5061/dryad.2dh0223. The data is also available on Movebank at doi:10.5441/001/1.3c4fv0m4.

7 Appendix

7.1 Violation of Triangle Inequality Proposed Dissimilarity Measure

Ultimately, any measure of dissimilarity or distance is intended to define a relationship between two elements of interest. This is most easily examined and visualized for 2D and 3D geometric problems. However, it is required in many application to measure dissimilarity or distance in a more abstract space. This space may be characterized by a complex processes

(such as in spline models), or in many statistical applications, the space is characterized by a large collection of variables.

In this section, we briefly show that a dissimilarity measure of interest is not a distance metric by violation of the triangle inequality. Let $d(X,Y) = 1 - I^*(X,Y)$ where $I^*(X,Y) = \frac{I(X,Y)}{I(Y,Y)}$ as mention in Section 5.1. The triangle equality holds under the condition that $d(X,Z) \leq d(X,Y) + d(Y,Z)$.

Substituting our proposed measure d, we have that

$$1 - \frac{I(X,Z)}{I(X,X)} \leq 1 - \frac{I(X,Y)}{I(X,X)} + 1 - \frac{I(Y,Z)}{I(Y,Y)}, \tag{7.1}$$

and further,

$$-\frac{I(X,Z)}{I(X,X)} \leq -\frac{I(X,Y)}{I(X,X)} + 1 - \frac{I(Y,Z)}{I(Y,Y)}. \tag{7.2}$$

Rewriting mutual information in terms of entropy $I(X,Y) = H(X) - H(X|Y)$, it follows that

$$-\frac{H(X) - H(X|Z)}{H(X) - H(X|X)} \leq 1 - \frac{H(X) - H(X|Y)}{H(X) - H(X|X)} - \frac{H(Y) - H(Y|Z)}{H(Y) - H(Y|Y)}. \tag{7.3}$$

Note that $H(X,X) = 0$ and $H(Y,Y) = 0$. With this fact, we multiply the inequality by $-H(X)$ which gives

$$H(X) - H(X|Z) \leq H(X) - H(X) - H(X|Y) + \frac{H(X)}{H(Y)}(H(Y) - H(Y|Z)). \tag{7.4}$$

The next several steps are simplifications of the inequality.

$$H(X) - H(X|Z) \leq H(X) - H(X|Y) - \frac{H(X)H(Y|Z)}{H(Y)}. \tag{7.5}$$

$$-H(X|Z) \leq -H(X|Y) - \frac{H(X)H(Y|Z)}{H(Y)}. \tag{7.6}$$

$$H(X|Z) \geq H(X|Y) + \frac{H(X)H(Y|Z)}{H(Y)}. \tag{7.7}$$

Since X, Y, Z are arbitrarily defined random variables, it is not implied that $H(X|Z) \geq H(X|Y)$, and therefore, it cannot be confirmed that a more extreme requirement of $H(X|Z) \geq H(X|Y) + \frac{H(X)H(Y|Z)}{H(Y)}$. Hence, $d(X, Y)$ is not a distance metric.

7.2 Alternate Binning Procedure results for Analytically Evaluated LMI Simulation

In this section, we report two other binning procedures referred to as "Equal Width Binning" and "Global Equal Width Binning." These procedures, although not exactly identical to the rudimentary binning procedure used to evaluate LMI analytically, are more similar to the analytic solution. More details on the implemented binning procedures can be found at the following source [48].

As shown in Figure 7.1 and 7.2, these binning procedures follow the analytical solution more closely. We emphasize that the binning procedure used in the analytical evaluation is a simplification of the binning process and it is only performed to confirm the similarity of the results from the computational approach implemented.

7.3 Sensitivity Analysis of Density-Based Knot Placement Procedure for Smoothing Spline Models

As mentioned in Section 6.3.1, smoothing animal movement superficially is straightforward, but, in the case of the Jaguar Movement Database, the raw time grid is realized with highly disparate densities in the collection of animal positions. Although they do not occur fre-

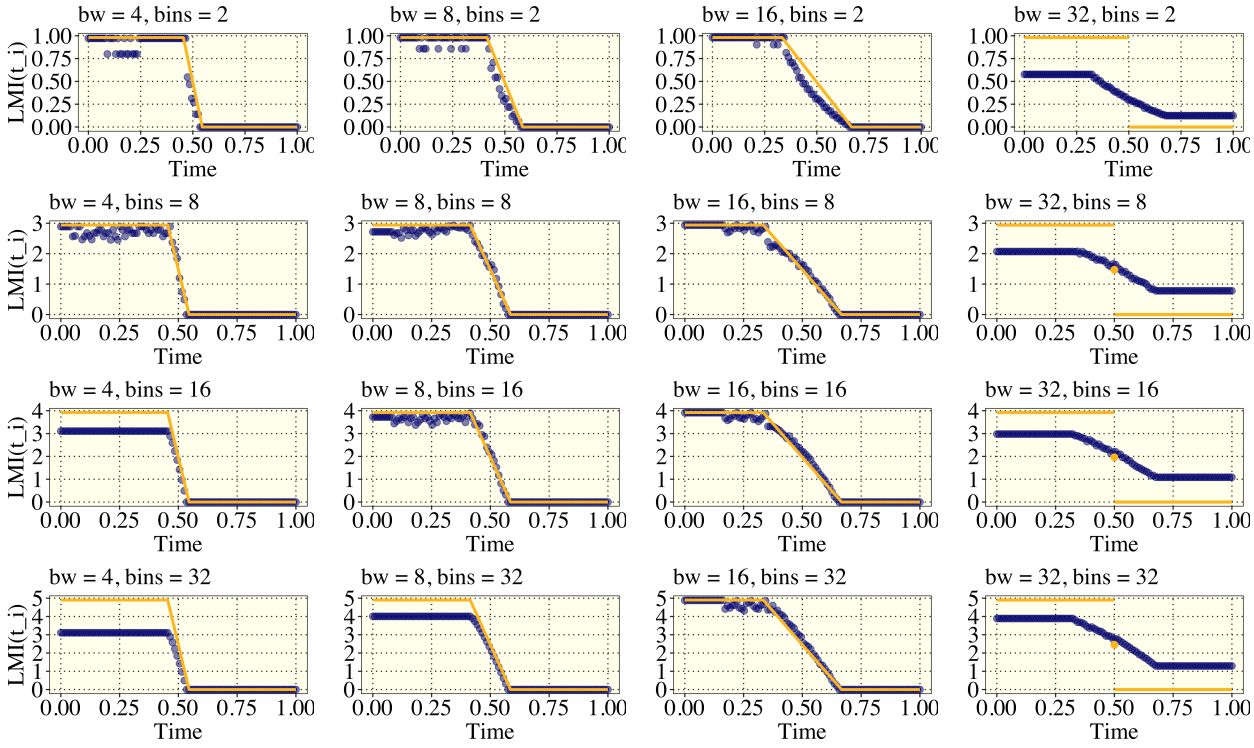

Figure 7.1: Implementation of Simulation 1 from Section 5.2.2 using *Equal Width Binning*. As is depicted the decline in LMI matches the timing of the decline from the analytic evaluation.

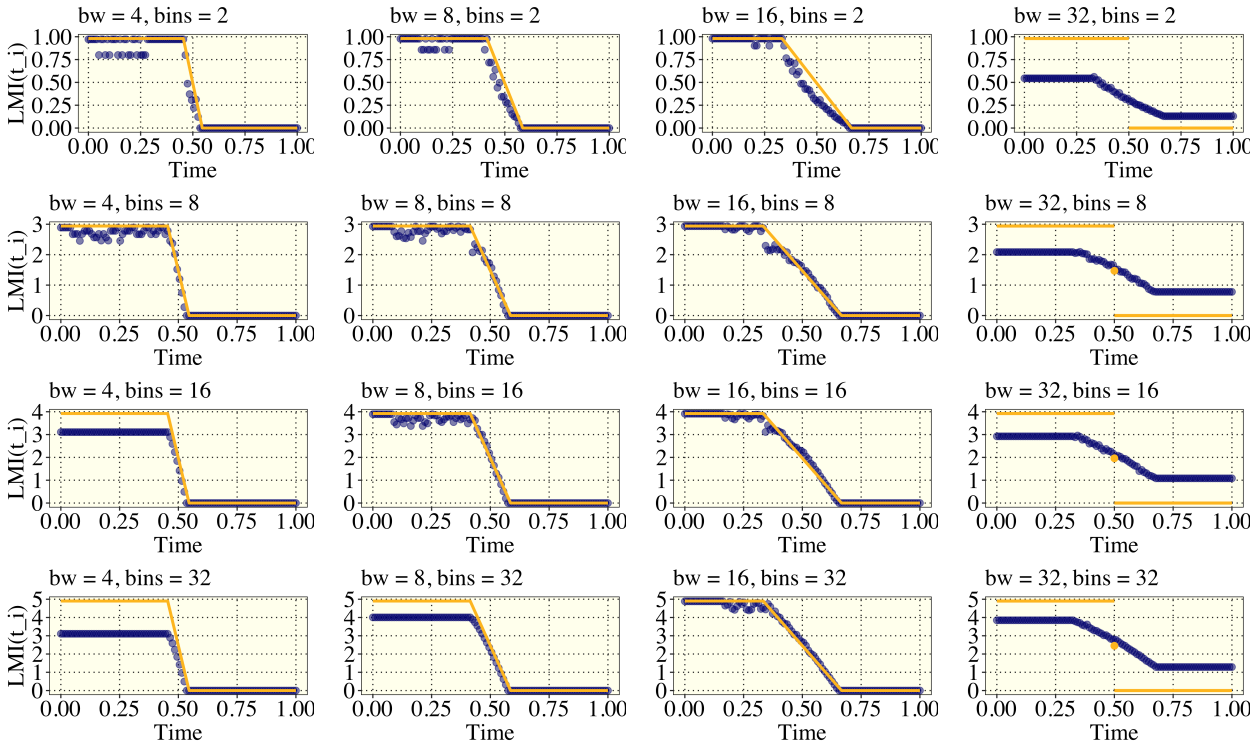

Figure 7.2: Implementation of Simulation 1 from Section 5.2.2 using *Global Equal Width Binning*. As is depicted the decline in LMI matches the timing of the decline from the analytic evaluation.

quently in the time domain, they occur enough to hinder the spline model from meaningfully characterizing jaguar movement for generic placement of equally spaced knot.

An density-based knot placement method has been proposed in this work to avoid the labor of manual knot selection, which is an arduous task when it is not always clear for larger datasets where the knots are best placed. Specifically, our objective here is to avoid over-fitting complex movement behavior in regions where we have no information about the movement of an animal. The knot placement procedure is summarized again below for convenience.

Let $(t_1, \ldots, t_n)$ be independently and identically distributed time samples from an unknown distribution f_h. We estimate the density of sampled times for a given jaguar using kernel density estimation defined by $\hat{f}_h(t) = \frac{1}{nh}\sum_{i=1}^{n} K(\frac{t-t_i}{h})$, where K is gaussian kernel function and h is a smoothing bandwidth parameter where higher values of h yield a smooth estimate of the density [62]. Let $k = \hat{f}_h(t^*)$ be selected as a threshold where t_i with $\hat{f}(t_i) > k$ define the collection of high density times $\{t_i | \hat{f}_h(t_i) > k\} = (\tau_1, \ldots, \tau_m)$ where $\tau_1 < \ldots < \tau_m$.

The method shows promise from our application section of this work, but it is instructive to further understand the sensitivity in the selection of the parameter k. We explore this for Jaguar 12 (Female, Age = 4) and Jaguar 81 (Male, Age = 4).

Figure 7.3 and 7.4 show the kernel density of the time grid for both animals. For both of their time domains, there is a high density of recorded animal positions, and there are infrequent drops in the density. It is clear from these images that a small bandwidth has been chosen to derive the density functions for both figures, and this is an intentional choice: we want to remove a sparse number of knots occurring in relatively short time spans. A rougher density function (with a smaller bandwidth) will retain information about low density areas on a small time domains than a smoother density function (with a larger bandwidth). In both figures, we have considered a selection of potential k-values which will be used to determine the location of knots. With an original selection of uniformly spaced knots on the time grid shown in these images, any knots located at a time where the density is above k will be

retained as knots in the smoothing process. Otherwise, the knot is removed.

In Figures 7.5 and 7.6, the smoothing spline models are visualized by their respective latitude and longitude components. As k decreases, we observe that the spline model estimates increasingly complex/extreme behavior in regions with lower raw time grid density. This is easiest to see visually in Figure 7.5 at $t = 480$ and in Figure 7.6 around $t = 550$. It is clear from these images that visual inspection and evaluation of knot placement is inadequate, and the density-based knot placement method is a versatile and simple method to improve spline model fit for data with variable/sporadic collection of information about a process.

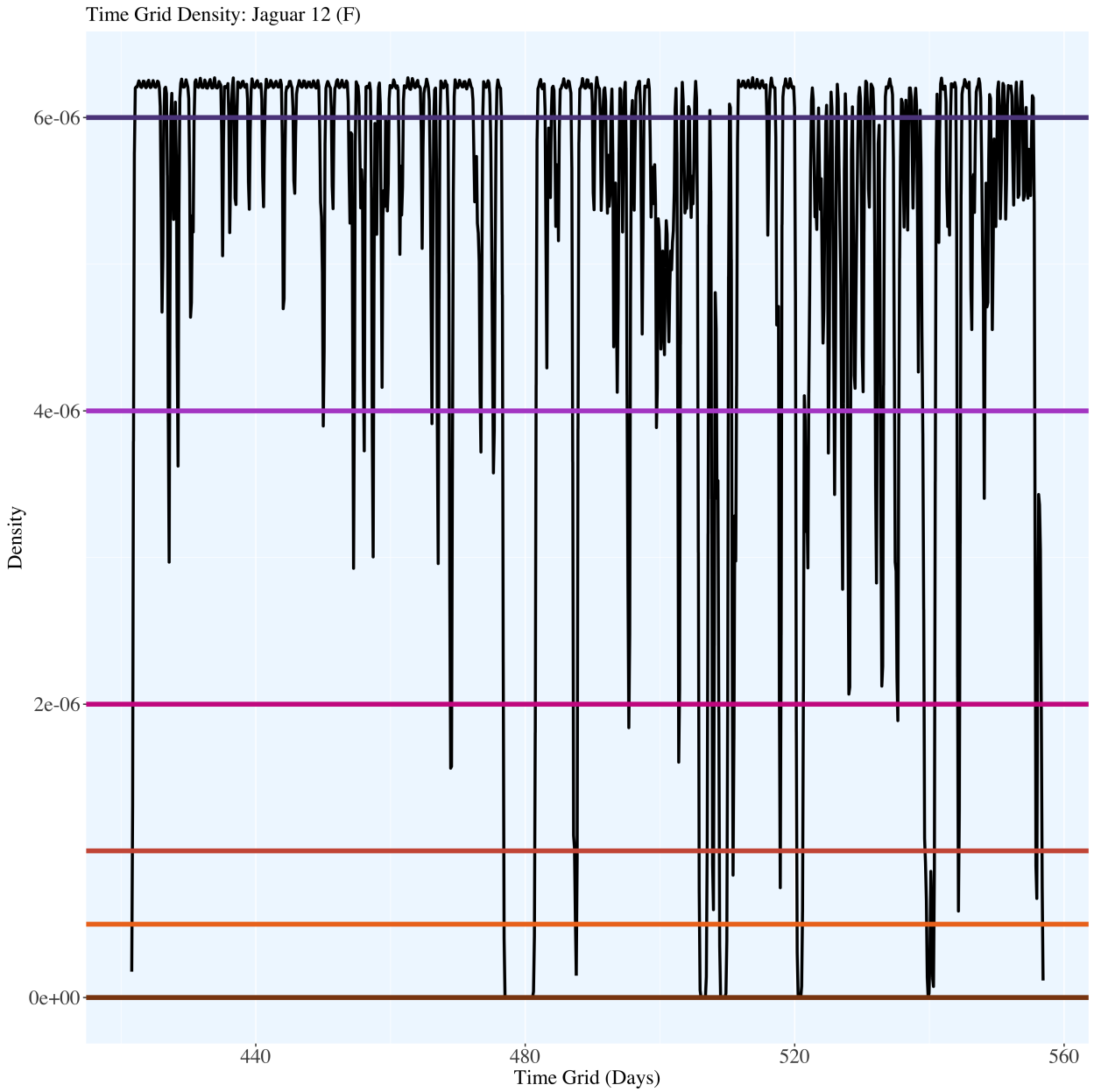

Figure 7.3: Density of the raw time grid for Jaguar 12 is shown as a kernel density plot. The selection k-values are marked by horizontal colored lines. Lower lines are characterized by having more knots in lower density portions of the time domain.

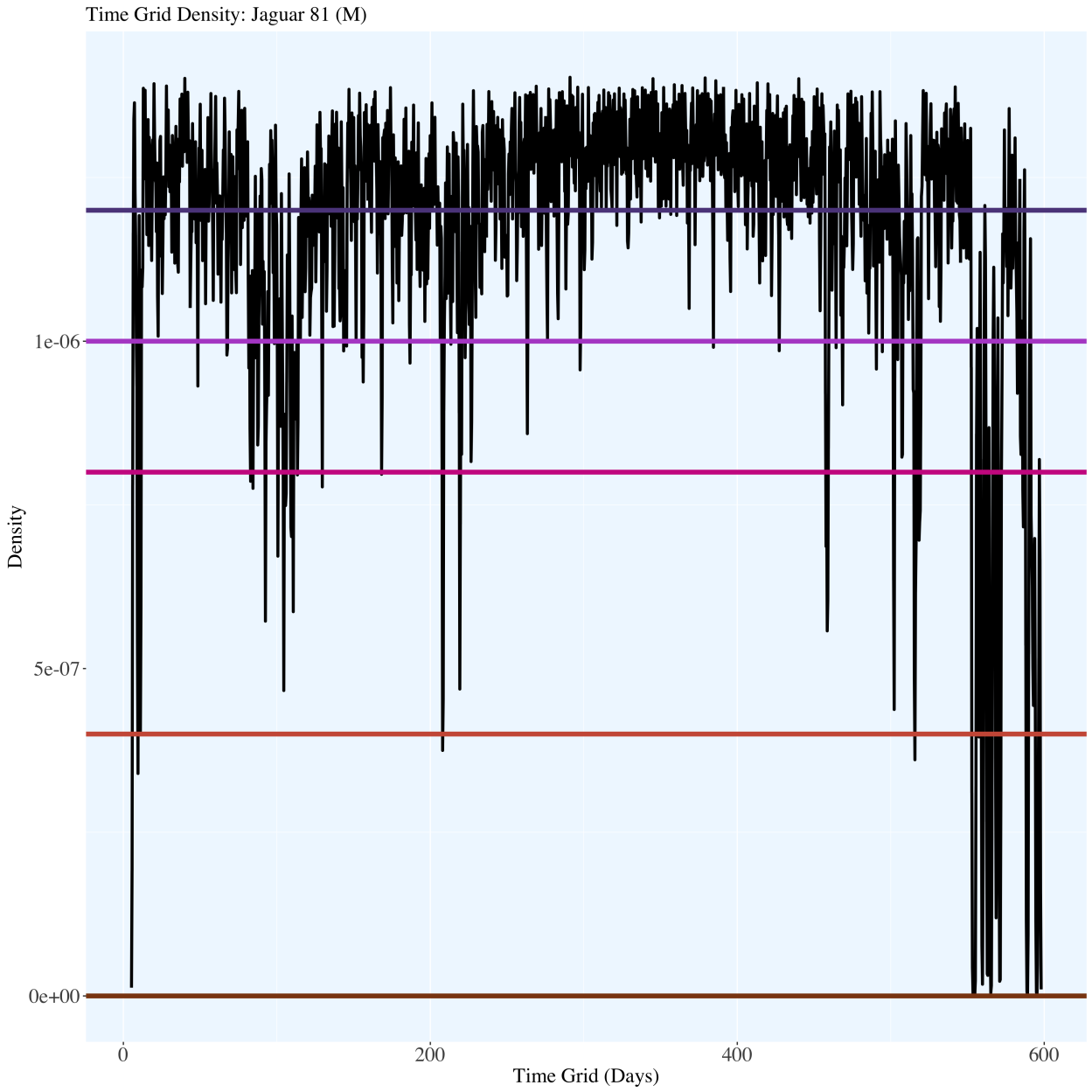

Figure 7.4: Density of the raw time grid for Jaguar 81 is shown as a kernel density plot. The selection k-values are marked by horizontal colored lines. Lower lines are characterized by having more knots in lower density portions of the time domain. Jaguar 81's time domain is approximately 4x longer that Jaguar 12's time domain, and the y-axis for these plots should not be compared directly.

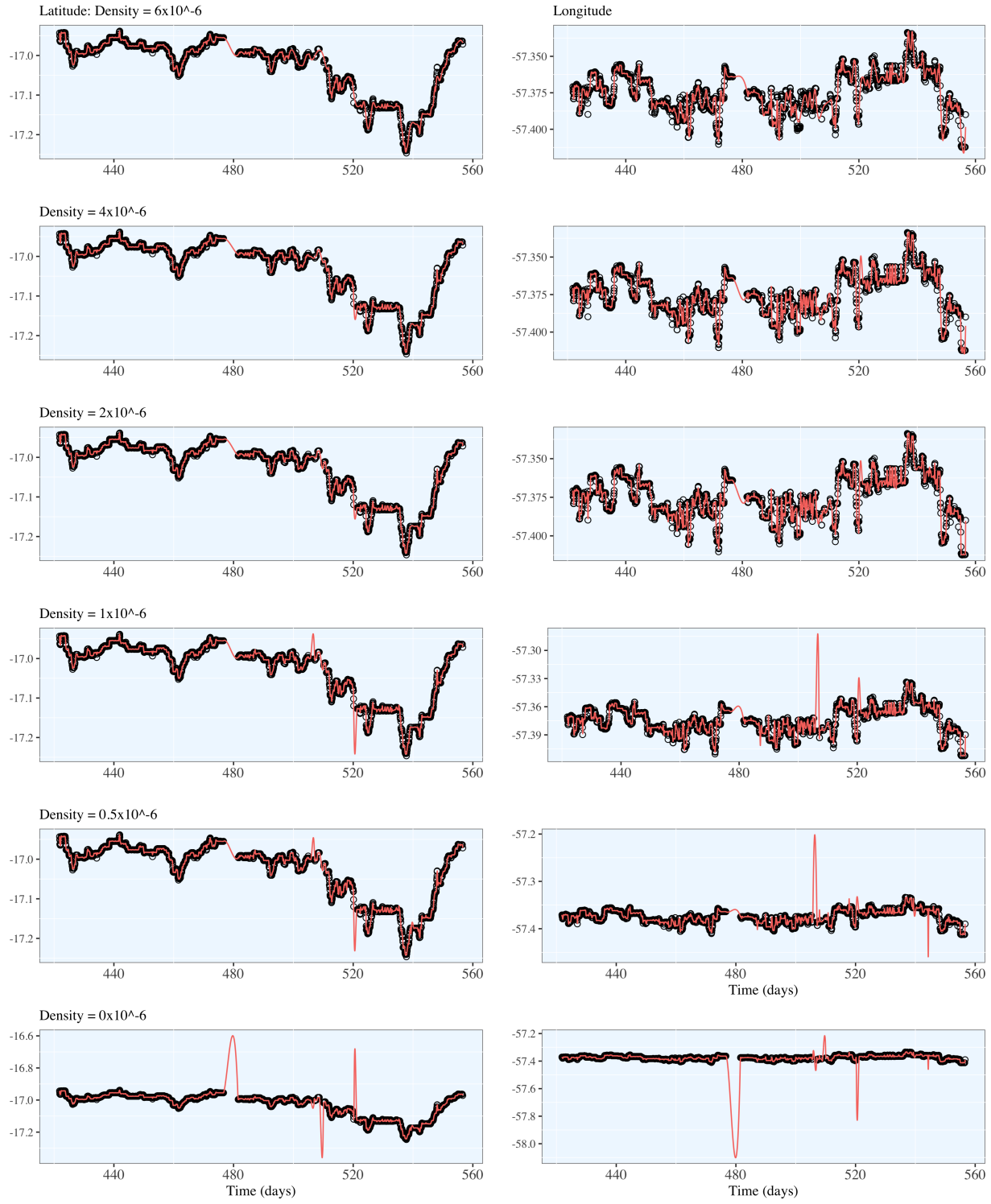

Figure 7.5: Smoothing splines for Jaguar 12 with 6 different magnitudes of k. As k decreases, we observe that the spline model estimates increasingly complex/extreme behavior in regions with lower raw time grid density.

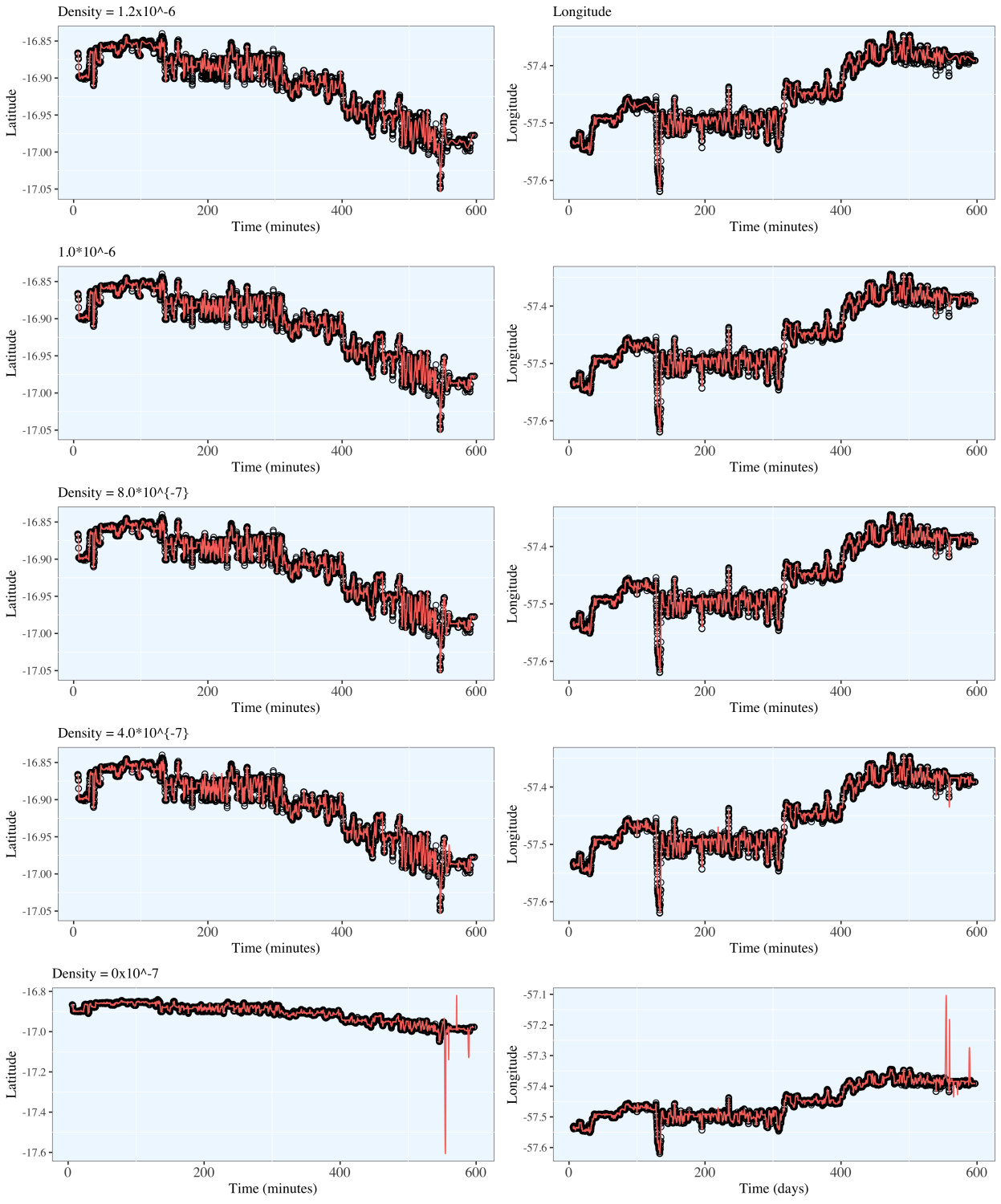

Figure 7.6: Smoothing splines for Jaguar 12 with 6 different magnitudes of k. As k decreases, we observe that the spline model estimates increasingly complex/extreme behavior in regions with lower raw time grid density. Jaguar 81's spline models are overall much better behaved across most values of k, near the end of the time domain note in Figure 7.4 the long period of lower density. The is the first region that the spline model begins to have issues estimating for very low values of k.

7.4 Starter Code for LMI

```
# Load packages for visualization and an array of information
# theoretic measures
library(infotheo)
library(ggplot2)
library(RColorBrewer)
library(gridExtra)

# LMI Function Proposed in the Whetten 2021 Preprint:
# November 2021
# DOI: 10.13140/RG.2.2.23971.37923/1  or
# https://www.researchgate.net/publication/356406518_
# Localized_Mutual_Information_Monitoring_of_Pairwise_
# Associations_in_Animal_Movement
# Project: Localized Mutual Information of Pairwise Animal Movement
# Association

# LMI Function
# Inputs:
# t_tilde - a (nx1) vector of times from the unified time grid (same
# time grid for both animals)
# animal1_x, animal2_x - the longitudinal (nx1) vectors for each
# animal's position
# animal1_y, animal2_y - the latitudinal (nx1) vectors for each
# animal's position
# bw - the bandwidth (lambda) value defining a neighborhood
```

```
# (of size 2*bw) of time points within a distance of bw
# from the center of the interval
# bins - the number of bins used to discretize the
# neighborhood/interval of width 2*bw

# Notes:
#-bins should be >= 2;
# bw can be >= 1 but note that bw's that are closer to one yield very
# noisy LMI functions.
# bw can be as large as length(t_tilde) but this would just give a
# function of global mutual information measures all of the
# same/similar value


local_mut_info <- function(t_tilde, animal1_x, animal1_y, animal2_x,
animal2_y, bw, numbins){
  # Create empty vectors to pass directional and joint components
  # of LMI
  loc_mut_lat <- as.numeric()
  loc_mut_lon <- as.numeric()
  loc_mut_joint <- as.numeric()
  loc_mut_max <- as.numeric()
  loc_mut_joint_max <- as.numeric()

  loc_mut_max_lon <- as.numeric()
  loc_mut_max_lat <- as.numeric()
```

```
# pass number of bins parameter
nb <- numbins

# For loop computing the LMI at each time t_i on a neighborhood of
# [t_i-bw, t_i +bw]
for (i in 1:length(animal1_x) ){
  # define neighborhood
  loc_time_sub <- (i-bw):(i+bw)
  # filter out time points outside of t_0 and t_f
  loc_time_sub <- loc_time_sub[loc_time_sub > 0]
  loc_time_sub <- loc_time_sub[loc_time_sub <= length(animal1_x)]
  if(length(loc_time_sub)-1 < 2*bw & max(loc_time_sub) ==
  max(length(t_tilde))){
    loc_time_sub <- (max(loc_time_sub-2*bw)):max(loc_time_sub)
  }
  if(length(loc_time_sub)-1 < 2*bw & min(loc_time_sub) ==1){
    loc_time_sub <- (min(loc_time_sub)):(min(loc_time_sub+2*bw))
  }
  # Compute LMI for lat, lon, and identify the max LMI for
  # each on the same interval

  loc_mut_lat[i] <- mutinformation(
      discretize(animal1_y[loc_time_sub],
          nbins = nb, disc = "equalfreq"),
      discretize(animal2_y[loc_time_sub],
          nbins = nb, disc = "equalfreq"))
  loc_mut_lon[i] <- mutinformation(
```

```
        discretize(animal1_x[loc_time_sub],
            nbins = nb),
        discretize(animal2_x[loc_time_sub],
            nbins = nb))
    loc_mut_max_lon[i] <- mutinformation(
        discretize(animal1_x[loc_time_sub],
            nbins = nb, disc = "equalfreq"),
        discretize(animal1_x[loc_time_sub],
            nbins = nb, disc = "equalfreq"))
    loc_mut_max_lat[i] <- mutinformation(
        discretize(animal1_y[loc_time_sub],
            nbins = nb),
        discretize(animal1_y[loc_time_sub],
            nbins = nb))
    # Compute joint LMI and joint max LMI
    loc_mut_joint[i] <- sqrt( (loc_mut_lat[i])^2 +
        (loc_mut_lon[i] )^2)
    loc_mut_joint_max[i] <- sqrt(loc_mut_max_lat[i]^2 +
    loc_mut_max_lon[i]^2)
}
# output final dataframe
#df_final <- as.data.frame(cbind(t_tilde, loc_mut_lat,
loc_mut_lon, loc_mut_joint, loc_mut_joint_max))
df_final <- as.data.frame(cbind(t_tilde, loc_mut_lat,
loc_mut_max_lat, loc_mut_lon, loc_mut_max_lon,
loc_mut_joint, loc_mut_joint_max))
#list_final <- list(df_final, bin_temp1, bin_temp_2)
```

```
  return(df_final)
  #return(list_final)

##############################################################
############ 1st Simulation from LMI Preprint ##########
##############################################################

# Refer to paper to see detailed explanation of this simulation
# This code also includes the ggplot2 code to replicate the
# first visualization

# Define function to generate movement model and compute
# LMI using LMI function from above
# Function outputs list with the LMI dataframe, the
# position dataframe and some other details.
shift_sen <- function(band, r_err_1, r_err_2, nbins){
  # band = 4
  # r_err_1 = 0
  # r_err_2 = 0
  # nbins = 2
  #
  vt <- seq(0, 1, length.out=100)
  noise_1 <- rnorm(100, mean = 0, sd = r_err_1)
  noise_2 <- rnorm(100, mean = 0, sd = r_err_2)
  animal_lat_1 <- vt + noise_1
  animal_lat_2 <- vt[vt < 0.5]  + noise_2[1:50]
  animal_lat_2 <-  c(animal_lat_2, vt[vt >= 0.5]*0 +
```

```
animal_lat_2[50] + noise_2[51:100])

animal_lon_1 <- (vt - 0.05)
animal_lon_2 <- vt[vt < 0.50]    + 0.05 #+ noise_2[1:90]
animal_lon_2 <-  c(animal_lon_2, vt[vt >= 0.5]*0 +
animal_lon_2[50] + noise_2[51:100])

position_df <- as.data.frame(cbind(animal_lon_1, animal_lat_1,
animal_lon_2, animal_lat_2))

# Overall GMI
# from t = [1, 15]
baseline_GMI <- sqrt(
      mutinformation(
          discretize(animal_lon_1[1:50]),
          discretize(animal_lon_2[1:50]))^2 +
      mutinformation(
          discretize(animal_lat_1[1:50]),
          discretize(animal_lat_2[1:50]))^2)
# t = [15, 30]
shift_GMI <- sqrt(
      mutinformation(
          discretize(animal_lon_1[51:100]),
          discretize(animal_lon_2[51:100]))^2 +
      mutinformation(discretize(animal_lat_1[51:100]),
          discretize(animal_lat_2[51:100]))^2)
```

```
  mut_df <-local_mut_info(t_tilde = vt,
                          animal_lon_1,
                          animal_lat_1,
                          animal_lon_2,
                          animal_lat_2,
                          bw = band,
                          numbins = nbins)
  list_return <- list("Overall GMI" = c(baseline_GMI, shift_GMI),
                      "Animal Positions" = position_df,
                      "LMI Bandwidth" = band,
                      "Noise Magnitude (normal random error)" =
                      c(r_err_1, r_err_2),
                      "LMI Function" =  mut_df)
  return(list_return)
}

# Write general function for generating the computed
# analytic solution for LMI
t_til <- seq(0, 1, length.out=100)
trans <- 0.5

analytic_sol <- function(t_tilde, trans_time, bw, bins){

  l <- length(t_tilde)
  lmi_a <- rep(0,100)
  prop <- rep(0,100)
  for (i in 1:l) {
```

```
    # i=1
    if(t_tilde[i + bw] < trans_time |
        is.na(t_tilde[i + bw]) ==TRUE){
      if(is.na(t_tilde[i + bw]) ==FALSE){
        lmi_a[i] <- log(bins)
        prop[i] = 1
        }
    }
    else if(t_tilde[i + bw] > trans_time &
        t_tilde[i - bw] < trans_time){
      l_window <- length(t_tilde[(i-bw):(i+bw)])
      sum_phase1 <- sum(t_tilde[(i-bw):(i+bw)] < trans_time)
      prop[i] <- sum_phase1/l_window

      # Compute analytic Solution
      lmi_a[i] <- prop[i]*log(bins)
    }

  }
  temp_df <- as.data.frame(cbind(lmi_a, prop))
  return(temp_df)
}

sim_1_err0_bw4 <- shift_sen(band = 4, r_err_1 = 0,
    r_err_2 = 0, nbins = 8)
sim_1_err0_bw8 <- shift_sen(band = 8,
    r_err_1 = 0, r_err_2 = 0, nbins = 8)
```

```
sim_1_err0_bw12 <- shift_sen(band = 12, r_err_1 = 0,
    r_err_2 = 0, nbins = 8)
sim_1_err0_bw16 <- shift_sen(band = 16, r_err_1 = 0,
    r_err_2 = 0, nbins = 8)
sim_1_err0_bw32 <- shift_sen(band = 32, r_err_1 = 0,
    r_err_2 = 0, nbins = 8)

sim_1_err0_bw4_b2 <- shift_sen(band = 4, r_err_1 = 0,
    r_err_2 = 0, nbins = 2)
sim_1_err0_bw8_b2 <- shift_sen(band = 8, r_err_1 = 0,
    r_err_2 = 0, nbins = 2)
sim_1_err0_bw12_b2 <- shift_sen(band = 12, r_err_1 = 0,
    r_err_2 = 0, nbins = 2)
sim_1_err0_bw16_b2 <- shift_sen(band = 16, r_err_1 = 0,
    r_err_2 = 0, nbins = 2)
sim_1_err0_bw32_b2 <- shift_sen(band = 32, r_err_1 = 0,
    r_err_2 = 0, nbins = 2)

sim_1_err0_bw4_b16 <- shift_sen(band = 4, r_err_1 = 0,
    r_err_2 = 0, nbins = 16)
sim_1_err0_bw8_b16 <- shift_sen(band = 8, r_err_1 = 0,
    r_err_2 = 0, nbins = 16)
sim_1_err0_bw12_b16 <- shift_sen(band = 12, r_err_1 = 0,
    r_err_2 = 0, nbins = 16)
sim_1_err0_bw16_b16 <- shift_sen(band = 16, r_err_1 = 0,
    r_err_2 = 0, nbins = 16)
sim_1_err0_bw32_b16 <- shift_sen(band = 32, r_err_1 = 0,
```

```
    r_err_2 = 0, nbins = 16)

sim_1_err0_bw4_b32 <- shift_sen(band = 4, r_err_1 = 0,
    r_err_2 = 0, nbins = 32)
sim_1_err0_bw8_b32 <- shift_sen(band = 8, r_err_1 = 0,
    r_err_2 = 0, nbins = 32)
sim_1_err0_bw12_b32 <- shift_sen(band = 12, r_err_1 = 0,
    r_err_2 = 0, nbins = 32)
sim_1_err0_bw16_b32 <- shift_sen(band = 16, r_err_1 = 0,
    r_err_2 = 0, nbins = 32)
sim_1_err0_bw32_b32 <- shift_sen(band = 32, r_err_1 = 0,
    r_err_2 = 0, nbins = 32)

# Blank Plot templates to overlay final LMI results
gg_time <- ggplot() +
  theme(text = element_text(family="Times",size=20),
        plot.title = element_text(size = 20, colour = "black"),
        plot.background = element_rect(fill = "white"),
        axis.text=element_text(size=20, color = "black"),
        axis.title = element_text(family="Times",size=20,
        colour = "black"),
        panel.background = element_rect(fill = "ivory1",
        colour = "black"),
        panel.grid.major = element_line(colour = "grey18",
        linetype = "dotted"),
        panel.grid.minor.x=element_blank(),
        panel.grid.minor.y=element_blank(),
```

```
        legend.position = "none") +  xlab("Time") + ylab("LMI(t_i)")
gg_pos <- ggplot() +
  theme(text = element_text(family="Times",size=20),
        plot.title = element_text(size = 20, colour = "black"),
        plot.background = element_rect(fill = "white"),
        axis.text=element_text(size=20, color = "black"),
        axis.title = element_text(family="Times",size=20,
        colour = "black"),
        panel.background = element_rect(fill = "ivory1",
        colour = "black"),
        panel.grid.major = element_line(colour = "grey18",
        linetype = "dotted"),
        panel.grid.minor.x=element_blank(),
        panel.grid.minor.y=element_blank(),
        legend.position = "none") +  xlab("Long_Position") +
        ylab("Lat_Position")


gg_pos <- gg_pos +
  geom_point(data = sim_1_err0_bw16$`AnimalPositions`,
  aes(animal_lon_1,animal_lat_1),
  col = "royalblue", alpha=0.4, size = 2.5) +
  geom_point(data = sim_1_err0_bw16$`Animal Positions`,
  aes(animal_lon_2,animal_lat_2),
  col = "lightsalmon", alpha=0.4, size =2.5)
gg_time <- gg_time +
  geom_point(data = sim_1_err0_bw16$`LMI Function`,
  aes(t_tilde,loc_mut_joint/loc_mut_joint_max),
```

```
  col = "navy", alpha=0.5, size =2.5)

# FIGURE 1
gg_pos



gg_time <- ggplot() +
  theme(text = element_text(family="Times",size=20),
        plot.title = element_text(size = 20, colour = "black"),
        plot.background = element_rect(fill = "white"),
        axis.text=element_text(size=20, color = "black"),
        axis.title = element_text(family="Times",size=20,
        colour = "black"),
        panel.background = element_rect(fill = "ivory1",
        colour = "black"),
        panel.grid.major = element_line(colour = "grey18",
        linetype = "dotted"),
        panel.grid.minor.x=element_blank(),
        panel.grid.minor.y=element_blank(),
        legend.position = "none") +  xlab("Time") + ylab("␣")

##########################################
##########################################

a_bw4 <- analytic_sol(t_tilde = t_til,trans_time = trans,
bw=4, bins = 2)
a_bw8 <- analytic_sol(t_tilde = t_til,trans_time = trans,
```

```
bw=8, bins = 2)
a_bw16 <- analytic_sol(t_tilde = t_til,trans_time = trans,
bw=16, bins = 2)
#a_bw32 <- analytic_sol(t_tilde = t_til,trans_time = trans,
bw=32, bins = 2)
gg_time_bw4 <- gg_time + ylab("LMI(t_i)") + ggtitle("bw = 4,
bins = 2")+
  geom_point(data = sim_1_err0_bw4_b2$`LMI Function`,
  aes(t_tilde,loc_mut_lat), col = "navy", alpha=0.5,
  size =2.5) +
  geom_line(aes(x=t_til, y=a_bw4$lmi_a), col = "goldenrod1",
  size = 1.2)
  col = "goldenrod1", size =1.25) +


gg_time_bw8 <- gg_time + ggtitle("bw = 8, bins = 2")+
  geom_point(data = sim_1_err0_bw8_b2$`LMI Function`,
  aes(t_tilde,loc_mut_lat), col = "navy", alpha=0.5,
  size =2.5) +
  geom_line(aes(x=t_til, y=a_bw8$lmi_a), col = "goldenrod1",
  size = 1.2)
gg_time_bw16 <- gg_time + ggtitle("bw = 16, bins = 2")+
  geom_point(data = sim_1_err0_bw16_b2$`LMI Function`,
  aes(t_tilde,loc_mut_lat), col = "navy", alpha=0.5,
  size =2.5) +
  geom_line(aes(x=t_til, y=a_bw16$lmi_a), col = "goldenrod1",
  size = 1.2)
```

```
gg_time_bw32 <- gg_time + ggtitle("bw = 32, bins = 2")+
  geom_point(data = sim_1_err0_bw32_b2$`LMI Function`,
  aes(t_tilde,loc_mut_lat), col = "navy", alpha=0.5,
  size =2.5) +
  geom_segment(aes(x=0,xend=0.5,y=log(2),yend=log(2)),
  col = "goldenrod1", size =1.25) +
  geom_segment(aes(x=0.5,xend=1.0,y=log(1),yend=log(1)),
  col = "goldenrod1", size =1.25)
gg_b2 <- grid.arrange(gg_time_bw4, gg_time_bw8,
gg_time_bw16, gg_time_bw32, ncol= 4 )



a_bw4 <- analytic_sol(t_tilde = t_til,trans_time = trans,
bw=4, bins = 8)
a_bw8 <- analytic_sol(t_tilde = t_til,trans_time = trans,
bw=8, bins = 8)
a_bw16 <- analytic_sol(t_tilde = t_til,trans_time = trans,
bw=16, bins = 8)

gg_time_bw4 <- gg_time + ylab("LMI(t_i)")+
     ggtitle("bw = 4, bins = 8")+
     geom_point(data = sim_1_err0_bw4$`LMI Function`,
     aes(t_tilde,loc_mut_lat), col = "navy",
     alpha=0.5, size =2.5) +
     geom_line(aes(x=t_til, y=a_bw4$lmi_a), col = "goldenrod1",
     size = 1.2)
gg_time_bw8 <- gg_time +  ggtitle("bw = 8, bins = 8")+
```

```
  geom_point(data = sim_1_err0_bw8$`LMI Function`,
  aes(t_tilde,loc_mut_lat), col = "navy", alpha=0.5, size =2.5) +
  geom_line(aes(x=t_til, y=a_bw8$lmi_a), col = "goldenrod1",
  size = 1.2)
gg_time_bw16 <- gg_time + ggtitle("bw = 16, bins = 8")+
  geom_point(data = sim_1_err0_bw16$`LMI Function`,
  aes(t_tilde,loc_mut_lat), col = "navy", alpha=0.5, size =2.5) +
  geom_line(aes(x=t_til, y=a_bw16$lmi_a), col = "goldenrod1",
  size = 1.2)
gg_time_bw32 <- gg_time + ggtitle("bw = 32, bins = 8")+
  geom_point(data = sim_1_err0_bw32$`LMI Function`,
  aes(t_tilde,loc_mut_lat), col = "navy", alpha=0.5, size =2.5) +
  geom_segment(aes(x=0,xend=0.5,y=log(8),yend=log(8)),
  col = "goldenrod1", size =1.25) +
  geom_segment(aes(x=0.5,xend=1.0,y=log(1),yend=log(1)),
  col = "goldenrod1", size =1.25) +
  geom_point(aes(x=0.5, y=0.5*log(8)),
  col = "goldenrod1", size = 2.5)
gg_b8 <- grid.arrange(gg_time_bw4, gg_time_bw8,
gg_time_bw16, gg_time_bw32, ncol = 4 )



a_bw4 <- analytic_sol(t_tilde = t_til,trans_time = trans,
bw=4, bins = 16)
a_bw8 <- analytic_sol(t_tilde = t_til,trans_time = trans,
bw=8, bins = 16)
a_bw16 <- analytic_sol(t_tilde = t_til,trans_time = trans,
```

```
bw=16, bins = 16)
#a_bw32 <- analytic_sol(t_tilde = t_til,trans_time = trans,
bw=32, bins = 16)
gg_time_bw4 <- gg_time + ylab("LMI(t_i)")+
  ggtitle("bw = 4, bins = 16")+
  geom_point(data = sim_1_err0_bw4_b16$`LMI Function`,
  aes(t_tilde,loc_mut_lat), col = "navy", alpha=0.5, size =2.5) +
  geom_line(aes(x=t_til, y=a_bw4$lmi_a),
  col = "goldenrod1", size = 1.2)
gg_time_bw8 <- gg_time +  ggtitle("bw = 8, bins = 16")+
  geom_point(data = sim_1_err0_bw8_b16$`LMI Function`,
  aes(t_tilde,loc_mut_lat), col = "navy",
  alpha=0.5, size =2.5) +
  geom_line(aes(x=t_til, y=a_bw8$lmi_a),
  col = "goldenrod1", size = 1.2)
gg_time_bw16 <- gg_time + ggtitle("bw = 16, bins = 16")+
  geom_point(data = sim_1_err0_bw16_b16$`LMI Function`,
  aes(t_tilde,loc_mut_lat), col = "navy", alpha=0.5, size =2.5) +
  geom_line(aes(x=t_til, y=a_bw16$lmi_a),
    col = "goldenrod1", size = 1.2)
gg_time_bw32 <- gg_time + ggtitle("bw = 32, bins = 16")+
  geom_point(data = sim_1_err0_bw32_b16$`LMI Function`,
  aes(t_tilde,loc_mut_lat), col = "navy", alpha=0.5, size =2.5) +
  geom_segment(aes(x=0,xend=0.5,y=log(16),yend=log(16)),
  col = "goldenrod1", size =1.25) +
  geom_segment(aes(x=0.5,xend=1.0,y=log(1),yend=log(1)),
  col = "goldenrod1", size =1.25) +
```

```
  geom_point(aes(x=0.5, y=0.5*log(16)),
  col = "goldenrod1", size = 2.5)
gg_b16 <- grid.arrange(gg_time_bw4, gg_time_bw8,
gg_time_bw16, gg_time_bw32, ncol = 4 )

a_bw4 <- analytic_sol(t_tilde = t_til,trans_time = trans,
bw=4, bins = 32)
a_bw8 <- analytic_sol(t_tilde = t_til,trans_time = trans,
bw=8, bins = 32)
a_bw16 <- analytic_sol(t_tilde = t_til,trans_time = trans,
bw=16, bins = 32)
a_bw32 <- analytic_sol(t_tilde = t_til,trans_time = trans,
bw=32, bins = 32)
gg_time_bw4 <- gg_time + ylab("LMI(t_i)")+
     ggtitle("bw = 4, bins = 32")+
     geom_point(data = sim_1_err0_bw4_b32$`LMI Function`,
     aes(t_tilde,loc_mut_lat), col = "navy", alpha=0.5, size =2.5) +
     geom_line(aes(x=t_til, y=a_bw4$lmi_a),
     col = "goldenrod1", size = 1.2)
gg_time_bw8 <- gg_time +  ggtitle("bw = 8, bins = 32")+
  geom_point(data = sim_1_err0_bw8_b32$`LMI Function`,
  aes(t_tilde,loc_mut_lat), col = "navy", alpha=0.5, size =2.5) +
  geom_line(aes(x=t_til, y=a_bw8$lmi_a),
  col = "goldenrod1", size = 1.2)
gg_time_bw16 <- gg_time + ggtitle("bw = 16, bins = 32")+
  geom_point(data = sim_1_err0_bw16_b32$`LMI Function`,
  aes(t_tilde,loc_mut_lat), col = "navy", alpha=0.5, size =2.5) +
```

```
  geom_line(aes(x=t_til, y=a_bw16$lmi_a),
  col = "goldenrod1", size = 1.2)
gg_time_bw32 <- gg_time + ggtitle("bw = 32, bins = 32")+
  geom_point(data = sim_1_err0_bw32_b32$`LMI Function`,
  aes(t_tilde,loc_mut_lat), col = "navy", alpha=0.5, size =2.5) +
  geom_segment(aes(x=0,xend=0.5,y=log(32),yend=log(32)),
  col = "goldenrod1", size =1.25) +
  geom_segment(aes(x=0.5,xend=1.0,y=log(1),yend=log(1)),
  col = "goldenrod1", size =1.25) +
  geom_point(aes(x=0.5, y=0.5*log(32)),
  col = "goldenrod1", size = 2.5)
gg_b32 <- grid.arrange(gg_time_bw4, gg_time_bw8,
gg_time_bw16, gg_time_bw32, ncol = 4 )

grid.arrange(gg_b2, gg_b8, gg_b16, gg_b32, ncol = 1)
}
```

REFERENCES

[1] Urbano, F., Cagnacci, F., Calenge, C., Dettki, H., Cameron, A., Neteler, M. (2010). Wildlife tracking data management: a new vision. Philosophical transactions of the Royal Society of London. Series B, Biological sciences, 365(1550), 2177–2185. https://doi.org/10.1098/rstb.2010.0081

[2] Lewis M.A., Fagan W.F., Auger-Méthé M., Frair J., Fryxell J.M., Gros C., Gurarie E., Healy S.D., Merkle J.A. Learning and Animal Movement. Frontiers in Ecology and Evolution. Vol 9. pp 441. https://www.frontiersin.org/article/10.3389/fevo.2021.681704.

[3] Cagnacci F., Urbano F.2008Managing wildlife: a spatial information system for GPS collars data. Environ. Modell. Softw. 23, 957–959 (doi:10.1016/j.envsoft.2008.01.003)

[4] Hooten, M., Buderman, F., Brost, B., Hanks, E., and Ivan, J. (2016), "Hierarchical Animal Movement Models for Population-Level Inference," Environmetrics, 27, 322–333.

[5] Hooten M.B., Johnson D.S., McClintock B.T., Morales J.M., References, Animal Movement, 10.1201/9781315117744, (273-290), (2017).

[6] Fleming, C., Deznabi, I., Alavi, S., Crofoot, M., Hirsch, B., Medici, E., Noonan, M., Kays, R., Fagan, W., Sheldon, D., Calabrese, J. (2021). Population-level inference for home-range areas. 10.1101/2021.07.05.451204.

[7] Buderman F.E. et. al. A functional model for characterizing long-distance movement behaviour. Methods in Ecology and Evolution. Volume7, Issue3 March 2016. Pages 264-273. https://doi.org/10.1111/2041-210X.12465

[8] McClintock, B.T., Johnson, D.S., Hooten, M.B. et al. When to be discrete: the importance of time formulation in understanding animal movement. Mov Ecol 2, 21 (2014). https://doi.org/10.1186/s40462-014-0021-6

[9] McClintock, B., London J., Cameron M., and Boveng P. 2015. Modeling animal movement using the Argos satellite telemetry location error ellipse. Methods in Ecology and Evolution, 6:266–277.

[10] Jonsen, I., Flemming J., and Myers R. 2005. Robust state-space modeling of animal movement data. Ecology, 45:589–598.

[11] Morales, J., Haydon D., Friar J., Holsinger K., and Fryxell J. 2004. Extracting more out of relocation data: building movement models as mixtures of random walks. Ecology, 85: 2436–2445.

[12] Parton, A., Blackwell P.G. Bayesian Inference for Multistate 'Step and Turn' Animal Movement in Continuous Time. JABES 22, 373–392 (2017). https://doi.org/10.1007/s13253-017-0286-5

[13] Hanks, E.M., Hooten M.B., and Alldredge M.W. "Continuous-time discrete-space models for animal movement." The Annals of Applied Statistics 9.1 (2015): 145-165

[14] Harris KJ, Blackwell PG. Flexible continuous-time modelling for heterogeneous animal movement. Ecol Model 2013, 255:29–37

[15] Johnson, D.S., et al. "Continuous-time correlated random walk model for animal telemetry data." Ecology 89.5 (2008): 1208-1215

[16] Gurarie E, Andrews RD, Laidre KL. A novel method for identifying behavioural changes in animal movement data. Ecol Lett. 2009; 12: 395–408. pmid:19379134

[17] Torres LG, Orben RA, Tolkova I, Thompson DR (2017) Classification of Animal Movement Behavior through Residence in Space and Time. PLOS ONE 12(1): e0168513. https://doi.org/10.1371/journal.pone.0168513

[18] Sur M, Skidmore AK, Exo K-M, Wang T, Ens BJ, Toxopeus A. Change detection in animal movement using discrete wavelet analysis. Ecol Inform. 2014; 20: 47–57.

[19] Fontes S.G., Morato R.G., Stanzani S.L., Pizzigatti Corrêa P.L. (2021) Jaguar movement behavior: using trajectories and association rule mining algorithms to unveil behavioral states and social interactions. PLOS ONE 16(2): e0246233. https://doi.org/10.1371/journal.pone.0246233

[20] Hastie, T., Tibshirani, R.,, Friedman, J. (2001). The Elements of Statistical Learning. New York, NY, USA: Springer New York Inc..

[21] Khaled Fawagreh, Mohamed Medhat Gaber, Eyad Elyan (2014) Random forests: from early developments to recent advancements, Systems Science and Control Engineering, 2:1, 602-609, DOI: 10.1080/21642583.2014.956265

[22] Gower, J.C., Properties of Euclidean and non-Euclidean distance matrices. Linear Algebra and its Applications. Volume 67. 1985. Pages 81-97. ISSN 0024-3795,https://doi.org/10.1016/0024-3795(85)90187-9.

[23] Boriah S., Chandola V., Kumar V. (2008). Similarity measures for categorical data: A comparative evaluation. In: Proceedings of the 8th SIAM International Conference on Data Mining, SIAM, p. 243-254.

[24] Whetten AB, Demler H. Detection of Multidecadal Changes in Vegetation Dynamics and Association with Intra-annual Climate Variability in the Columbia River Basin. In ArXiv e-prints (May 2021). arXiv: 2105.08864 [q-bio.QM]

[25] Binbin Lu, Martin Charlton, Paul Harris, A. Stewart Fotheringham (2014) Geographically weighted regression with a non-Euclidean distance metric: a case study using hedonic house price data, International Journal of Geographical Information Science, 28:4, 660-681, DOI: 10.1080/13658816.2013.865739

[26] Kendall, M. G. (1938). A new measure of rank correlation, Biometrika, 30, 81–93. doi: 10.1093/biomet/30.1-2.81.

[27] Schaeffer, M. S., Levitt, E. E. (1956). Concerning Kendall's tau, a nonparametric correlation coefficient. Psychological Bulletin, 53(4), 338–346. https://doi.org/10.1037/h0045013

[28] Cover, T.M.; Thomas, J.A. (1991). Elements of Information Theory (Wiley ed.). ISBN 978-0-471-24195-9.

[29] Gervini, D. and Khanal, M. (2019). Exploring patterns of demand in bike sharing systems via replicated point process models. Journal of the Royal Statistical Society Series C: Applied Statistics 68 585-602.

[30] Owoeye K., Musolesi M., Hailes S. Characterizing animal movement patterns across different scales and habitats using information theory. bioRxiv 311241. 2018. doi: https://doi.org/10.1101/311241

[31] S. Butail, F. Ladu, D. Spinello, and M. Porfiri. Information flow in animal-robot interactions. Entropy, 16(3):1315–1330, 2014.

[32] S. Butail, V. Mwaffo, and M. Porfiri. Model-free information-theoretic approach to infer leadership in pairs of zebrafish. Physical Review E, 93(4):042411, 2016

[33] F. Hu, L.-J. Nie, and S.-J. Fu. Information dynamics in the interaction between a prey and a predator fish. Entropy, 17(10):7230–7241, 2015.

[34] M. Kadota, E. J. White, S. Torisawa, K. Komeyama, and T. Takagi. Employing relative entropy techniques for assessing modifications in animal behavior. PLOS ONE, 6(12):1–6, 2011.

[35] W. M. Lord, J. Sun, N. T. Ouellette, and E. M. Bolt. Inference of causal information flow in collective animal behavior. IEEE Transactions on Molecular, Biological and Multi-Scale Communications, 2(1):107–116, 2016.

[36] Rocchini, D.; Thouverai, E.; Marcantonio, M.; Iannacito, M.; Da Re, D.; Torresani, M.; Bacaro, G.; Bazzichetto, M.; Bernardi, A.; Foody, G.M.; et al. rasterdiv—An Information Theory tailored R package for measuring ecosystem heterogeneity from space: To the origin and back. Methods Ecol. Evol. 2021, 12, 1093–1102.

[37] Jeffrey J. Thompson, Ronaldo G. Morato, et. al. (2021) Environmental and anthropogenic factors synergistically affect space use of jaguars. Current Biology. 31 (15): 3457-3466. ISSN 0960-9822. https://doi.org/10.1016/j.cub.2021.06.029.

[38] Dai S., Zhan S., Song N. Adaptive Active Contour Model: a Localized Mutual Information Approach for Medical Image Segmentation. (2015). KSII Transactions on Internet and Information Systems, 9(5). https://doi.org/10.3837/tiis.2015.05.016

[39] Klein S., et. al. Automatic segmentation of the prostate in 3D MR images by atlas matching using localized mutual information.2008. Volume35, Issue4.Pages 1407-1417. https://doi.org/10.1118/1.2842076

[40] Whetten A.B., Smoothing Splines of Apex Predator Movement: Functional modeling strategies for exploring animal behavior and social interactions. Ecology and Evolution. Vol 11 (21). DOI: 10.1002/ece3.8294

[41] Torres LG, Thompson DR, Bearhop S, Votier SC, Taylor GA, Sagar PM, et al. White-capped albatrosses alter fine-scale foraging behavior patterns when associated with fishing vessels. Mar Ecol Prog Ser. 2011; 428: 289–301.

[42] Green, P. J.; Silverman, B.W. (1994). Nonparametric Regression and Generalized Linear Models: A roughness penalty approach. Chapman and Hall.

[43] Hastie, T. J.; Tibshirani, R. J. (1990). Generalized Additive Models. Chapman and Hall. ISBN 978-0-412-34390-2.

[44] Ramsay, J.O., and Silverman, B.W. (2005). Functional Data Analysis (second edition). Springer, New York.

[45] Ramsay J., Dalzell C. (1991). Some Tools for Functional Data Analysis. Journal of the Royal Statistical Society. Series B (Methodological), 53(3), 539-572.

[46] De Boor C. 1978. A practical guide to splines.

[47] Gel'fand, I.M.; Yaglom, A.M. (1957). "Calculation of amount of information about a random function contained in another such function". American Mathematical Society Translations. Series 2. 12: 199–246. doi:10.1090/trans2/012/09. ISBN 9780821817124. English translation of original in Uspekhi Matematicheskikh Nauk 12 (1): 3-52.

[48] Meyer, P. E. (2008). Information-Theoretic Variable Selection and Network Inference from Microarray Data. PhD thesis of the Universite Libre de Bruxelles.

[49] Wong JB, Lisovski S, Alisauskas RT, English W and others (2021) Arctic terns from circumpolar breeding colonies share common migratory routes. Mar Ecol Prog Ser 671:191-206. https://doi.org/10.3354/meps13779

[50] Palomares, F. et. al. (2018). Scraping marking behaviour of the largest Neotropical felids. PeerJ, 6, e4983. https://doi.org/10.7717/peerj.4983

[51] Towns V. et. al. (2017). Marking behaviours of jaguars in a tropical rainforest of southern Mexico. CAT news. 66. 33-35.

[52] Ullah S., Finch C.F. ((2013). Applications of functional data analysis: A systematic review. BMC Med Res Methodol 13, 43.

[53] Hooten M.B., Johnson D.S., Basis Function Models for Animal Movement, Journal of the American Statistical Association, 10.1080/01621459.2016.1246250, 112, 518, (578-589), (2016).

[54] Henning B., Kist A., Pinheiro A., Camargo R.L, Batista T.M., Carneiro E.M, dos Reis S.F., Modelling Animal Activity as Curves: An Approach Using Wavelet-Based Functional Data Analysis, Open Journal of Statistics, 10.4236/ojs.2017.72016, 07, 02, (203-215), (2017).

[55] Hefley T.J., Broms K.M., Brost B.M., Buderman F.E., Kay S.L., Scharf H.R., Tipton J.R., Williams P.J., Hooten M.B., The basis function approach for modeling autocorrelation in ecological data, Ecology, 10.1002/ecy.1674, 98, 3, (632-646), (2017).

[56] Anderson-Sprecher R., and Lenth R.V. "Spline estimation of paths using bearings-only tracking data." Journal of the American statistical association 91.433 (1996): 276-283.

[57] Morato R.G., Stabach J.A., Fleming C.H., Calabrese J.M., Paula R.C.D., Ferraz K.M.P.M., et al. Space Use and Movement of a Neotropical Top Predator: The Endangered Jaguar. PLOS ONE. 2016; 11: e0168176. https://doi.org/10.1371/journal.pone.0168176 PMID: 28030568

[58] Cavalcanti SMC, Gese EM. Spatial Ecology and Social Interactions of Jaguars (Panthera onca) in the Southern Pantanal, Brazil. J Mammal. 2009; 90: 935–945. https://doi.org/10.1644/08-MAMM-A-188.1

[59] Sneha J., Shuangge Ma. Functional Measurement Error in Functional Regression. Candian Journal of Statistics. Volume48, Issue2.2020.https://doi.org/10.1002/cjs.11529

[60] Cai X. Methods for handling measurement error and sources of variation in functional data models. Columbia Commons. 2015. Doctoral Thesis. https://doi.org/10.7916/D8M907CJ

[61] Hooten, M.B., et al. "Animal movement models for migratory individuals and groups." Methods in Ecology and Evolution 9.7 (2018): 1692-1705

[62] Wand, M.P; Jones, M.C. (1995). Kernel Smoothing. London: Chapman Hall/CRC. ISBN 978-0-412-55270-0.

[63] Noonan M.J., Fleming C.H., Akre T.S. et al. Scale-insensitive estimation of speed and distance traveled from animal tracking data. Mov Ecol 7, 35 (2019). https://doi.org/10.1186/s40462-019-0177-1

[64] Buderman F.E., et al. "Large-scale movement behavior in a reintroduced predator population." Ecography 41.1 (2018): 126-139.

[65] Hijman R.J. (2019). geosphere: Spherical Trigonometry. R package version 1.5-10. https://CRAN.R-project.org/package=geosphere

[66] Harmsen B.J., Foster R.J., Gutierrez S.M., Marin S.Y., Doncaster C.P., Scrape-marking behavior of jaguars (Panthera onca) and pumas (Puma concolor), Journal of Mammalogy, Volume 91, Issue 5, 15 October 2010, Pages 1225–1234, https://doi.org/10.1644/09-MAMM-A-416.1

[67] Scharf, H.R., et al. "Dynamic social networks based on movement." The Annals of Applied Statistics 10.4 (2016): 2182-2202.

[68] Scharf, H.R., et al. "Process convolution approaches for modeling interacting trajectories." Environmetrics 29.3 (2018): e2487.

[69] Hamdy M., arXiv:1906.10221 [stat.ME]

[70] Langley R. 1999. Dilution of precision. — GPS World 10: 52–59.

[71] Morato R.G., Thompson J.J., Paviolo A., Torre J.A. de L, Lima F., McBride R.T., et al. Jaguar movement data- base: a GPS-based movement dataset of an apex predator in

the Neotropics. Ecology. 2018; 99: 1691– 1691. https://doi.org/10.1002/ecy.2379 PMID: 29961270

[72] Morato R.G., Kantek D.L.Z., Miyazaki S., Deluque T., de Paula R.C. (2021) Data from: Jaguar movement database—a GPS-based movement dataset of an apex predator in the Neotropics. Movebank Data Repository. doi:10.5441/001/1.3c4fv0m4

[73] Wickham H. ggplot2: Elegant Graphics for Data Analysis. Springer-Verlag New York, 2016.

[74] Baptiste A. (2017). gridExtra: Miscellaneous Functions for "Grid" Graphics. R package version 2.3. https://CRAN.R-project.org/package=gridExtra

[75] Charlotte E. Eriksson, et. al. Extensive aquatic subsidies lead to territorial breakdown and high density of an apex predator. bioRxiv 2021.03.29.437596; doi: https://doi.org/10.1101/2021.03.29.437596

[76] Hijmans R.J. (2019). geosphere: Spherical Trigonometry. R package version 1.5-10. https://CRAN.R-project.org/package=geosphere

[77] Meyer P.E. (2014). infotheo: Information-Theoretic Measures. R package version 1.2.0. https://CRAN.R-project.org/package=infotheo

[78] Kantek D.L.Z and Onuma S.S.M. Jaguar Conservation in the region of Taiamã Ecological Station, Northern Pantanal, Brazil. Publicatio UEPG Biológicas e da Saúde. 2013. DOI: 10.5212/Publ.Biologicas.v.19i1.0008

[79] Cavalcanti S. et. al. (2012). The status of the jaguar in the Pantanal. Cat News. 7.

[80] Sollmann R. et. al. (2008). Jaguar Conservation in Brazil: The Role of Protected Areas. Cat News Spec. Issue. 4.

[81] Cullen J.L., Sana D.A., Lima F., Abreu K.C. de, Uezu A. Selection of habitat by the jaguar, Panthera onca (Carnivora: Felidae), in the upper Paraná River, Brazil. Zoologia (Curitiba). 2013;30: 379–387.

[82] Darudi A., Rezaeifar S., and Bayaz M.H.J.D, "Partial mutual information based algorithm for input variable selection For time series forecasting," 2013 13th International

Conference on Environment and Electrical Engineering (EEEIC), 2013, pp. 313-318, doi: 10.1109/EEEIC-2.2013.6737928.

[83] Conde D.A., Colchero F., Zarza H., Christensen N.L., Sexton J.O., Manterola C., et al. Sex matters: Modeling male and female habitat differences for jaguar conservation. Biological Conservation. 2010; 143: 1980– 1988. https://doi.org/10.1016/j.biocon.2010.04.049

[84] de Azevedo F.C.C., Dennis Lewis Murray. Spatial organization and food habits of jaguars (Panthera onca) in a floodplain forest. Biological Conservation. 2007. Volume 137. Issue 3.Pages 391-402. https://doi.org/10.1016/j.biocon.2007.02.022.

[85] Towns V., et. al. Marking behaviours of jaguars in a tropical rainforest of southern Mexico. CAT News. 2017. ISSN 1027-2992.

[86] Togunov R.R., Derocher A.E., Lunn N.J., Auger-Méthé M.. Characterising menotactic behaviours in movement data using hidden Markov models. Methods in Ecology and Evolution.2021. https://doi.org/10.1111/2041-210X.13681